PASSIVE ACOUSTIC SHIP DETECTION PERFORMANCE NEAR THE PORT OF SEPT-ÎLES, QUEBEC, CANADA

By

Marina Antipina

Submitted in partial fulfilment of the requirements for the degree of Master of Science

At

Dalhousie University
Halifax, Nova Scotia
September 2022

DEDICATION

This thesis is dedicated to Scott Carr for being by my side every step of the way, and all his unconditional love, support and encouragement. This accomplishment would not have been possible without you. I am forever grateful.

TABLE OF CONTENTS

LIST OF TABLES

LIST OF FIGURES

ABSTRACT

An AMAR acoustic recorder was deployed near the Port of Sept-Îles, Quebec, Canada in the Fall of 2020 and collected one year of data. Vessels were detected using narrowband tonals. Sound pressure level (SPL) for each minute of data in the 40–315 Hz decidecade shipping band was then computed. These SPLs were then searched for the highest 1 min SPL which was identified as the CPA time for each acoustic contact. Interpolated vessel track data from the AIS were used to compute CPAs for vessels carrying an AIS transponder during the deployment period. A DEMON detector was implemented based on DEMON processing. Then, the AIS CPA was compared to the JASCO and DEMON CPA to calculate the number of true positive and false negative CPAs for each detector. The combination of the two detectors was used to improve JASCO's vessel detector's performance, and its results are discussed.

ACKNOWLEDGEMENTS

I am extremely grateful to my advisor Dr. David Barclay, and my committee – Dr. Bruce Martin, Dr. Mae Seto, and Dr. Len Zedel. Your continuous support, guidance, and expertise throughout my studies made this master's thesis possible.

I would like to thank JASCO for funding and assisting with my research.

I am thankful to my family and friends for their love and support throughout my years of study. I would also like to express gratitude to my professors and colleagues for motivating and inspiring me.

Finally, I would also like to thank my cats, Kai and Malia, for always being there for me.

Chapter 1: Introduction

This thesis presents the results of the analysis aimed to improve the detection of vessels in acoustic data collected with a JASCO Applied Sciences (Dartmouth, Nova Scotia, Canada) AMAR recorder deployed near the Port of Sept-Îles in Saint Lawrence River (Quebec, Canada) between November 2020 and October 2021. It consists of the introductory part where the motivation and the objectives of the research are presented, a theory section discussing the elements of ship generated noise, followed by a description of the methods, data analysis, and the detection algorithms used, and finished with a presentation of research results, a discussion and conclusions.

1.1 Background

The St. Lawrence River flows from Lake Ontario into the Gulf of St. Lawrence (Figure 1) (Great Lakes Guide, from https://greatlakes.guide/watersheds/st-lawrence, last viewed August 1, 2022; Perlman et al., 2017). The St. Lawrence Seaway connects the Great Lakes to the Atlantic Ocean (Shaw et al., 2015; Perlman et al., 2017).

Figure 1: Map of the St. Lawrence River, Great Lakes and St. Lawrence Seaway (Perlman et al., 2017).

The Port of Sept-Îles is located on the North Shore of the St. Lawrence River, and about 650 kilometers from Quebec City (Port of Sept-Îles, from https://www.portsi.com/port/?lang=en, last viewed December 14, 2021). In French Sept-Îles means the "Seven Islands" which can be seen in the distance in Figure 2.

Figure 2: The Port of Sept-Îles, and the Seven Islands in the distance (Canadian Sailings, 2018).

Major iron and mining companies are located in Sept-Îles and the town's Port is the largest mineral port in North America (Port of Sept-Îles, from https://www.portsi.com/port/?lang=en, last viewed December 14, 2021). The port is a natural harbour with a 10 km wide semi-circular bay. It is a centre for the shipping of iron and other minerals between North America, Europe and Asia, and it is open year-round (Port of Sept-Îles, from https://www.portsi.com/port/?lang=en, last viewed December 14, 2021).

Shipping to and from the Port of Sept-Îles passes through or close to many marine protected areas and reserves (Figure 3).

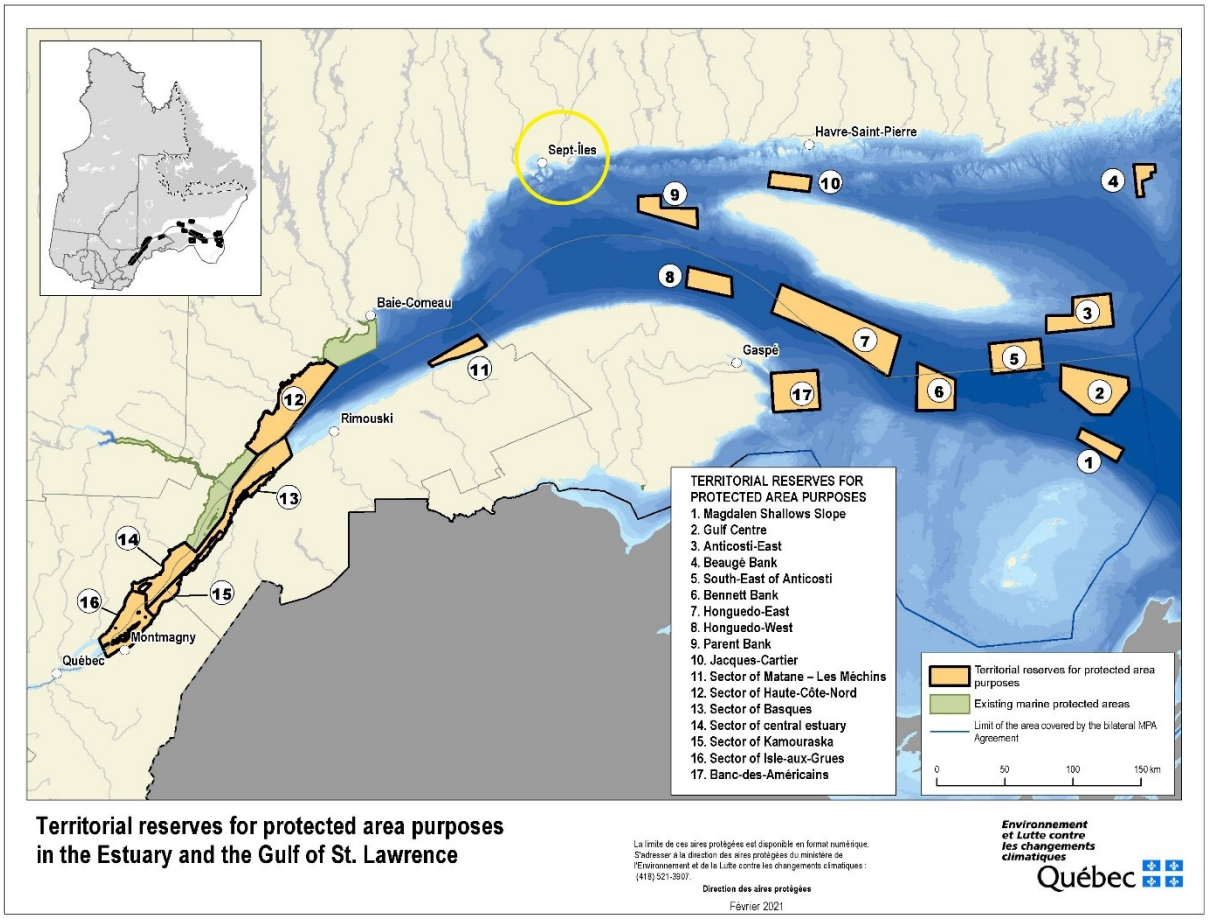

Figure 3: Marine Protected Areas and Territorial Reserves for Protected Area Purposes in the Estuary and the Gulf of St. Lawrence (Retrieved from https://www.environnement.gouv.qc.ca/biodiversite/aires_protegees/aire-marine/reserve-golf-estuaire-st-laurent-en.htm).

Active marine mammal presence was documented from May through September in 2017 (Figure 4) near the Port of Sept-Îles, which stands between the Saguenay-St. Lawrence Marine Park and the Gulf of St. Lawrence (INREST, 2017).

Figure 4 taken from the INREST report (INREST, 2017), provides a general overview of marine mammal's presence in the area around the Port of Sept-Îles and shows whale and seal sightings in the region near where the AMAR was deployed.

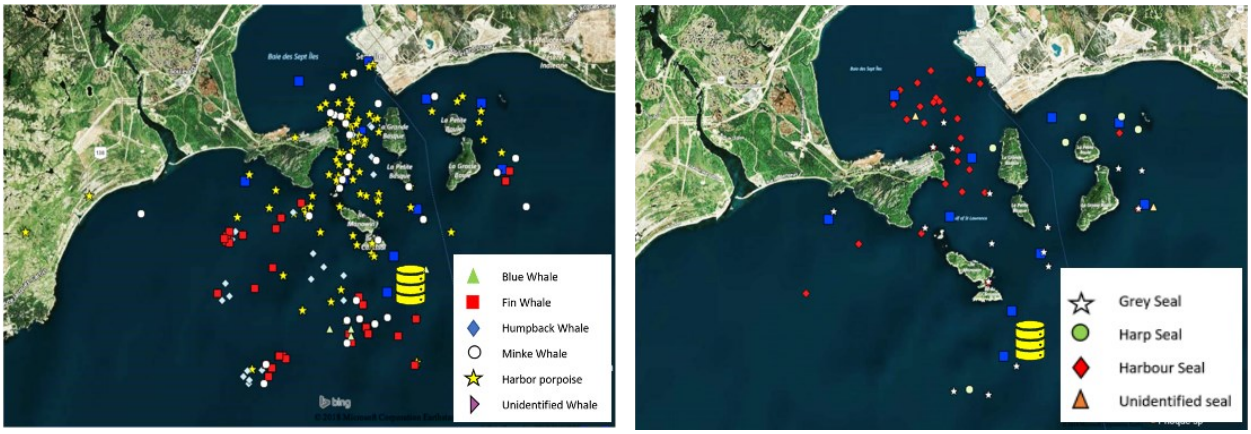

Figure 4: Whale and Seal Sightings near the AMAR (May – September 2017) (INREST, 2017). The AMAR is indicated as the yellow cylinder.

Figure 5 shows the 2019 AIS ship traffic near the Port of Sept-Îles (MarineTraffic Density Maps, 2021). Increased shipping traffic has caused growing concerns about the impact of underwater ship noise on marine life since marine mammals heavily rely on sound for their survival (Southall et al., 2017; Halliday et al., 2017; NOAA, 2021). Ship noise has been demonstrated to have physiological and behavioural effects in a range of marine animals (Southall, 2007; Southall et al., 2017; Erbe et al., 2019; Southall et al., 2021). Potential effects include disruption of behavior, temporary or permanent hearing thresholds shifts, and auditory masking (Southall, 2005; Southall et al., 2007; Southall et al., 2017; Southall et al., 2019; Erbe et al., 2019).

These impacts have been documented in mysticetes and odontocetes (Erbe et al., 2019). Mysticetes (i.e.baleen whales) are affected by the low-frequency ship noise (Parks et al., 2007; Cranford et al., 2015; Erbe et al., 2019), whereas odontocetes (i.e., toothed whales, dolphins, and porpoises) are more sensitive to the higher frequency noise (Marley et al., 2017; Erbe et al., 2019). For example, humpback whales (Blair et al., 2016; Erbe et al., 2019) and harbor porpoises (Wisniewska et al., 2018; Erbe et al., 2019) alternate their

behavior in relation to ship noise, and fin whales demonstrated some changes in acoustic behavior (Castellote et al., 2012; Erbe et al., 2019).

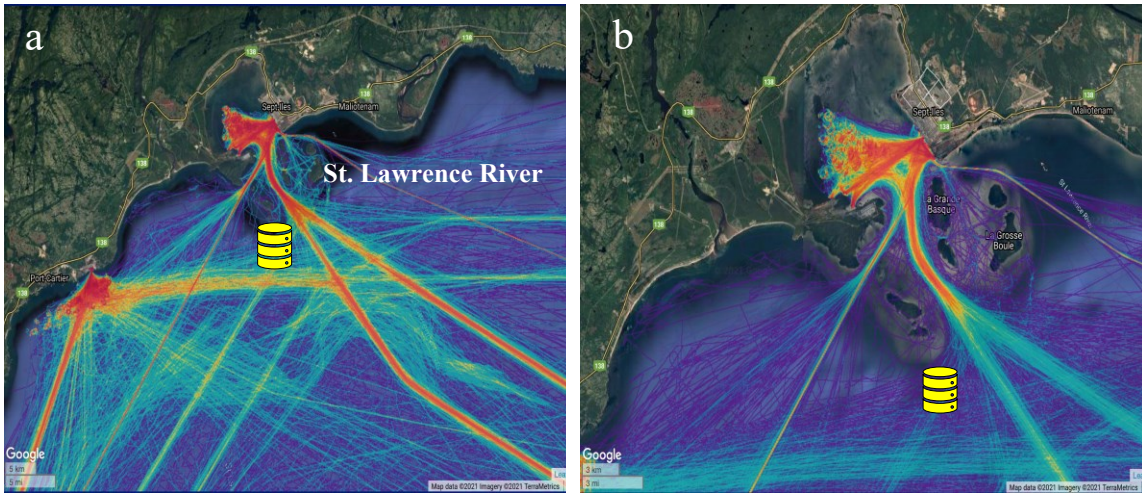

Figure 5: AIS ship traffic in 2019 (MarineTraffic Density Maps, 2021). Plot (a) shows the main shipping lanes around the Port of Sept-Îles. Plot (b) demonstrates shipping going in and out of the Port of Sept-Îles. The AMAR is indicated as the yellow cylinder.

1.2 Motivation

To monitor the presence of vessels outside the port of Sept-Îles, several methods might be employed, such as ground based or satellite visual observations, Automatic Identification System (AIS), active sonar systems, or passive acoustic surveillance (Seto, 2021). Passive acoustic monitoring (PAM) systems have several advantages. They are environmentally friendly because they do not radiate energy into the marine environment (Pollara et al., 2016; Pollara et al., 2017a). They are also stealthy, robust, and relatively cost-effective (Pollara et al., 2016; Pollara et al., 2017a; Mooney et al., 2020). In addition, they allow long-term monitoring of vessel activity without human interaction (Pollara et al., 2017a; Mooney et al., 2020).

Automatic Identification System is a key method for surveillance of ships, however, there is no legal requirement for some vessel types to carry or use an AIS transmitter (Lowes et al., 2022). PAM is an alternative method, relying only on a vessels' radiated noise that can be used for stealthy vessel detection and classification (Fillinger et al., 2011; Pollara et al., 2016; Pollara et al., 2017a) and to assess and document the number of ships in an area. PAM is an important surveillance method because some vessels can be involved in illegal or criminal activities such as smuggling and transporting illegal drugs and contraband, or illegal fishing and unlawful passage of vessels (Pollara et al., 2016; Pollara et al., 2017a). Hence, using PAM for monitoring vessel activity is crucial for detecting illicit activities (Pollara et al., 2016; Pollara et al., 2017a).

1.3 Research Objectives

JASCO (JASCO Applied Sciences, Dartmouth, Nova Scotia, Canada) developed a vessel detector (Martin, 2013) to identify when vessels are present in passive acoustic data. This detector has been used in many commercial and academic publications, but its performance has never been quantified, especially for duty cycled data.

The main goal of this thesis is to assess, analyse, and improve the performance of JASCO's vessel detector using AIS ship positioning data for vessel presence validation. Therefore, the first research objective is to assess how well the JASCO's existing vessel detector agrees with the AIS data.

The JASCO vessel detection algorithm has been developed and updated by many scientists over a period of several years. However, the analysis of the different detection parameters (e.g. signal energy thresholds in different bands over different periods) used to determine a vessel's presence in the algorithm has not been done. Therefore, the second

research objective is to analyse the detector performance for different parameter thresholds and determine optimal performance parameters to optimize the existing JASCO vessel detection criteria.

The third objective is to use Detection of Envelope Modulation on Noise (DEMON) processing as the acoustic detection method and compare its performance to that of the JASCO detector.

The fourth and final objective is to use the JASCO algorithm together with DEMON processing as an enhanced vessel detector and evaluate its combined performance.

Chapter 2: Ship Noise Theory

This section begins with an overview of ship noise. Commercial shipping is a dominant source of low frequency (5 to 500 Hz band) noise in the oceans (Arveson et al., 2000; Hildebrand, 2004; Pricop et al., 2010; McKenna et al., 2012). Commercial shipping vessels produce acoustic underwater radiated noise (URN) where each ship may have a unique radiated noise signature (Hildebrand, 2004; Seto, 2021).

The ship's radiated source levels depend on the vessel class, size, speed, maneuvering, onboard machinery states, cargo hold (if any) contents, hull design, propeller characteristics, hull-propeller interactions, vessel draught, sea state etc. (Pricop et al., 2010; McKenna et al., 2012; Simard et al., 2016; Seto, 2021; MacGillivray et al., 2021).

The ship's URN can be quantified through its power spectral density which shows how the radiated sound power is distributed over the frequency bands (Arveson et al., 2000; Lobo, 2002; Seto, 2021). Figure 6 shows an example of a ship spectrum consisting of continuous (broad band) noise with discrete (narrowband) frequency lines (tones) (Arveson et al., 2000; Lobo, 2002; Pricop et al., 2010; Fillinger et al., 2011; Seto, 2021).

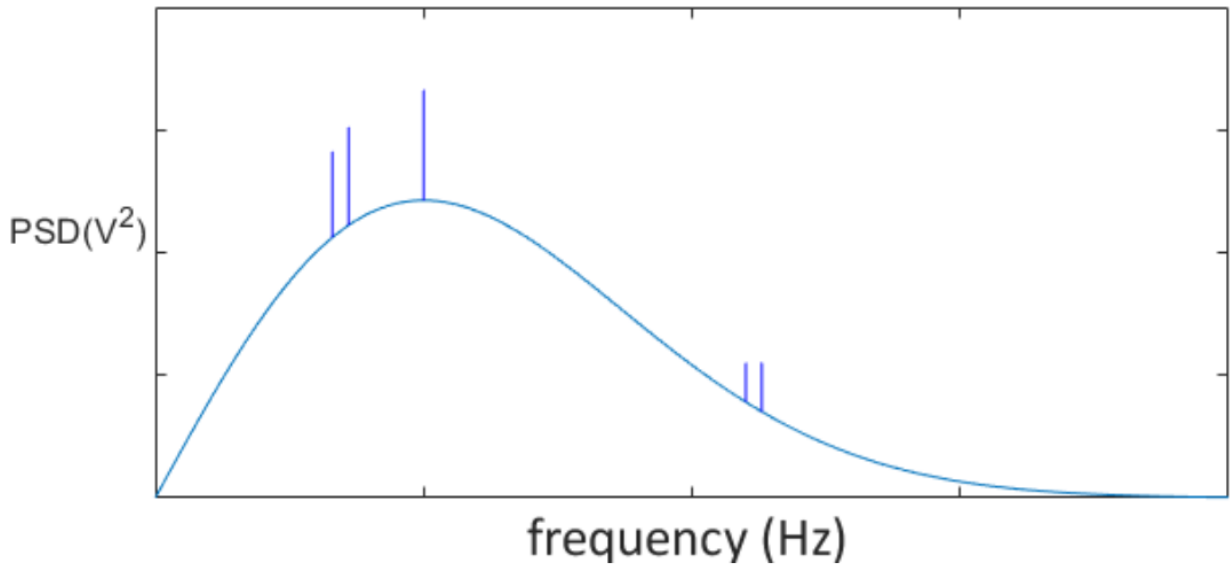

Figure 6: Typical frequency spectrum for a ship's radiated acoustic noise. Note that it consists of a continuous spectrum as well as narrowband lines (p.18, lecture "Acoustics of Motorized In-Water Vehicles", Seto, 2021).

A knowledgeable sonar operator can use power spectral analysis of the URN to identify the on-board equipment that created a particular tonal set in a ship's underwater radiated noise signature by examining the band of the noise (Figure 7), and the harmonic relationships between tones (Lobo, 2002; Pricop et al., 2010; Seto, 2021).

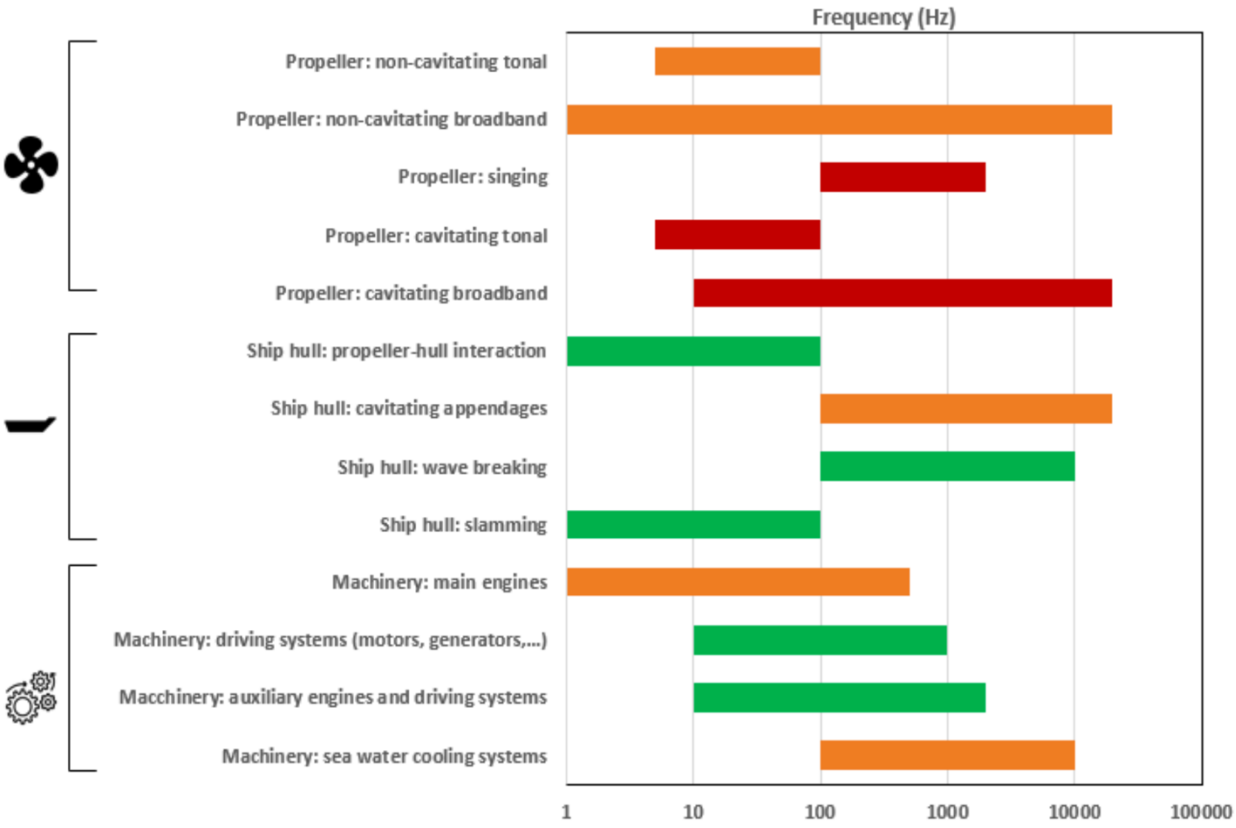

Figure 7: "Overview of continuous underwater noise sources from ships, in terms of frequency range and expected contribution to URN (Bretschneider et al., 2014): red – high contribution; orange – medium contribution; green – low contribution" (p. 16) (Cruz et al., 2021).

Most of the ship URN is in the 10 Hz to 2 kHz range (Lobo, 2002; Pricop et al., 2010). Generally, URN due to machinery dominates at low ship speeds, whereas propeller cavitation noise contributes more at higher ship speeds (Arveson et al., 2000; Lobo, 2002; Audoly, 2015; Seto, 2021). There are four main contributors (noise sources) to the ship URN as shown in Table 1 (Arveson et al., 2000; Lobo, 2002; Oliveira et al., 2010; Abrahamsen, 2012; Audoly, 2015; Seto, 2021; Cruz et al., 2021). These four contributors are discussed next.

Table 1: Noise type and source.

Noise type	Noise source
Machinery noise	• Propulsion drive train: prime mover (e.g. diesel engines and electric motors), transmission (gears) and turbines. • Auxiliary machinery: "generators, pumps, and air conditioning equipment" (p.9393) (Oliveira et al., 2010), etc.
Propeller noise	• Cavitation
Hydrodynamic noise	• "Hydrodynamic flow over the ship's hull and hull appendages" (p.4) (Hildebrand, 2004).
Other noise	• Other

2.1.1 Machinery Noise

Machinery noise is a strong noise source for ships under normal operating conditions (Lobo, 2002; Pricop et al., 2010; Seto, 2021), and is dominant at low speeds (Arveson et al., 2000; Lobo, 2002; Audoly, 2015; Seto, 2021).

Machinery noise comes from main and auxiliary equipment (Audoly, 2015) which generates "tones at frequencies related to their operation" (p.1) (Pollara et al., 2017a). The URN for a ship is mostly the cumulation of all on-board machinery (Lobo, 2002; Audoly, 2015; Seto, 2021).

The machinery noise generated on-board, which manifests as vibrations or pressure waves, can take various paths (Audoly, 2015; Seto, 2021; Cruz et al., 2021). One path is to transmit the vibrations to the ship structure then the hull and finally into the water (Arveson et al., 2000; Lobo, 2002; Pricop et al., 2010; Audoly, 2015; Seto, 2021; Cruz et al., 2021). Once it is in the water the vibrational energy radiates as underwater acoustic pressure waves (Abrahamsen, 2012). These waves may travel only locally trapped in the near field or radiate into the far field (Abrahamsen, 2012; Seto, 2021). It is the far field radiated component that is of interest for PAM. The machinery generated noise can also

insonify the air and other ship structures and take other paths which may or may not transmit into the water (Audoly, 2015; Seto, 2021; Cruz et al., 2021).

Main machinery

The on-board machinery that contributes notably to the URN is usually the main propulsion system's drive train (Oliveira et al., 2010; Arveson et al., 2000; Lobo, 2002; Audoly, 2015; Seto, 2021; Cruz et al., 2021).

The dominant machine in the drive train is the prime mover (Seto, 2021; Cruz et al., 2021). As examples, the prime mover could be an electric propulsion motor or a two- or four-stroke propulsion diesel engine with corresponding number of cylinders that fire in a particular sequence within a cycle (Lobo, 2002; Arveson et al., 2000; Pricop et al., 2010; Audoly, 2015; Seto, 2021). "Vibrations from the prime mover of a vessel will usually occur at frequencies related to the firing rates of individual cylinders and the overall firing rate of the engine" (p.1) (Pollara et al., 2017a). Their firing rate is proportional to the propulsion demand which is driven by the ship speed (Arveson et al., 2000; Audoly, 2015; Seto, 2021). The prime mover's activity is (usually) seen in the URN spectrum (Pricop et al., 2010; Audoly, 2015). The prime mover's firing rate and propeller shaft rates can be detectable as tonal features in the URN's spectrum (Audoly, 2015; Seto, 2021; Cruz et al., 2021).

Generally, electric propulsion motors are quieter than propulsion diesel engines (Audoly, 2015; Lobo, 2002; Seto, 2021). Propulsion systems that are direct drive would not require reduction gearing or transmission systems so they will be quieter (Pricop et al., 2010; Seto, 2021).

However, for propulsion systems that require transmissions, the second loudest sound source is the reduction gear boxes (Lobo, 2002; Pricop et al., 2010; Audoly, 2015; Seto, 2021) between the prime mover and the propeller shaft (Pricop et al., 2010). In some instances, the transmission could produce more noise than the prime mover (Lobo, 2002; Pricop et al., 2010).

The third dominant machinery sound source, in terms of sound intensity, are the turbines. These include propulsion turbines and turbine generator (Audoly, 2015). Turbines are certainly a dominant noise source for ships driven by steam turbines (Audoly, 2015).

The dominant machinery URN frequencies associated with the drive train – the prime mover, transmission, propeller shaft and turbine are, not unexpectedly, functions of ship speed (Arveson et al., 2000; Lobo, 2002; Pricop et al., 2010; Oliveira et al., 2010; Audoly, 2015; Seto, 2021). Generally, higher ship speeds distribute more acoustic power at higher frequencies (Seto, 2021). Machinery activity manifests in the URN spectrum as tonals or lines and with higher ship speeds the lines migrate to higher frequencies in the URN spectrum (Lobo, 2002; Pricop et al., 2010; Oliveira et al., 2010; Seto, 2021). In contrast, this is not the case for on-board auxiliary machinery (Lobo, 2002; Pricop et al., 2010; Oliveira et al., 2010; Seto, 2021).

Auxiliary machinery

The URN signature of auxiliary machinery does not change notably as a function of ship speed (Arveson et al., 2000; Lobo,2002; Pricop et al., 2010; Oliveira et al., 2010; Seto, 2021). That is their frequencies, amplitudes and line thicknesses persist at all ship speeds (Arveson et al., 2000; Seto, 2021). Given this, the URN signature of onboard

auxiliary machinery could identify a ship class or even a particular ship (Lobo, 2002; Damas et al., 2006; Oliveira et al., 2010; Seto, 2021).

The proportion that the auxiliary machinery URN contributes to a ship's acoustic signature, relative to the propulsion drive train, depends on the ship class (Audoly, 2015; Seto, 2021; Cruz et al., 2021).

2.1.2 Propeller Noise

The propeller rotates in water to generate thrust to move a ship forward. In the process it also generates URN (Arveson et al., 2000; Lobo, 2002; Audoly, 2015; Seto, 2021). This URN is divided into cavitating and non-cavitating components and is demarcated by the cavitation inception speed (Audoly, 2015; Seto, 2021; Cruz et al., 2021). Research and naval ships are interested in non-cavitating noise whereas commercial shipping is less concerned with cavitating noise until it affects ship endurance or performance (Seto, 2021).

Figure 8 shows the propeller noise contributions as a function of frequency (Bahtiarian, 2019). Cavitation generates sound over a wide range of frequencies. Large container ships would be at the lower frequency end of the propeller cavitation noise as their shaft/propeller rotation rates are slower. As vessels get smaller, their propellor rotation rates tend to increase moving the propeller cavitation noise up in frequency (Figure 7 and Figure 8). Propeller cavitation generally has a broadband peak around 50 Hz for large single propeller vessels, and 100 – 300 Hz for other vessel types (Figure 8) "followed by a continuum that decreases by 6 db per octave" (annex 1, p.2) (IMO, 2010).

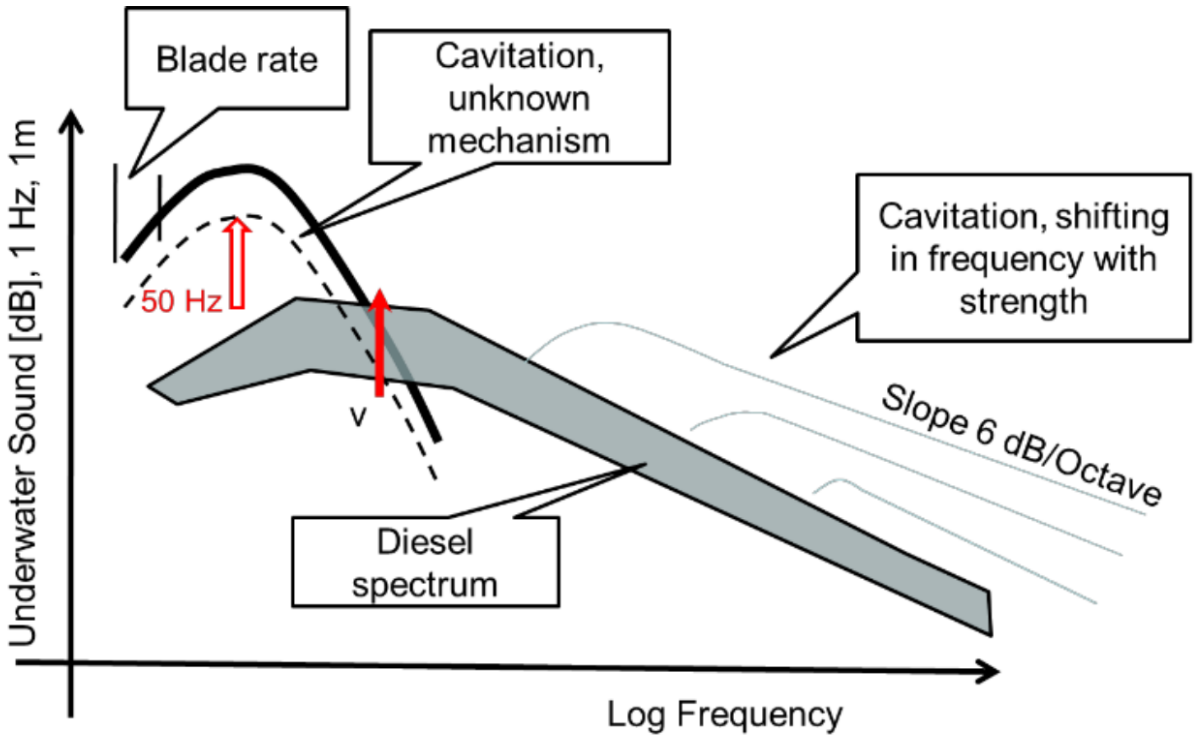

Figure 8: "Illustration of propeller noise contributions" (p.13) (Bahtiarian, 2019).

Non-Cavitating Noise

The URN spectrum of the non-cavitating propeller has low frequency tones (blade frequencies) followed by broadband noise at higher frequencies (Audoly, 2015).

Blade Rate (tonal) URN

As a propeller blade rotates one face is the pressure side and the back face, the suction side (Audoly, 2015; Seto, 2021). This pressure difference across a blade generates a pressure (acoustic) wave (and its harmonics) which radiates away from the blade (Audoly, 2015; Seto, 2021). The blade generates this noise continuously at every point in its rotation. As the propeller blade passes a receiver, at a given location, the receiver will (eventually) detect that pressure signal and do so cyclically every time the blade passes that location at the blade pass frequency (Arveson et al., 2000; Audoly, 2015; Seto, 2021). If

the propeller has multiple blades, then the blade rate is multiple times the single blade (or shaft rate) pass frequency (Seto, 2021). This means the propeller blade carries a pressure gradient with it.

Propellers operate in a circumferentially varying wake pressure field (Audoly, 2015; Seto, 2021). At the very minimum the top part of the propeller disc has a lower pressure than the bottom part (Arveson et al., 2000; Audoly, 2015). The blade's rotation (passage) through the circumferentially varying pressure field in the propeller disc modulates this circumferentially varying pressure field at the blade rate (Abrahamsen, 2012; Audoly, 2015; Seto, 2021).

Broadband URN

Broadband URN has contributions from the time-varying turbulence in the propeller inlet flow conditions, propeller trailing edge noise, and hull fouling among others (André et al., 2010; Audoly, 2015; Seto, 2021). This creates a varying pressure field that propagates over a wide range of higher frequencies (Seto, 2021).

The sound generated at the propeller radiates directly as a source. Additionally, this sound can also excite (insonify) the ship hull so the ship hull becomes a secondary sound source (Seto, 2021). In the radiated URN spectrum, propeller-related activity, due to its periodicity and thus phase correlation, appear as lines or tones (Audoly, 2015; Seto, 2021). This is true of the propeller shaft and blade rates (integral multiple of shaft rate) at lower ship speeds (Seto, 2021).

Cavitation Noise

With increased ship speed, cavitation inception will occur at mid to high frequencies (Audoly, 2015; Seto, 2021). It is characterized by a notable increase in the sound pressure levels (Cruz et al., 2021).

Cavitation occurs when the water pressure drops below the local vapour pressure as in the case of heavily loaded propellers (Seto, 2021; Cruz et al., 2021). In regions around the propeller where this occurs the air will condense out of the water in the form of air bubbles. The bubbles attach to the low pressure portion of the propeller blade (Seto, 2021). When this propeller blade moves into a region of pressure that is above the vapour pressure (potentially the bottom half of the propeller disc due to the nonuniform propellor inflow velocity), the bubble will collapse (Arveson et al., 2000; Audoly, 2015; Seto, 2021). This collapse is cavitation and creates large (acoustic) pressure waves and thus URN (Arveson et al., 2000; Lobo, 2002; Audoly, 2015; Seto, 2021; Cruz et al., 2021). This can occur every time the blade passes through these propeller disc regions of low and high pressure and thus cavitation can occur at the blade rate and its harmonics (Arveson et al., 2000; Audoly, 2015; Seto, 2021).

Due to the impulsive collapse the resulting URN is white noise that can go to high non-acoustic frequencies (~ MHz) (André et al., 2010; Audoly, 2015; Seto, 2021).

There are several types of propeller cavitation (Audoly, 2015; Cruz et al., 2021). A treatment of them is beyond the scope of this section. Suffice it to say that there is cavitation that can occur at the blade rate which amplifies the non-cavitating blade rate lines (increased amplitude) (Audoly, 2015; Seto, 2021). There are other types of cavitation that are less dependent and contribute to the broadband signal.

At higher speeds, propeller singing may occur where a blade's trailing edge vortex shedding frequency becomes synchronous with the blade tip's structural resonant frequency (Lobo, 2002; Abrahamsen, 2012; Audoly, 2015; Seto, 2021). This can appear in the URN spectrum as higher amplitude tonals. It can also have a low frequency component as well (Seto, 2021).

2.1.3 Hydrodynamic Flow Noise

"Hydrodynamic flow over the ship's hull and hull appendages" (p.4) (Hildebrand, 2004) generates major noise particularly with increased ship speed (Lobo, 2002; Hildebrand, 2004; Abrahamsen, 2012). "It is an important broadband noise-generating mechanism" (p.4) (Hildebrand, 2004). Also, the longer ship, the more water it is moving, generating more flow noise, especially in case of maneuvering (Seto, 2021).

2.1.4 Other Noise

Other noise generated within the ship could include crew activity, slamming hatches and doors, navigation aids such as sonar, and venting underwater exhaust (Lobo, 2002; Seto, 2021).

Chapter 3: Methods

3.1 Data Collection

3.1.1 Deployment Location

The AMAR was deployed for two six-month periods, on a C-Lander mooring (JASCO Applied Sciences, Dartmouth, Nova Scotia, Canada) which can be seen in Figure 9, near the entrance to the Port of Sept-Îles in St. Lawrence River, at the location shown in Figure 10. The deployment coordinates for the two deployments are given in Table 2.

Table 2: C-Lander Deployment Coordinates.

	Latitude	Longitude	Depth (m)	Deployment	Retrieval	Durations (days)
Deployment 1	50° 2' 14.1" N	66° 22' 15.96" W	~75	04-Nov-20	04-May-21	181
Deployment 2	50° 2' 9.816" N	66° 22' 7.536" W	~75	04-May-21	29-Oct-21	181

Figure 9: JASCO AMAR integrated on C-Lander mooring.

Figure 10: JASCO AMAR on a C-Lander mooring in St. Lawrence River (Delarue, 2021).

The bathymetry around the Port of Sept-Îles can be seen in Figure 11. The C-Lander was deployed to ~75 metres depth, and its location is indicated as the red dot. As can be seen, the water gets shallower towards the shoreline (Figure 11).

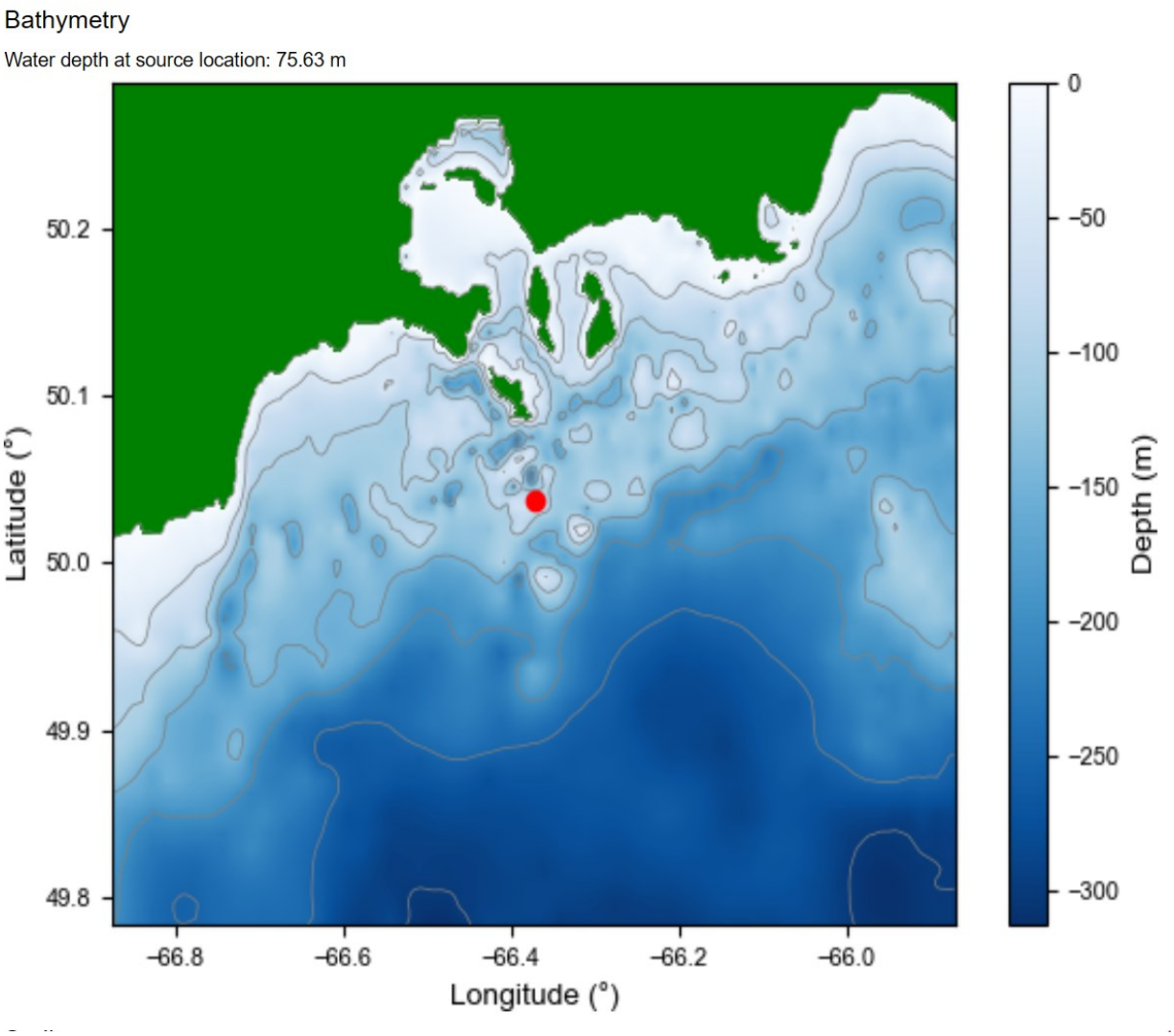

Figure 11: The bathymetry around the Port of Sept-Îles. The C-Lander location is indicated as the red dot.

3.1.2 AMAR

JASCO's AMAR was integrated on a C-Lander mooring (JASCO Applied Sciences, Dartmouth, Nova Scotia, Canada) (Figure 9). The AMAR and C-Lander specifications can be found in Appendix B: Equipment Specifications. It was fitted with 10 TBs of memory on removable SD cards and had four omnidirectional GeoSpectrum M36-V35-100 hydrophones configured as a tetrahedral array (Delarue, 2021).

The system was configured to record on a duty cycle consisting of:

- 340 s of recording at 32 kHz (24 bit) on 4 channels
- 60 s of recording at 256 kHz (24 bit) on 1 channel
- 500 s of sleep

This configuration allowed for the planned six-month deployments. The AMAR recorder was calibrated prior to deployment and again after retrieval to assess if any sensitivity loss occurred during the 6 month data collection period. No significant losses were observed (Delarue, 2021).

3.1.3 AIS Data

The Automatic Identification System (AIS) is an automated tracking system for transmitting and receiving a vessel's position, course, speed, identity, and other relevant information (Maritime Information Portal, 2020). Dynamic information is transmitted as often as every 2 to 10 seconds, and every 6 minutes while anchored. Static or voyage related information is transmitted every 6 minutes (MarineTraffic, from https://help.marinetraffic.com/hc/en-us/articles/205426887-What-kind-of-information-is-AIS-transmitted-, last viewed July 5, 2022). The AIS data were obtained from MERIDIAN (Marine Environmental Research Infrastructure for Data Integration and Application Network), Dalhousie University. As mentioned above, there is no legal requirement for some smaller vessel types to carry or use an AIS transmitter (Lowes et al., 2022). The International Maritime Organization (IMO) regulation (December 31, 2004) requires AIS to be fitted (IMO, from https://www.imo.org/en/OurWork/Safety/Pages/AIS.aspx, last viewed July 5, 2022):

- “aboard all ships of 300 gross tonnage and upwards engaged on international voyages

- cargo ships of 500 gross tonnage and upwards not engaged on international voyages and
- all passenger ships irrespective of size" (para. 2).

There are different AIS categories of ships including: Cargo, Tugs, Fishing, Towing, Search and rescue vessels, Tankers, Passenger Ships, and other types, including research vessels.

Interpolated AIS data were used to ground truth the JASCO and DEMON estimated closest point of approach.

3.2 Data Analysis

The next five sub-sections introduce the data analysis. Section 3.2.1 shows the determination of vessel closest point of approach using AIS data. Section 3.2.2 present a review of the JASCO acoustic analysis process, and section 3.2.3 demonstrates the JASCO acoustic CPA determination. Section 3.2.4 shows the DEMON Processing, and Section 3.2.5 is the DEMON CPA determination.

3.2.1 Determination of Vessel Closest Point of Approach Using AIS Data

AIS data were obtained for each 6-month deployment period. The goal of this section was to determine the closest points of approach for a subset of the AIS vessel data determined by selections of maximum range and minimum speed.

All ships with a reported speed over ground (SOG) of less than one knot (Figure 12) were removed, to exclude those alongside, moored or at anchor.

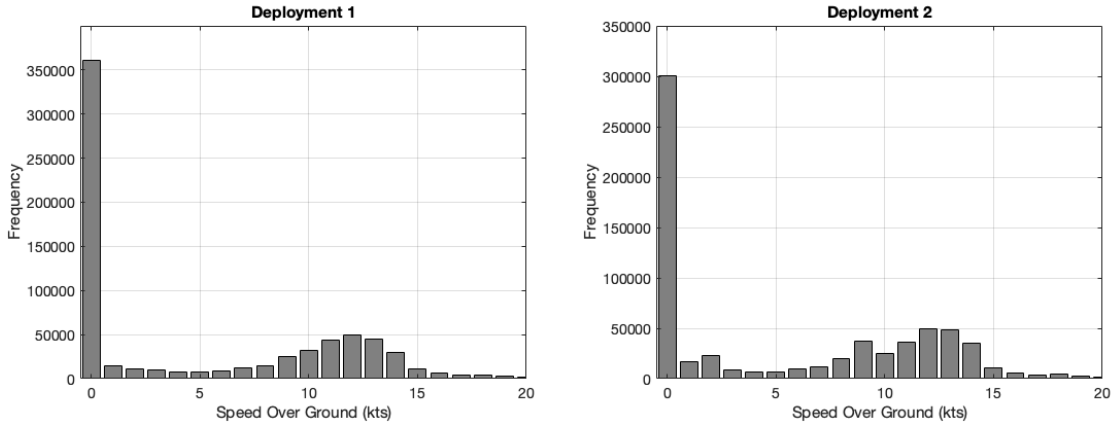

Figure 12: Histogram of speed over ground values for the two 6-month deployments.

The next step was to calculate the distance of all AIS contacts to the AMAR. Figure 13 shows the distribution of the vessel ranges to the AMAR for each of the two deployments. The peaks near 17 km (deployment 1) and 18 km (deployment 2) represent vessels in the Port of Sept-Îles while the peaks at around 29 km (deployment 1) and 30 km (deployment 2) represent vessels in the Port of Cartier (Figure 13).

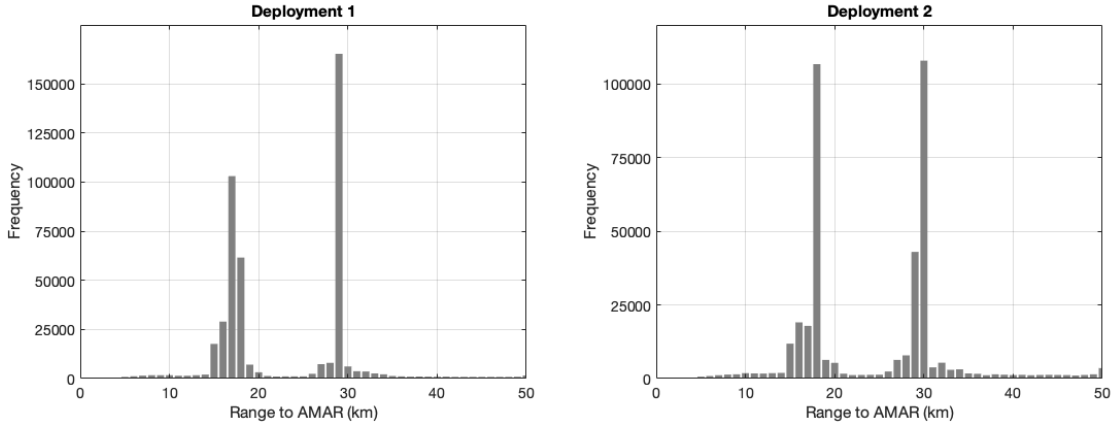

Figure 13: Histogram of vessel ranges to 50 km for the two 6-month deployments.

Next data for ranges greater than 1.5 times the maximum range of interest (10 km) was removed. The range data were then interpolated to a 10 second time basis to determine the CPA of all vessels each time they transited past the AMAR. For this step the Maritime Mobile Service Identity (MMSI), a number which uniquely identifies a vessel or boat (Government of Canada, 2021; Lowes et al., 2022) was selected. For each MMSI, unique ship transit data were determined by looking for time differences between two consecutive AIS times of more than 2 hours. The result was time segments for each MMSI in the AIS data set.

Each MMSI segment was then checked for a minimum of 3 data points. If there was less than 3 points, insufficient data to determine a CPA was indicated. MMSI segments with more than 3 data points were interpolated using the MATLAB retime function with a time step of 10 seconds. The minimum of the interpolated range for each MMSI segment was then identified as the CPA for that vessel and time segment and saved along with its corresponding time. The next step was to check whether the minimum range corresponded to the first or last point of the MMSI segment. If it did, it was indicated that no local minimum was found, and a CPA could not be identified, but that the data point identified was the closest AIS time for that transit in the data set. All other segments resulted in a u-shape pattern showing a local minimum and were classified as a true AIS CPA.

Next the CPA dataset was further down selected by specifying minimum speed over ground of 8 knots and a maximum range of 10 km. A distribution of the remaining SOG of interest are shown in Figure 14.

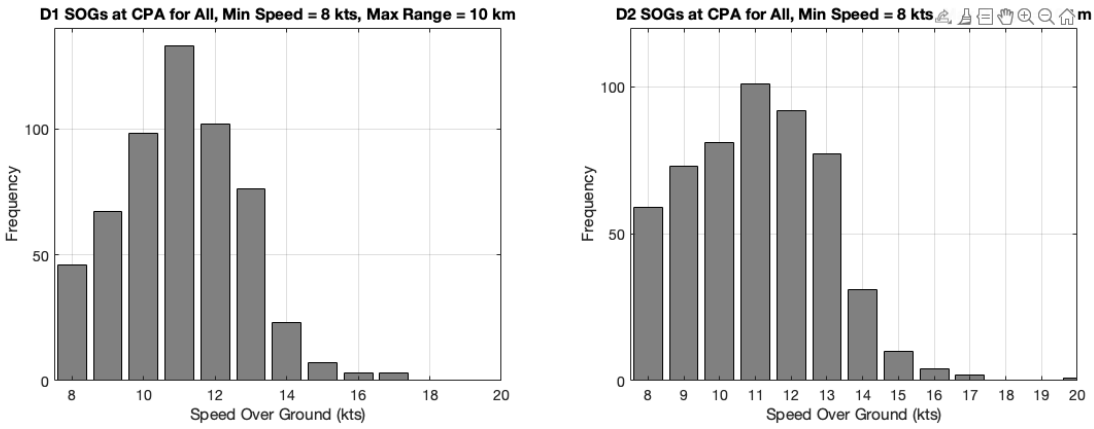

Deployment 1 Deployment 2

Figure 14: Histogram of speed over ground values at CPA for the two 6-month deployments.

The minimum speed was based on the expected propeller cavitation inception speed for cargo vessels which was identified to occur around 10 knots (Arveson et al., 2000). However, "for an older ship, with some fouling or damage on the propeller, a lower inception speed could be expected" (p.122) (Arveson et al., 2000). Also, propeller loading could be a factor (Abrahamsen, 2012; Cruz et al., 2021; Seto, 2021). If propeller loading is beyond the design range, the propeller will start cavitating regardless of speed. For example, propeller cavitation could occur when a vessel is towing or overloaded (Seto, 2021). To account for these factors a minimum speed of 8 knots was selected.

A distribution of the remaining CPA ranges of interest are shown in Figure 15.

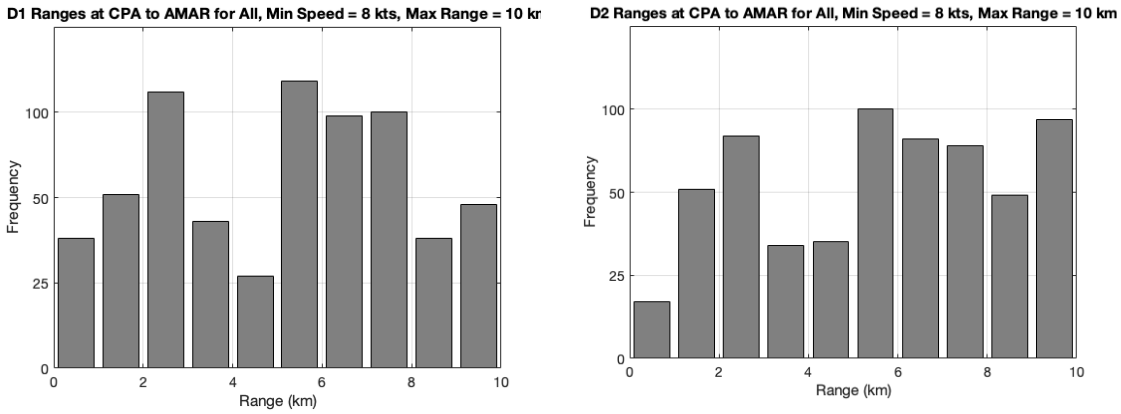

Deployment 1 Deployment 2

Figure 15: Histogram of vessel ranges at CPA for the two 6-month deployments.

The 10 km radius was chosen based on discussions regarding the AMAR's past performance in similar environments along with expectations of ranges at which JASCO's vessel detector was expected to perform well.

3.2.2 JASCO Automated Acoustic Data Analysis Using PAMlab

PAMlab, JASCO's acoustic processing, analysis, and annotation tool, was used to automatically analyze the recorded acoustic datasets. It performed automated analysis of total ocean noise, vessel and boat noise, and marine mammal vocalizations (Delarue, 2021). The automated analysis generates the following relevant outputs (JASCO Applied Sciences, JASCO internal document "Detection_levels", last viewed May 18, 2022):

- **10 Hz and above Sound Pressure Level (SPL) / unweighted root-mean-square (rms) SPL**: The 1-minute average sound pressure level computed from 1-second Fast Fourier Transforms (FFTs) of the data after applying the frequency dependent calibration coefficients, and finding the SPL in the 10 Hz to Nyquist frequency band. Units: dB re 1 μPa^2.

- **Shipping tonals**: The number of constant frequency tones detected in 1-minute of data using an FFT with 0.125 Hz resolution (8 seconds of input data, 6 second overlap). The 0.125 Hz resolution is recommended for separating and detecting individual tones (Martin, 2013). The tonals are detected as lines that were at least 32 seconds long, in the band of 10 – 1000 Hz.
- **40 - 315 Hz decidecade bands**: "Decidecade resolution, in which a factor of 10 in frequency (e.g. from 1–10 kHz) has 10 frequency bins, is suitable for many applications, such as quantifying weighted sound levels of human activities, or comparing sound levels to the hearing capabilities of marine and terrestrial life" (p.2) (Martin et al., 2021). It is the arithmetic sum of the power in the 40-315 Hz decidecade bands (Table 3), which are the bands measured to determine the presence of vessels. Units: dB re 1 μPa^2.

Table 3: Decidecade low, centre, high and nominal centre frequencies from 40 to 315 Hz (Martin, 2019).

Lower bound (Hz)	Centre frequency (Hz)	Upper bound (Hz)	Nominal centre frequency
35.48	39.81	44.67	40 Hz
44.67	50.12	56.23	50 Hz
56.23	63.10	70.79	63 Hz
70.79	79.43	89.13	80 Hz
89.13	100	112.2	100 Hz
112.2	125.9	141.3	125 Hz
141.3	158.5	177.8	160 Hz
177.8	199.5	223.9	200 Hz
223.9	251.2	281.8	250 Hz
281.8	316.2	354.8	315 Hz

"The centre frequency of the *i*th decidecade band, $f_c(i)$, is defined as

$$f_c(i) = 10^{i/10}$$

and the low (f_{lo}) and high (f_{hi}) frequency limits of the *i*th decidecade band are defined as:

$$f_{lo} = f_c(i) * 10^{-1/20}$$

$$f_{hi} = f_c(i) * 10^{1/20}$$

where (i) is from 17 to 26" (p. 27-28) (Martin, 2019).

> "In general mammals perceive exponential increases in frequency rather than linear increases (Scharf, 1970; Saunders et al. 1979). Therefore, splitting the spectrum into 1 Hz bands is not representative of how mammals perceive sound; rather analyzing a sound spectrum with bands that increase exponentially in size gives data that are more meaningful. In underwater acoustics, a spectrum is commonly split into bands that are $1/10^{th}$ of a decade where each decade represents a 10-fold increase in frequency" (p. 27) (Martin, 2019).

- **Lowest of the left and right sided 360 minute mean for 40 Hz - 315 Hz:** The mean SPL in the 40-315 Hz decidecade band is computed for six hours before and after the time under consideration. The lower of the two values is used as the 'average' background. The current SPL in the band must be at least 3 dB higher than this value for a possible vessel detection to occur. Units: dB re 1 µPa².
- **11-minutes-moving-average-number-of-tonals**: Averages over 11 minutes (5 minutes before, 1 current minute, 5 minutes after) to help with times when the tones are either drowned out by the cavitation or there is enough frequency change due to Doppler effect that the frequency does not stay stable for the detector's duration of 32 seconds. This value must be greater than 3 for a vessel detection to occur.

- **Shipping detection flag**: 0 indicates no detection, 1 detection, 4 ‘shoulder’ period = 10 minutes before and after the ‘1’ values. This system of 1 and 4 attempts to distinguish between vessels that are nearer and further from the AMAR, i.e. for large vessels the sequence is typically a series of flags of 4 (approach), then 1 (over/nearest), then 4 (departure).
- **Vessel CPA Flag**: The highest 1 min SPL in the vessel detection band, which is then identified as the closest point of approach time.
- **Ambient smoothed flag**: This flag is set for any time which does not have any shipping, seismic, or biophony detections within a window of time either before or after the current time slice.

3.2.3 JASCO Acoustic CPA Determination

The JASCO algorithm detects vessels in two steps (Martin, 2013). First it attempts “to detect constant, narrowband tones, produced by a vessel’s propulsion system and other rotating machinery (Arveson et al., 2000)” (p.7) (Delarue, 2021). Tonal peaks are obtained from the background using a split-window normalizer (Struzinski, 1984; Martin, 2013). According to Baldacci et al. (2006) “the split-window normalizer places guard bands around the point of interest to avoid a spill of the target’s energy into the background” (p.1), and hence “to separate the signal from the noise” (p.1).

Next it “assesses the SPL for each minute of data in the 40–315 Hz decidecade shipping frequency band, which commonly contains most of the sound energy produced by mid-sized to large vessels” (p.7) (Delarue, 2021).

The JASCO algorithm was originally developed for the Arctic in the summer. The following thresholds values were chosen empirically. A vessel is detected (Martin, 2013; Delarue, 2021) when :

- The SPL in the 40–315 Hz decidecade shipping band is at least 3 dB (double the energy of the mean) above the lowest of the left and right sided 360-minute mean for the 40-315 Hz decidecade shipping band for at least 5 minutes, and
- At least three tonals (moving average number of tonals over 11 minutes) (0.125 Hz bandwidth) are present for at least 1 minute per 5 minute window, and
- The SPL in the 40–315 Hz decidecade shipping band is within 12 dB of the system unweighted SPL. 12 dB was chosen to exclude seismic and biological signals, such as walrus.

When all these conditions are true, a ship event is detected. The highest 1 min SPL in the vessel detection band is then identified as the closest point of approach time (Delarue, 2021) and designated as the JASCO detector CPA.

Figure 16 demonstrates the JASCO vessel detection example, where the orange line is 40-315 Hz SPL, the yellow line is 12 hour 40-315 Hz SPL, the dark red line is the unweighted SPL, the grey lines are the number of tonals, the black line is the 11-minute-moving-average-number-of-tonals, and the green lines are the JASCO vessel detections.

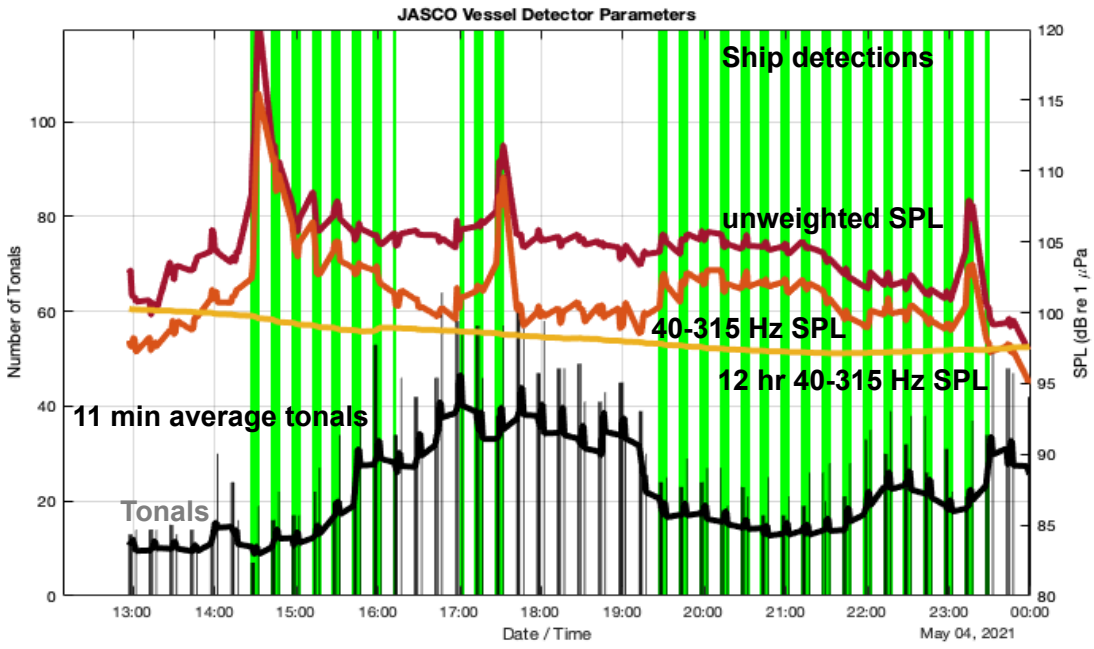

Figure 16: JASCO vessel detection example. The orange line is 40-315 Hz SPL, the yellow line is 12 hour 40-315 Hz SPL, the dark red line is the unweighted SPL, the grey lines are the number of tonals, the black line is the 11-minute-moving-average-number-of-tonals, and the green lines are the JASCO vessel detection.

The next step involved comparing the time stamps of each AIS CPA with the JASCO CPAs. A true positive match is determined when the timestamp of the AIS CPA and the nearest JASCO CPA are within 21 minutes of each other. 21 minutes was chosen as it represents two AMAR record sessions (2 x 5 minutes, 40 seconds) and a sleep session (9 minutes, 20 seconds).

However, in some cases, the results also demonstrate that the AIS CPA and JASCO CPAs do not align in time within the given window of 21 minutes. In this case the time of the closest one minute of JASCO data corresponding to the AIS CPA time was saved to help with further analysis.

3.2.4 DEMON Processing

Propeller cavitation generally has a peak below 300 Hz, however, energy is generated over a broad range of frequencies. The sound energy at higher frequencies (for example 500 – 1500 Hz) is often amplitude modulated by the vessel's blade and shaft rates. DEMON processing is designed to detect the amplitude modulation in the higher frequencies.

This thesis considers frequencies in 8000 to 15000 Hz band for DEMON processing of propeller cavitation. DEMON processing "extracts the frequencies which modulate this high frequency cavitation noise" (p.1) (Pollara et al., 2016). The (lower) extracted frequencies are relate the shaft and blade rates (and their harmonics) (Pollara et al., 2016; Pollara et al., 2017a). Cavitation noise is amplitude-modulated by the shaft and blade rates (and their harmonics) (Arveson et al., 2000; Audoly, 2015; Pollara et al., 2016; Pollara et al., 2017a; Seto, 2021; Lowes et al., 2022). The amplitude modulation is the envelope which is caused by the shaft or blade rates (Seto, 2021). Therefore, evaluation of the envelope can be used for ship detection and classification. This estimation method for the envelope modulation is known as DEMON (Fillinger et al., 2009; Fillinger et al., 2011; Chung et al., 2011; Pollara et al., 2016; Pollara et al., 2017a; Pollara et al., 2017b; Reis et al., 2019; Lowes et al., 2022).

Analysis of the DEMON-processed spectrum makes it possible to identify tonals (e.g. shaft and blade rate) (Chung et al., 2011; Pollara et al., 2016; Pollara et al., 2017a; Pollara et al., 2017b; Lowes et al., 2022). The steps in DEMON Processing (Chung et al., 2011) are shown in Figure 17.

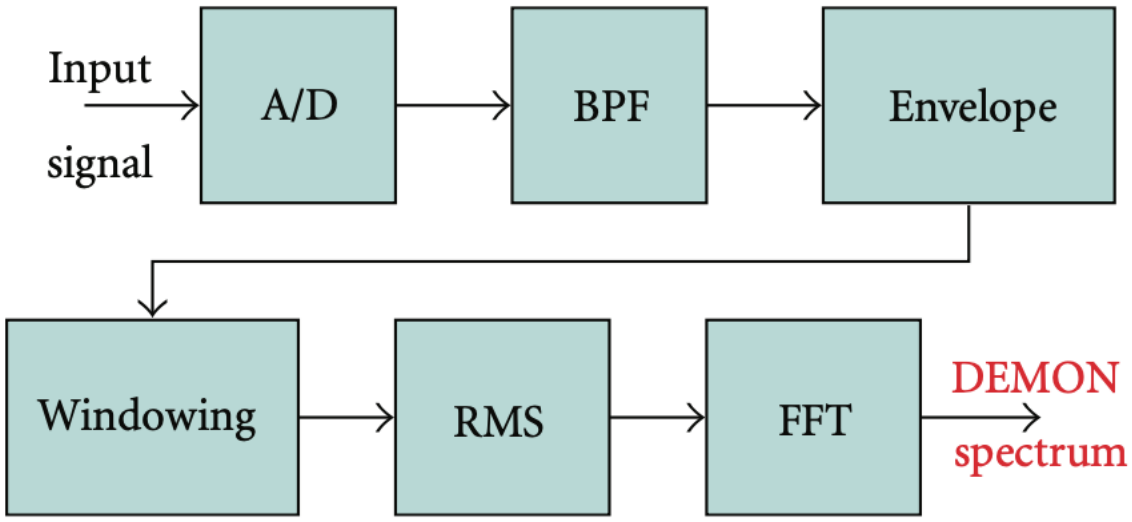

Figure 17: Block diagram of the DEMON Processing (p.3) (Chung et al., 2011). A/D is Analog to Digital Converter, BPF is Bandpass Filter, RMS is Root Mean Square, and FFT is Fast Fourier Transform.

3.2.4.1 Analog to Digital Conversion

First, the acoustic wave is transduced into an electrical signal which is input into the analog-to-digital converter (A/D) which digitizes it into a discrete time and amplitude signal (Tilden et al., 2011; Chung et al., 2011). This step occurs on the AMAR recorder.

3.2.4.2 Bandpass filter (BPF)

Then, the digitized signal is bandpass filtered (BPF) (Chung et al., 2011), so that only a specific range (band) of frequencies is passed, and the frequencies both above and below this range are attenuated (SOS, https://www.soundonsound.com/glossary/band-pass-filter-bpf, last viewed May 8, 2022). This step aims to isolate the typical band of interest for propeller cavitation noise. The specific parameters will be defined in the 3.2.5 DEMON CPA Determination section.

3.2.4.3 Envelope Extraction

Next is to extract the real envelope of the digitized and now filtered signal using a Hilbert transform (Chung et al., 2011; Yang, 2017). The Hilbert transform is used to obtain the imaginary part to generate a complex representation of the real valued signal (Viswanathan, 2017). It mathematically convolves the digitized and filtered signal with the signal $1/\pi t$, which is the impulse response of "a linear time-invariant filter (called a Hilbert transformer)" (p.1) (Kschischang, 2015). The output is a filtered impulse response of the signal which is complex. The real component is the envelope (Kschischang, 2015; Yang, 2017).

3.2.4.4 Windowing and Spectral Leakage

Spectral leakage is caused by the finite length of the time record (Harris, 1978; Hewlett-Packard, 1985; Merchant et al., 2015). It occurs when a time record is not periodic and contains a nonintegral number of cycles (Harris, 1978; Hewlett-Packard, 1985; Cerna et al., 2000; Seto, 2021). For example, "the sine wave does not begin and end at the same phase in its cycle in the time record – not phased-synchronized" (p.7, lecture "Fast Fourier Transform – Windowing", Seto, 2021).

"Spectral leakage distorts the measurement in such a way that energy from a given frequency component is spread over adjacent frequency lines or bins" (p.10) (Cerna et al., 2000). Also, it can mask small components of the total signal (Hewlett-Packard, 1985; Cerna et al., 2000; Merchant et al., 2015). Spectral leakage can be reduced through windowing (Harris, 1978; Hewlett-Packard, 1985; Cerna et al., 2000; Merchant et al., 2015; Seto, 2021). Window functions are designed to control spectral leakage (Harris, 1978; Merchant et al., 2015). The time record is multiplied by a window function (in the

time domain) that is tapered to zero at the ends of the time record and thus largest in the middle, so the Fast Fourier Transform is concentrated on the middle of the time record, and the edges of the time record are diminished (Hewlett-Packard, 1985; Cerna et al., 2000; Merchant et al., 2015; Seto, 2021).

3.2.4.5 Root-Mean-Square (RMS)

Next, "the average value of the real envelope is computed using the Root Mean Square" (p.6) (Chung et al., 2011). "RMS stands for root-mean-square and is calculated by squaring all the values, adding the squares, then dividing by the number of measurements (mean) and taking the square root of the result" (p.43) (Hewlett-Packard,1985). The key parameter for an RMS calculation is "a duration over which to average the pressure of the signal" (para.8, DOSITS, from https://dosits.org/science/advanced-topics/introduction-to-signal-levels/, last viewed May 12, 2022). The RMS amplitude or pressure is related to the energy carried by the pressure wave which is related to the power or intensity of the signal (DOSITS, from https://dosits.org/science/advanced-topics/introduction-to-signal-levels/, last viewed May 12, 2022). Therefore, RMS provides accurate estimates of the signal plus noise ratio (Hewlett-Packard,1985).

3.2.4.6 Fast Fourier Transform (FFT)

The DEMON spectrum is calculated using the FFT algorithm which transforms digitized data from the time domain to the frequency domain (Hewlett-Packard, 1985; Chung et al., 2011). The FFT acts like "a set of parallel filters" (p.4) (Cerna et al., 2000), and its bandwidth can consist of multiple frequency bins (Hewlett-Packard, 1985; Cerna et al., 2000).

3.2.4.7 Peak detection

After the FFT is computed, peak detection is performed on the DEMON spectrum. Propeller shaft and blade rates can be estimated from the peaks in the spectrum (Pollara et al., 2016; Pollara et al., 2017a; Pollara et al., 2017b; Lowes et al., 2022). Usually, the shaft rate will be the lowest frequency tone (Pollara et al., 2017a; Seto, 2021). Also, as mentioned above, the existence of spectral peaks, the time evolution of them, and their relative magnitudes can be used for ship detection and classification (Pollara et al., 2016; Pollara et al., 2017a; Lowes et al., 2022; Seto, 2021). The ratio between blade rate and shaft rate is an estimate of the number of propeller blades (Equation 1) (Pollara et al., 2017a; Lowes et al., 2022).

$$\text{No. Blades} = \frac{Blade\ Rate\ (Hz)}{Shaft\ Rate\ (Hz)}$$

Equation 1: Number of propeller blades.

3.2.5 DEMON CPA Determination

A subset of AMAR acoustic wav files corresponding to days when AIS showed vessel CPAs within the maximum range and minimum speed criteria was identified. Each unique wav file containing 5 minutes 40 seconds of recording time was then divided into 1-minute data segments using a Hamming window with 75% overlap resulting in 20 data segments for each unique acoustic wav file. JASCO's DEMON processing algorithm (Port of Vancouver, 2020) was then run on each 1-minute data segment to obtain their DEMON spectrum in the 1–90 Hz band. This was done using the parameters shown in Table 4. The frequencies in 8000 to 15000 Hz band aims to isolate the typical band of interest for propeller cavitation noise.

Table 4: DEMON Processing parameters.

Parameter	Threshold (Hz)
Maximum DEMON frequency	90.0
Minimum DEMON frequency	1
Minimum distance (in Hz) between peaks in the DEMON spectrum	0.5
Filter bank lowest frequency	8000.0
Filter bank highest frequency	15000.0
Bandwidth	1000.0

Then, for each segment the largest peak magnitude, its corresponding time and frequency, along with an estimated Shaft Rate (SR) and validity flag were determined and saved. Next, only peaks with valid shaft rate were considered. The DEMON data were divided into unique segments by looking for time differences between consecutive DEMON data points of more than 15 minutes. These segments were assumed to be different ship events. Then, on the DEMON spectrum data corresponding to each day the local peak detection was performed, and the largest peak for each segment was saved. These peaks were labelled as the DEMON CPAs.

As was done with the JASCO CPAs, the next step was to compare a time stamp of AIS CPA with a time stamp of all DEMON CPAs. If the time difference between AIS CPA and one of the peaks was within the tolerance of 21 minutes, then it was categorized as a true positive DEMON CPA.

DEMON Processing was also run on low rms SPL (< 90 dB) data, and no valid peaks were observed.

Chapter 4: Research Results

In this section, examples of vessel detection by the JASCO and DEMON detectors are discussed by comparing the CPAs determined by them to those of the ground truth AIS CPA data set. Both detectors demonstrated better performance on single vessel cases, whereas more complicated cases such as multiple vessels, two vessels operating at close range and time, and maneuvering vessels posed some challenges for the JASCO and DEMON detectors.

4.1 Overview of Figures Use to Present Results

Figure 18 and Figure 19, which are representative of the plots discussed in this section are described here for clarity. Figure 18 shows all the vessels for a given day, whereas Figure 19 only displays the vessels of interest.

Figure 18 is a geospatial plot of the AIS data for a given day. It shows the AMAR position as a yellow star, ship AIS data points as circles of distinct colors, where each color corresponds to a different ship (MMSI number), and AIS CPAs as red diamonds.

Figure 19 shows time aligned data from AIS, JASCO and DEMON detectors. The x-axis is the same date and time range for all four plots. AIS data are displayed in the top plot. The y-axis is vessel's range from the AMAR in kilometers. In this plot a single vessel's AIS track shows a vessel approaching the AMAR recorder with a CPA of approximately 5.8 km at 22:48. The green (or other color) dots are the actual received AIS data transmission points while the red diamond is the interpolated AIS CPA.

Next, the acoustic plot (second from top) presents the status of the JASCO vessel detector which is shown as the green diamonds indicating times when the JASCO algorithm has detected vessels. The six symbols correspond to 5 minutes 40 seconds of

AMAR recording, whereas the gaps indicate times when the AMAR is sleeping. The red diamond is the JASCO CPA.

The next plot (second from bottom) shows the 1-minute DEMON data with 75% overlap. It shows the peak frequency (y-axis) and peak magnitude (colorbar) of the demodulated output in Hz and dB respectively as a function of time (x-axis). The red diamond is the DEMON CPA.

The bottom plot shows the speed over ground (SOG) of the vessel in knots.

4.2 Single Vessel Transit Examples

4.2.1 June 6th, 2021: Single Vessel With Speed Increase

The AIS data from June 6th, 2021 are shown in Figure 18, with the corresponding detection data shown in Figure 19. The single vessel example in Figure 19 demonstrates the change in peak frequency due to a speed increase of the vessel.

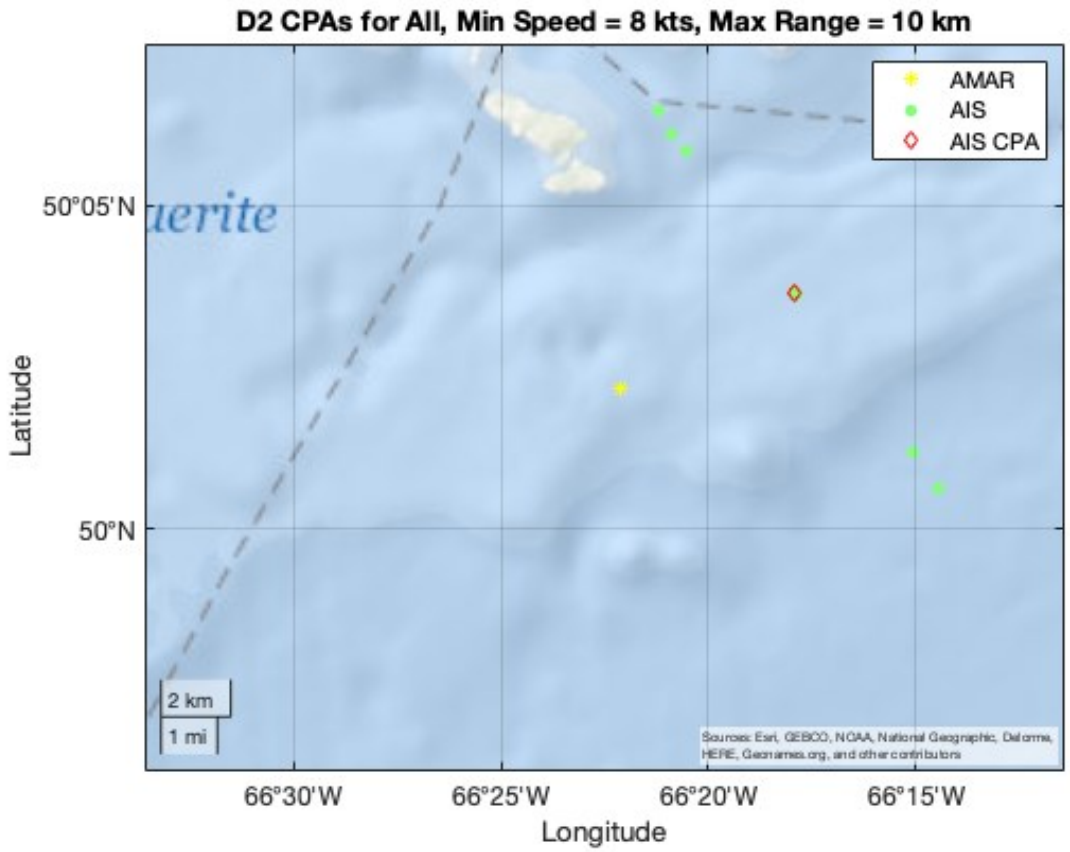

Figure 18: Single vessel on June 6th (deployment 2). The yellow star is the AMAR position, the green dots are the actual AIS data points, and the red diamond is the AIS CPA.

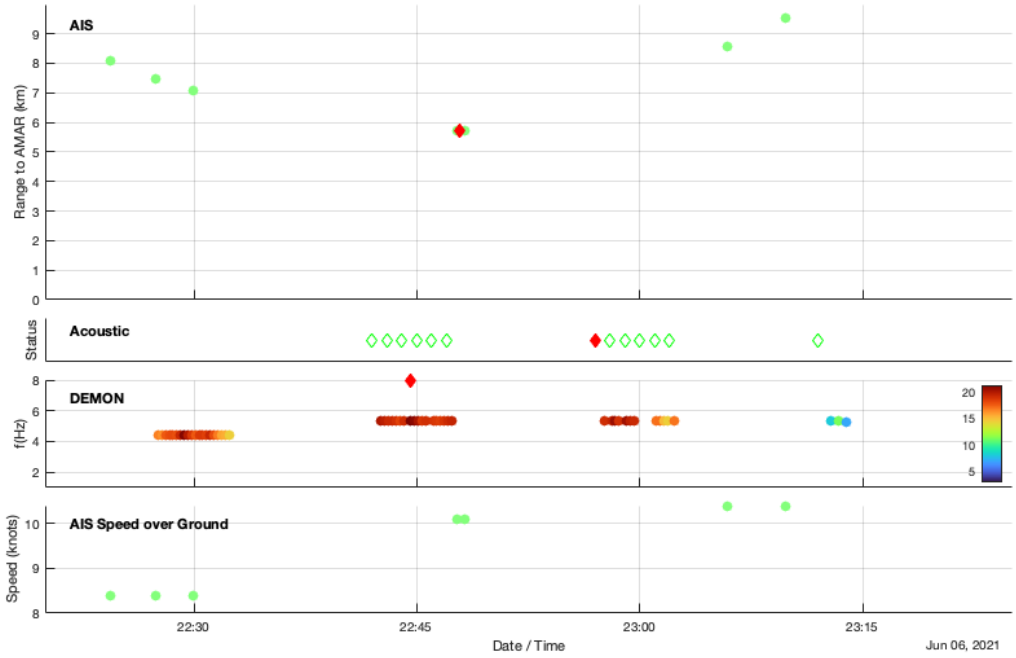

Figure 19: The AIS, JASCO, and DEMON data on June 6th (deployment 2).

AIS (top): Shows the actual received AIS transmission points as circles of different colors, where each color corresponds to a different ship (MMSI number), while the red diamond is the interpolated AIS CPA.

Acoustic (second from top): The green diamonds indicate when the JASCO algorithm detects a vessel, and the red diamond is JASCO CPA.

DEMON plot (second from bottom): Shows the peak frequency (y-axis) and peak magnitude (colorbar) of the 1-minute DEMON data with 75% overlap, and the red diamond is DEMON CPA.

The AIS speed over ground (bottom): Shows the speed over ground in knots.

The AIS data display a straight-line AIS track which corresponds to one ship travelling past the AMAR. The vessel shown in green has an AIS CPA at 22:47, with a corresponding JASCO CPA at 22:57, and DEMON CPA at 22:44.

The plot of the corresponding DEMON peak frequency shows a clear step change in frequency between 22:32 and 22:42 pm. The peak frequency initially falls around 4.4 Hz which is then followed by a step change to 5.3 Hz. This is suggested to be caused by a

change in speed of the vessel. This can be seen in the bottom portion of the plot where the AIS SOG is observed to increase from about 8.4 knots to 10.4 knots.

To further verify the suggestion, the DEMON peak magnitude data are further analyzed.

The AIS data show that initially the range decreases indicating that the vessel approaches the AMAR until it is at CPA (red diamond), and then increases as the vessel moves away from the acoustic recorder's location. Noise from a vessel passing an AMAR would increase as it approaches, reach a maximum near the CPA and then decrease as it moves away. This would be indicated by a peak magnitude intensity change in color from light, to dark, and back to light again (Lowes et al., 2022). Therefore, the peak magnitude data indicate a single vessel's presence and is consistent with an increase in speed of the vessel.

4.2.2 May 4th, 2021: Single Vessel With Speed Decrease

AIS data from May 4th, 2021 are shown in Figure 20 with the detector's performance shown in Figure 21. The single vessel example in Figure 21 displays the change in peak frequency due to a speed decrease of the vessel.

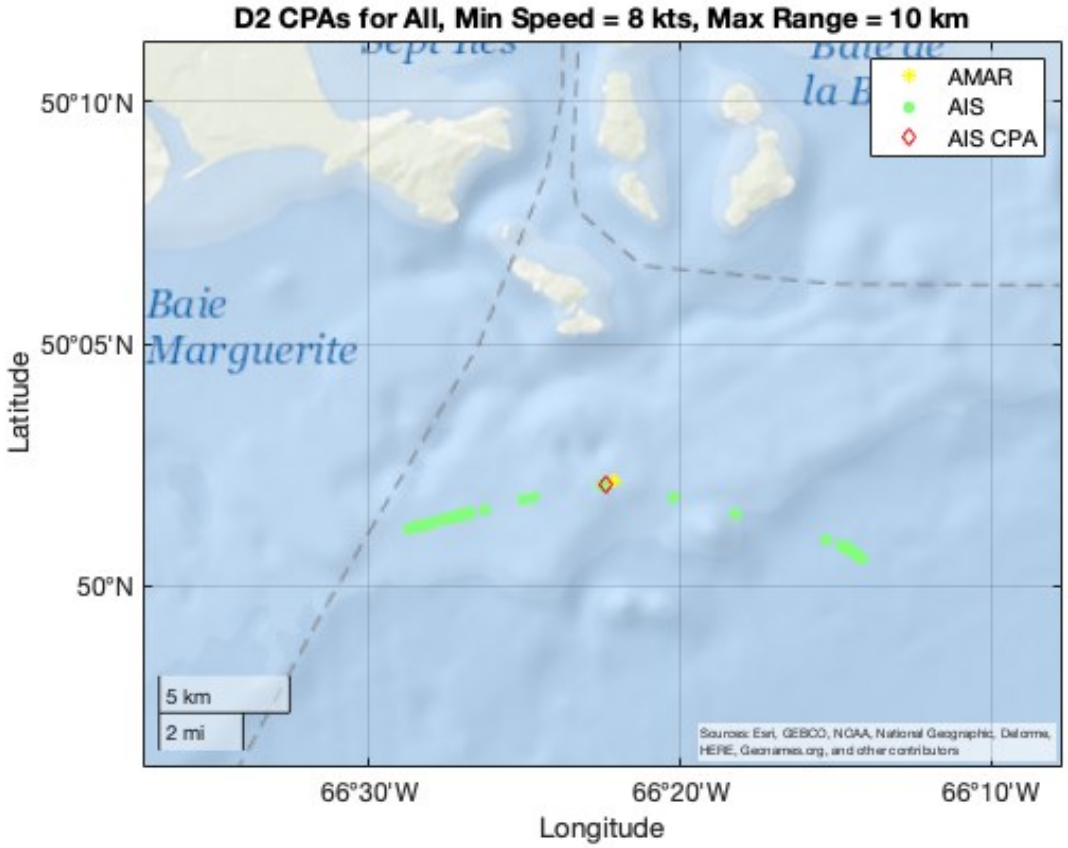

Figure 20: Single vessel on May 4th (deployment 2). The yellow star is the AMAR position, the green dots are the actual AIS data points, and the red diamond is the AIS CPA.

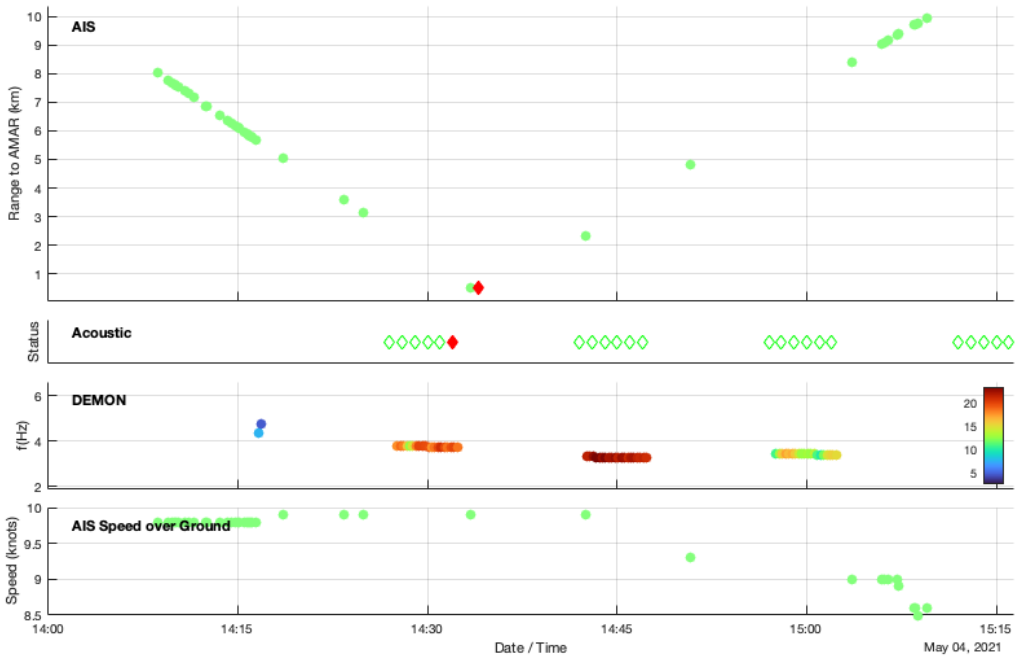

Figure 21: The AIS, JASCO, and DEMON data on May 4th (deployment 2). For the detailed description of symbols see Figure 19.

The AIS data display a u-shape track which corresponds to a single vessel (in green) with an AIS CPA at 14:34, and corresponding JASCO CPA at 14:32, and DEMON CPA at 14:43.

Once again, the DEMON plot shows a change in frequency between consecutive acoustic datasets at 14:32 and 14:42. The peak frequency drops from about 3.7 Hz to about 3.3 Hz with an associated AIS SOG decrease from about 9.6 knots to 8.5 knots. Once again, the peak magnitude data indicate a single vessel's presence and is consistent with a decrease in speed of the vessel..

4.2.3 May 17th, 2021: Single Vessel With SOG Change Not Observed in DEMON Data

AIS data from May 17th, 2021 are shown in Figure 22, with the detection details shown in Figure 23. This plot (Figure 23) demonstrates a change in SOG which is likely due to the sea/ocean conditions or use of a variable pitch propeller.

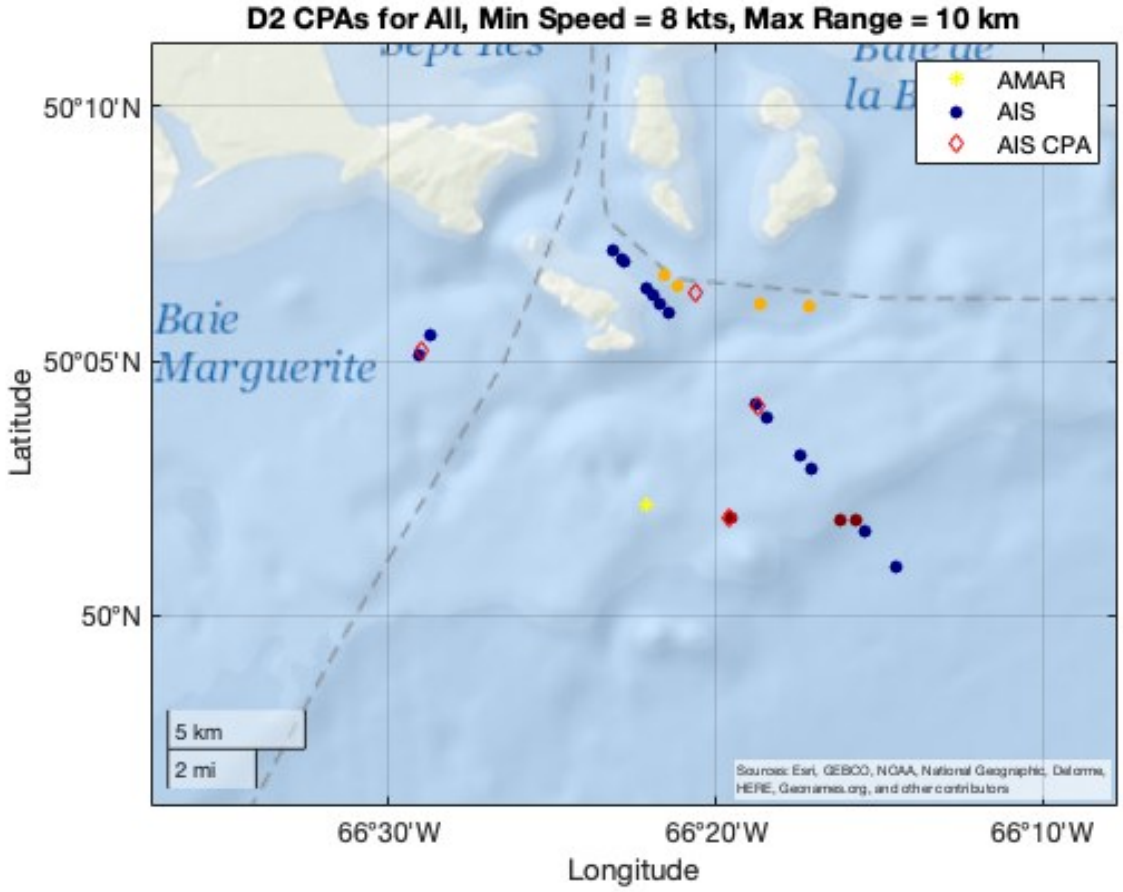

Figure 22: Multiple vessel presence on May 17th (deployment 2). The yellow star is the AMAR position, the circles of different colors correspond to a different ship, and the red diamond is the AIS CPA.

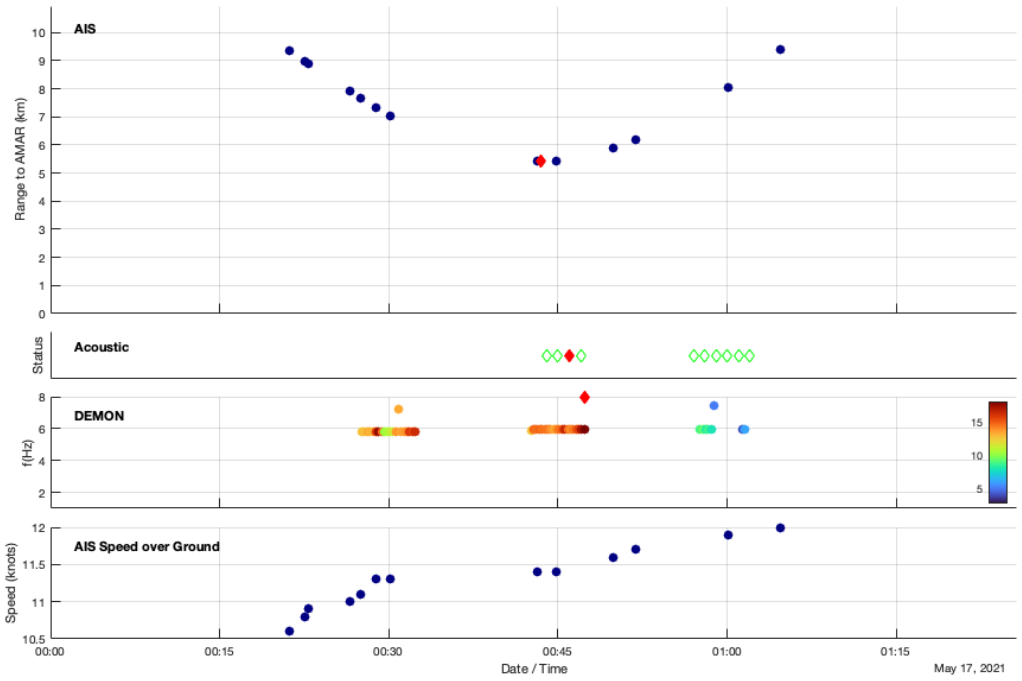

Figure 23: The AIS, JASCO, and DEMON data on May 17th for a single vessel of interest (deployment 2).

For the detailed description of symbols see Figure 19.

The AIS data display a straight-line AIS track (in blue) corresponding to one ship. The vessel (in blue) has AIS CPA at 00:43, and there is a corresponding JASCO CPA at 00:46, and DEMON CPA at 00:47.

The DEMON plot shows a distinctive peak frequency trend around 6 Hz from a single vessel. However, although the SOG changes from about 10.5 knots to 12 knots, it is not reflected in the DEMON data. One of the reasons could be that the vessel's SOG changes because of the sea/ocean conditions. For example, if the vessel was transiting with a current resulting from tidal flow, its SOG could change. Another potential reason could be that the change in speed is due to a ship with a variable pitch propeller. With variable pitch propeller, the change in the position of blades can move a ship forward or backwards while the propeller rotation speed remains constant (Bright Hub Engineering, 2009).

4.3 Multiple Vessel Transit Examples

4.3.1 May 5th, 2021: Multiple Vessels With Two CPAs Close in Time

Figure 24 shows five separate AIS tracks from May 5th, 2021 corresponding to five different vessels whose detection details are plotted in Figure 25. This example (Figure 25) shows that the DEMON detector found four out of five vessel CPAs while the JASCO detector identified three out of five vessel CPAs. Also, Figure 26 demonstrates the case when both detectors were not able to distinguish between two vessels CPAs close in time.

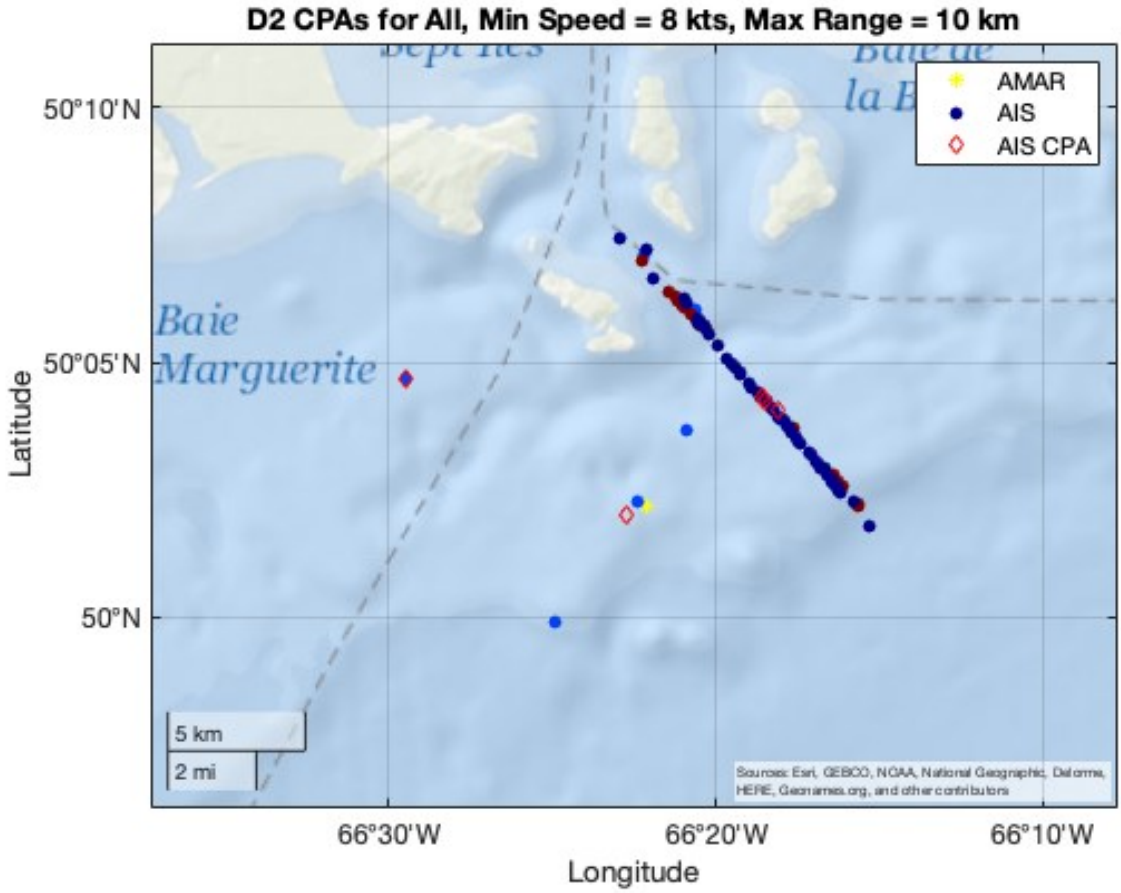

Figure 24: Multiple vessel presence on May 5th (deployment 2). The yellow star is the AMAR position, the circles of different colors correspond to a different ship, and the red diamond is the AIS CPA.

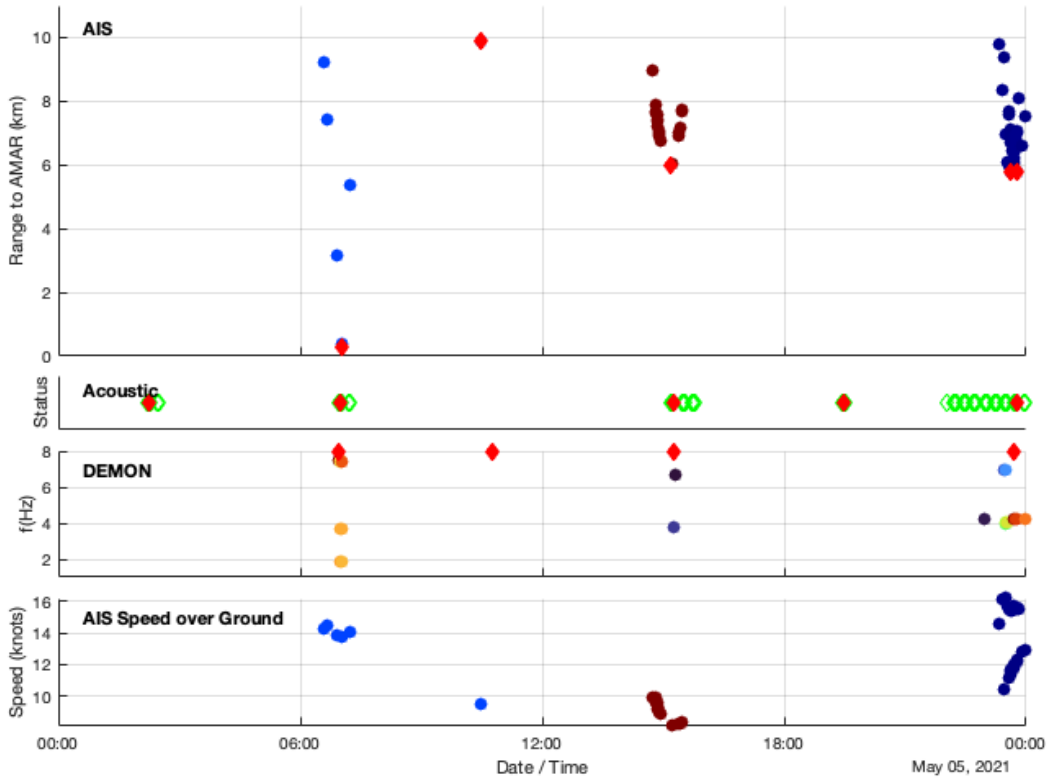

Figure 25: The AIS, JASCO, and DEMON data on May 5th (deployment 2). For the detailed description of symbols see Figure 19.

The first vessel (light blue) has an AIS CPA at 07:02 with corresponding JASCO and DEMON CPAs at 07:00 and 06:58. The second vessel has an AIS CPA at 10:29 at approximately 10 km range. It should be noted that only the CPA can be seen for the second vessel as the AIS data are at longer ranges which are beyond 10 km. There is no corresponding JASCO CPA. This vessel was initially classified as a false negative CPA in the JASCO detector. However, the DEMON detector identifies a CPA occurring at 10:44. Therefore, this vessel is classified as a true positive CPA by the DEMON and combined detectors.

The third vessel (brown) has an AIS CPA at 15:10 with a corresponding JASCO CPA at 15:16, and DEMON CPA at 15:15. The fourth vessel (dark blue) and fifth vessel

(also in dark blue) shown in more detail in Figure 26 have AIS CPAs at 23:36 and 23:45 respectively.

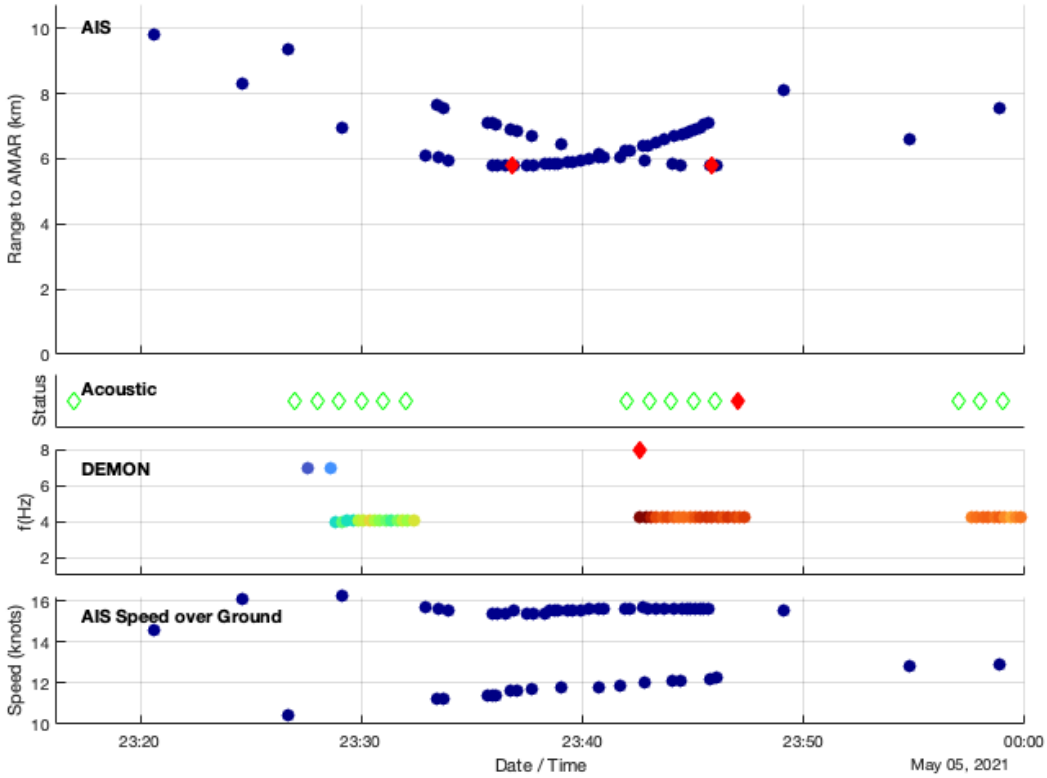

Figure 26: The AIS, JASCO, and DEMON data on May 5th (deployment 2). For the detailed description of symbols see Figure 19.

The detectors identify single CPAs at 23:47 (JASCO) and 23:42 (DEMON). Both detectors were not able to distinguish between two vessels CPAs close in time, and therefore only detected one of the vessels. Overall, the DEMON detector found four out of five vessel CPAs while the JASCO detector identified three out of five vessel CPAs. The connection between what the vessels are doing and what the JASCO algorithm is evaluating can be seen in Figure 27.

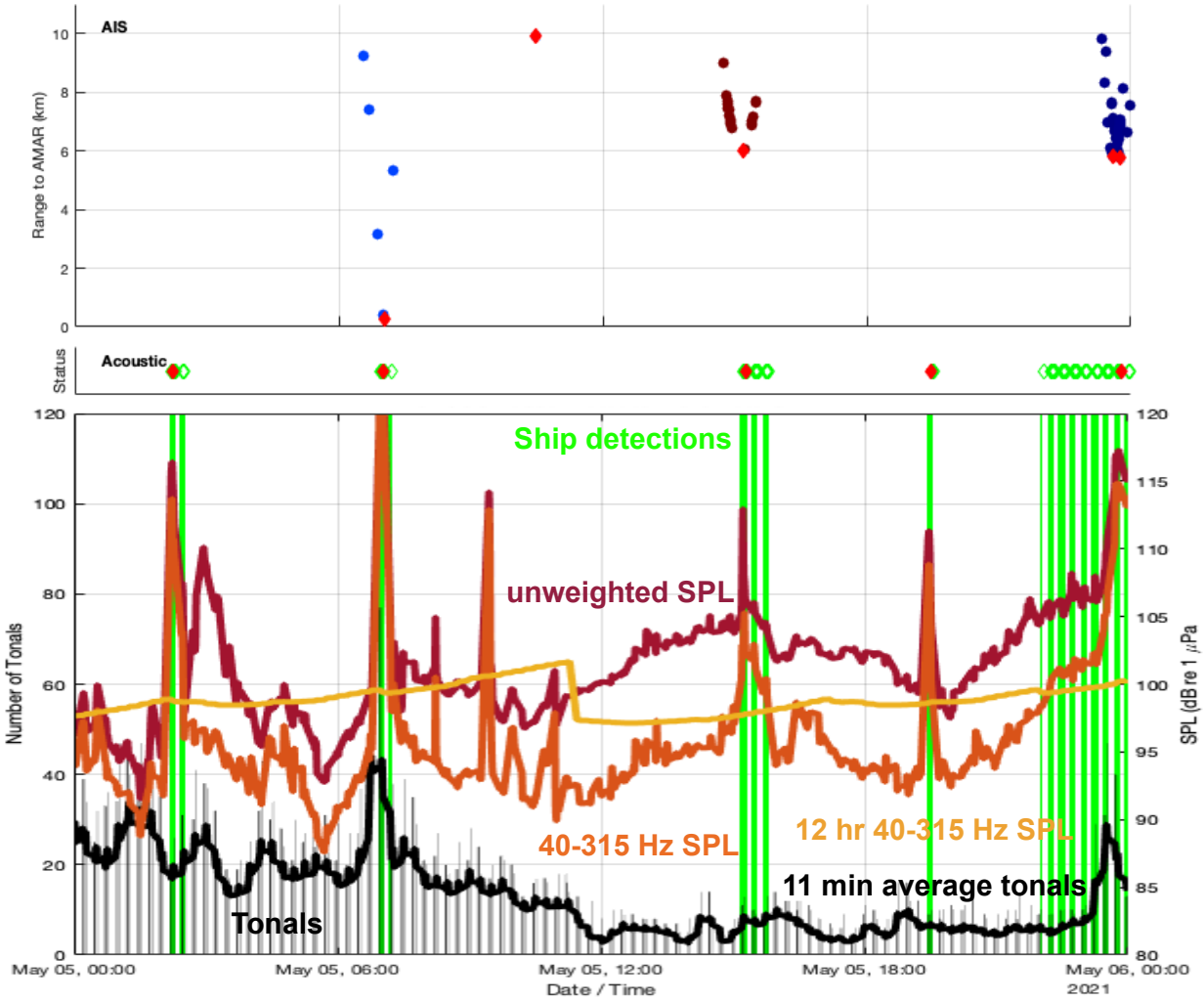

Figure 27: JASCO vessel detection example on May 5th (deployment 2).

AIS plot: Shows the actual received AIS transmission points as circles of different colors, where each color corresponds to a different ship (MMSI number), while the red diamond is the interpolated AIS CPA.

Acoustic plot: The green diamonds indicate when the JASCO algorithm detects a vessel, and the red diamond is JASCO CPA.

The bottom plot: The orange line is 40-315 Hz SPL, the yellow line is 12 hour 40-315 Hz SPL, the dark red line is the unweighted SPL, the grey lines are the number of tonals, the black line is the 11-minutes-moving-average-number-of-tonals, and the green lines are the JASCO vessel detection.

4.3.2 May 18th, 2021: Two Vessels With CPAs Within an Hour of Each Other

AIS data from May 18th, 2021 are shown in Figure 28, with the associated detector results shown in Figure 29. The example of Figure 29 displays that both detectors successfully detected the CPAs of the two vessels.

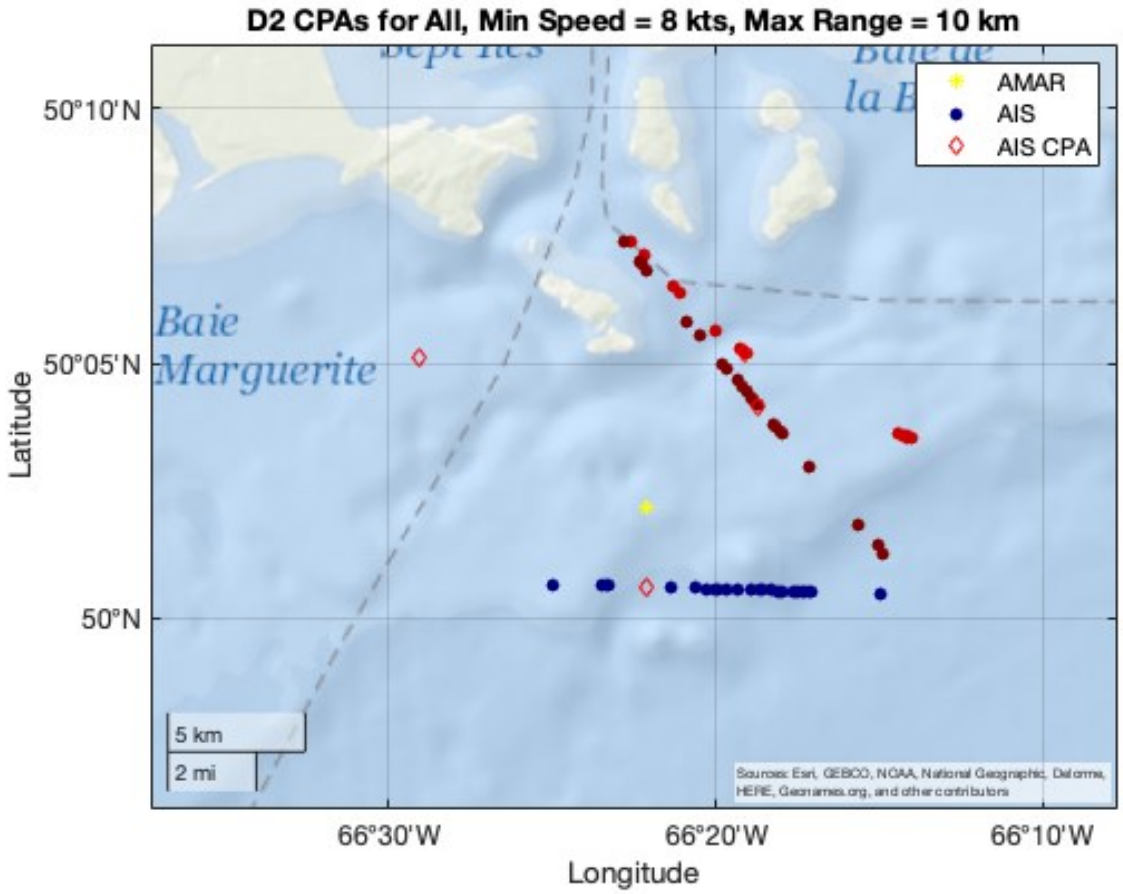

Figure 28: Multiple vessel presence on May 18th (deployment 2). The yellow star is the AMAR position, the circles of different colors correspond to a different ship, and the red diamond is the AIS CPA.

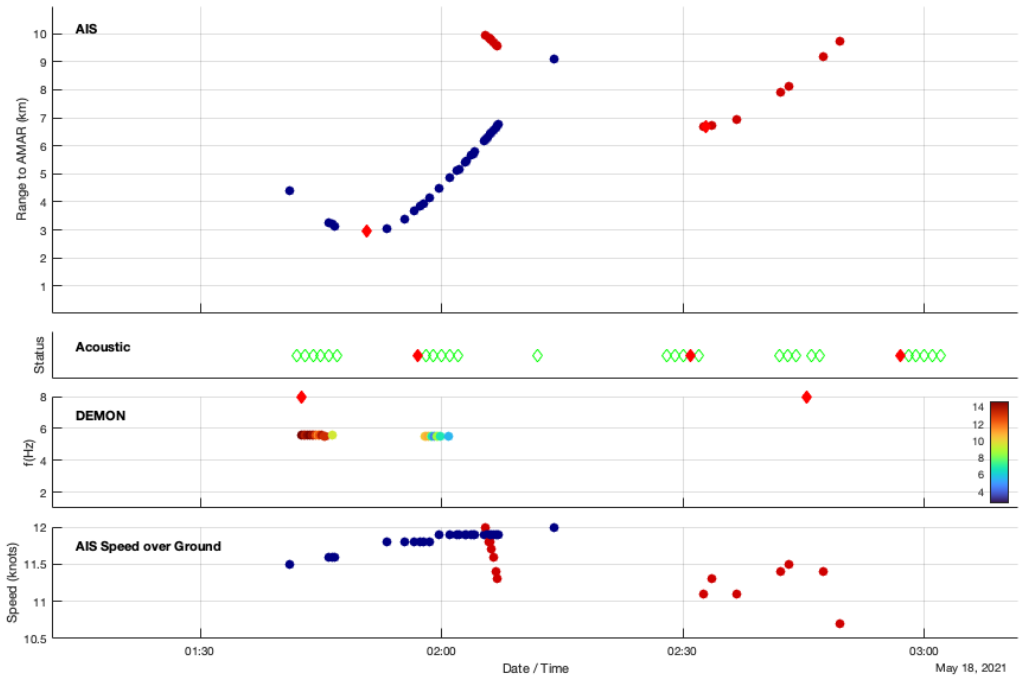

Figure 29: The AIS, JASCO, and DEMON data on May 18th (deployment 2). For the detailed description of symbols see Figure 19.

Two ships are seen. The first vessel (dark blue) has an AIS CPA at 01:50, and there is a corresponding JASCO CPA at 01:57, and DEMON CPA at 1:42. The second vessel (red) has an AIS CPA at 02:32, and there is a corresponding JASCO CPA at 02:31, and DEMON CPA at 2:45. It should be noted, that the reason why there is no DEMON data shown in the plot (Figure 29) for the second vessel is that the DEMON data is at high frequencies. Both detectors successfully detected the CPAs of the two vessels.

4.3.3 May 24th, 2021: Two Close Vessels With One Changing Course Resulting in Two CPAs

Figure 30 and Figure 31 show the AIS tracks and detector results from May 24th, 2021. The vessel (yellow) changes course by almost 90 degrees (Figure 30) and as a result has two CPAs.

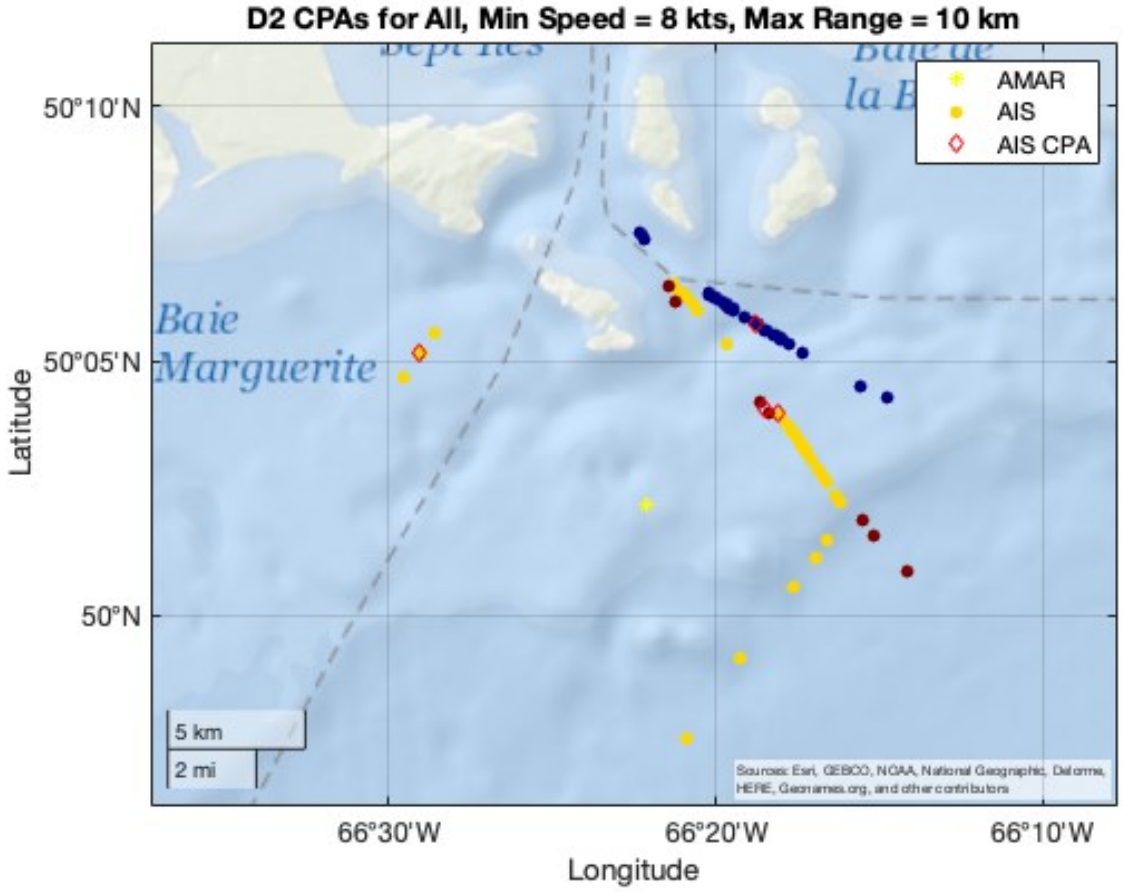

Figure 30: Multiple vessel presence on May 24th (deployment 2). The yellow star is the AMAR position, the circles of different colors correspond to a different ship, and the red diamond is the AIS CPA.

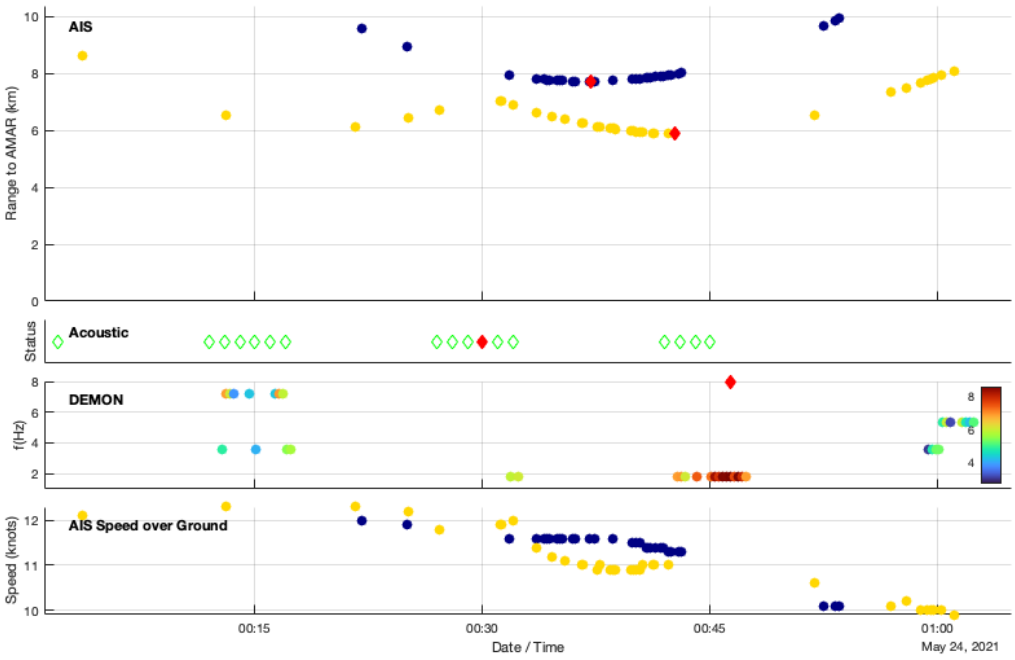

Figure 31: The AIS, JASCO, and DEMON data on May 24th (deployment 2). For the detailed description of symbols see Figure 19.

Two vessels are present. The first vessel (yellow) has an AIS CPA at 00:42, and the second vessel (dark blue) has an AIS CPA at 00:37. There is a corresponding JASCO CPA at 00:30, and DEMON CPA at 00:46. Both the JASCO and DEMON detectors were unable to distinguish between two vessels present at similar time and range. Therefore, they only detected one vessel out of the two.

The vessel (yellow) changes course by almost 90 degrees (Figure 30) and as a result has two CPAs. However, the current AIS analysis is done in the way that it breaks the data apart by unique vessel time differences and therefore only identifies one CPA (Figure 31). The AIS analysis could be improved upon in the future.

4.3.4 June 17th, 2021: Missed DEMON CPA

AIS data from June 17th, 2021 are shown in Figure 32 along with detection data shown in Figure 33. The DEMON detector was not able to identify CPA for the second vessel (royal blue) (Figure 33).

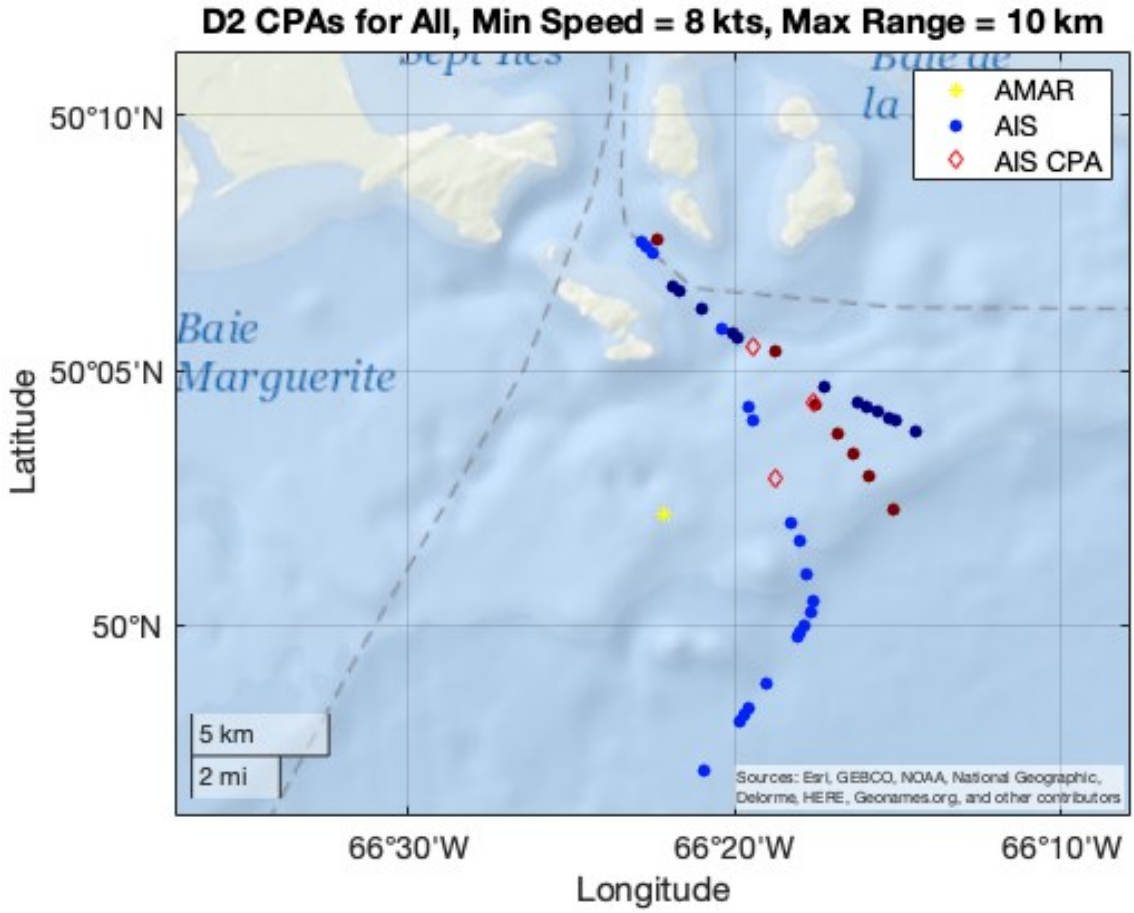

Figure 32: AIS of multiple vessels on June 17th (deployment 2). The yellow star is the AMAR position, the circles of different colors correspond to a different ship, and the red diamond is the AIS CPA.

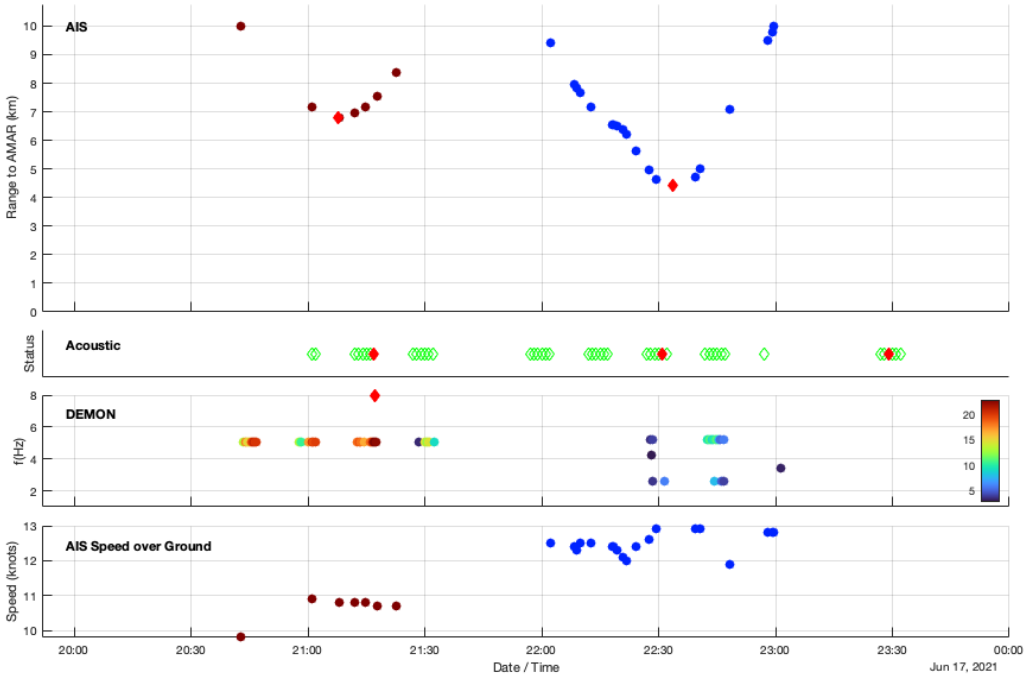

Figure 33: The AIS, JASCO, and DEMON data from June 17th (deployment 2). For the detailed description of symbols see Figure 19.

Two ships are present. The brown has an AIS CPA at 21:07, and there is a corresponding JASCO CPA at 21:17, and DEMON CPA at 21:17. The royal blue vessel has an AIS CPA at 22:33, and there is a corresponding JASCO CPA at 22:31. However, there is no corresponding DEMON CPA for this vessel. This vessel was initially classified as a false negative CPA in the DEMON detector. However, it is classified as a true positive CPA in the JASCO and combined detectors.

The DEMON detector was not able to identify CPA for the second vessel (royal blue), because there is additional DEMON data at higher frequencies (not displayed in Figure 33). Hence, the second vessel was not distinguished as a separate vessel since there was never 15 minutes difference between two consecutive DEMON data points. Therefore, the further improvements for the DEMON detector are needed.

4.3.5 May 30th, 2021: Missed CPAs and the Need for Additional DEMON Data

The AIS data from May 30th, 2021 are shown in Figure 34, with the detection details shown in Figure 35. The DEMON data show two distinctive trends which correspond to two separate vessels.

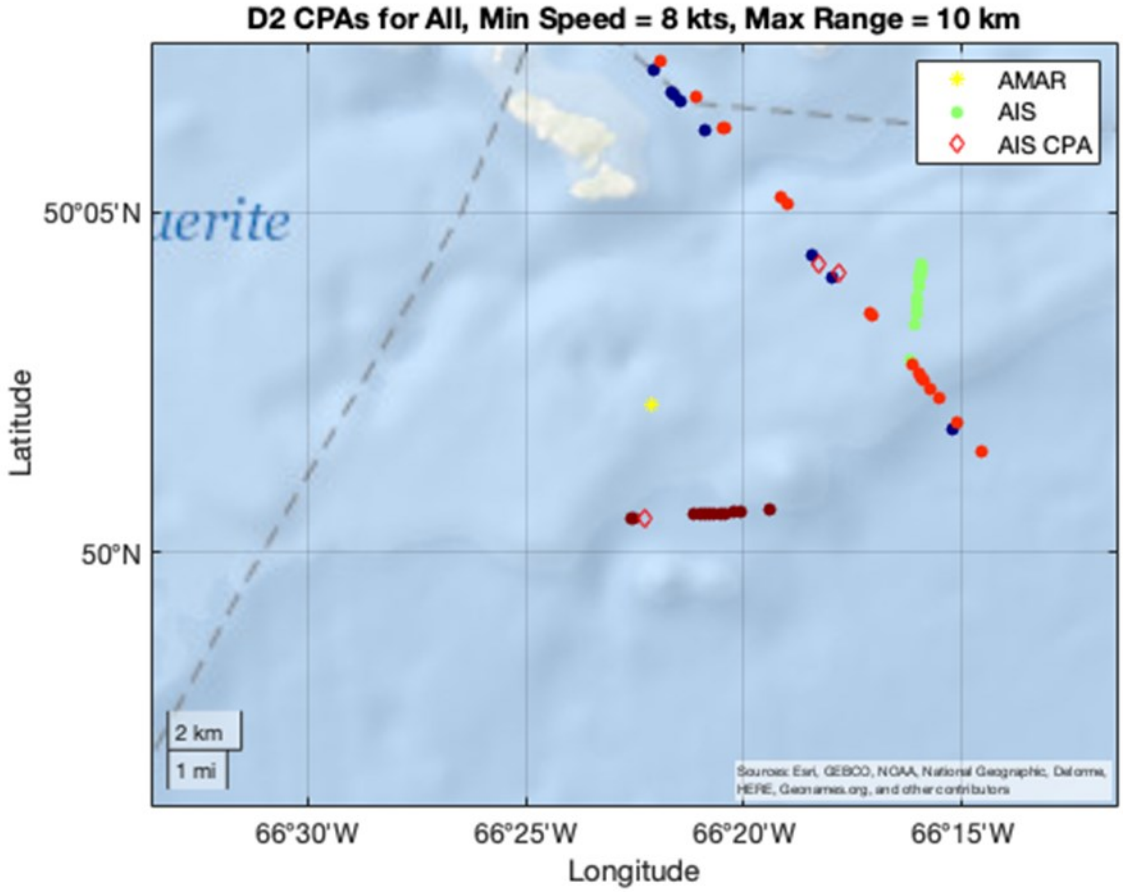

Figure 34: Multiple vessel presence on May 30th (deployment 2). The yellow star is the AMAR position, the circles of different colors correspond to a different ship, and the red diamond is the AIS CPA.

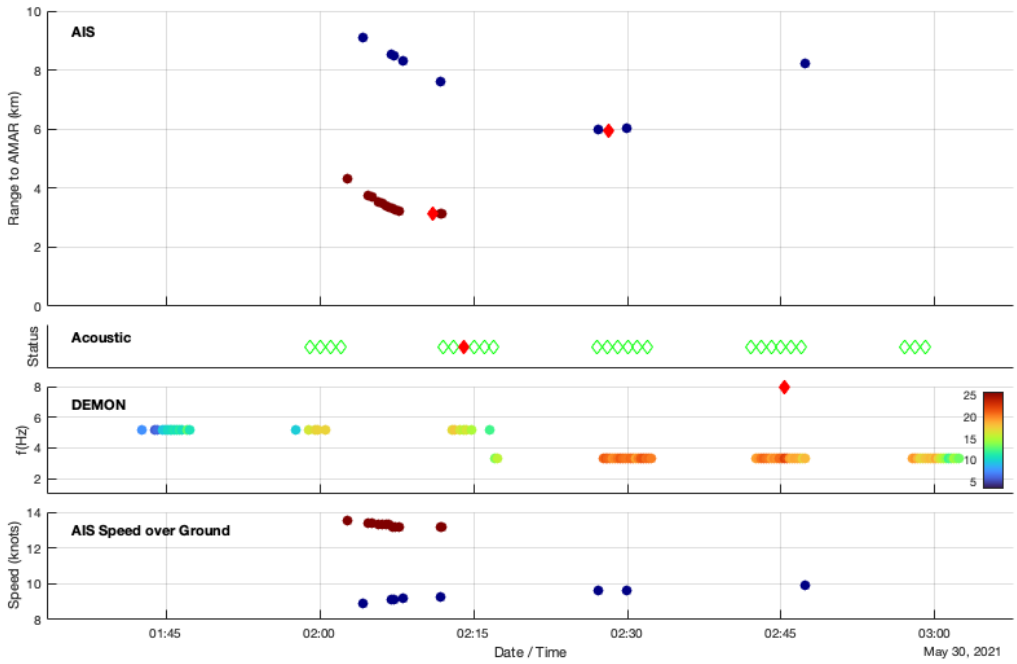

Figure 35: The AIS, JASCO, and DEMON data on May 30th (deployment 2). For the detailed description of symbols see Figure 19.

The first vessel (brown) has an AIS CPA at 02:11, and the second vessel (dark blue) has an AIS CPA at 02:28. There is a corresponding JASCO CPA at 02:14, but no corresponding DEMON CPA for the first vessel. However, there is a corresponding DEMON CPA at 02:45 for the second vessel.

A potential reason for why the trace of the first vessel (brown) seems to disappear on the AIS plot (Figure 35) is that the vessel may have stopped transmitting AIS data for unknown reasons. Therefore, it is recommended to check the AIS Navigational Status of this particular vessel (MarineTraffic, from https://help.marinetraffic.com/hc/en-us/articles/205426887-What-kind-of-information-is-AIS-transmitted-, last viewed July 5, 2022). A potential reason why the trace of the first vessel (brown) seems to disappear on the DEMON plot (Figure 35) is that only the peak with the highest magnitude was saved. It appears that when the second vessel arrives (dark blue), its ship noise dominates the first

vessel. Therefore, it is recommended to track and save additional DEMON peaks for further analysis. The additional peaks could help with vessel detection, especially for the case of identifying two or more vessels transiting past the recorder at similar times.

The JASCO detector was unable to distinguish between the two vessels operating at a similar time and range. Therefore, it only detected one vessel out of two. The DEMON detector, as expected, was only able to detect the second vessel since the time difference between two consecutive DEMON peaks has to be more than 15 minutes to be distinguished as separate vessel events. However, the peak frequency shows a step change in frequency occurring between 02:16 and 02:27. The first peak frequency trend is around 5 Hz which is then followed by a sudden drop to 3.3 Hz. The peak magnitude and frequency data show two distinctive trends which might correspond to two separate vessels. Note that as the SOG plot shows that the SOG for each vessel remains relatively constant, the change in peak frequency must be due to separate vessels as opposed to a single vessel with a speed change. However, even though, the DEMON detector was able to separate two vessels, it did not find a CPA for the first vessel as discussed above. This indicates that the DEMON detector requires further steps for optimization. Nevertheless, it was shown that it is possible to identify multiple vessels operating close in time. Overall, both detectors detected one vessel out of two.

To summarise, it has been shown that the DEMON detector is able to reliably detect vessels with AIS data to ground truth the detection result. Therefore, DEMON Processing data are valuable, especially in case of false negative CPAs. It proved to provide reliable vessel detection in some cases where the JASCO detector fails.

Chapter 5: Detector Performance

This section presents the confusion matrix for the performance of the acoustic detectors. The AIS CPAs were compared to the JASCO and DEMON CPAs, and their performance results were evaluated.

5.1 Confusion Matrix

The confusion matrix represents the detector performance results (Reis et al., 2019; Hildebrand et al., 2022). The columns of the confusion matrix show the number of vessel occurrences according to the AIS data, while the rows show the number of vessel occurrences according to the acoustic (JASCO, DEMON, or the combined) detectors.

The four resulting categories for the detectors are shown below (Lowes et al., 2022):

- True Positive (TP) represents the times when the AIS CPA and the acoustic detector CPA agree that a vessel is present within the tolerance of 21 minutes.
- False Positive (FP) represents the times when the acoustic detector does not have a corroborating AIS CPA within the tolerance of 21 minutes.
- False Negative (FN) represents the times when the AIS CPA does not have a corroborating acoustic detector CPA within the tolerance of 21 minutes.
- True Negative (TN) represents the times when both the AIS CPA and the acoustic detector, agree that there is no vessel present within the tolerance of 21 minutes.

The number of false positive CPAs is not available for the JASCO, DEMON, and combined detectors at this stage. One of the reasons is that the AIS CPAs were compared to the JASCO and DEMON CPAs. Therefore, this comparison can only provide the number of true positive and false negative CPAs.

5.2 Acoustic Detector Performance

A subset of 1009 CPAs from the AIS data representing vessel data to a maximum of 10 km and with a minimum speed of 8 knots was compared to the acoustic data to evaluate detection accuracy of the JASCO, DEMON, and combined detectors. Results for the three acoustic detectors are discussed below.

5.2.1 JASCO Vessel Detector (JVD)

Table 5 shows the results for the JASCO detector on the deployments 1 and 2 combined 1009 point AIS CPA data set.

Table 5: Detection results for the JASCO detector.

Confusion matrix		AIS (1009 CPAs)	
		CPA	No CPA
JASCO detector	CPA	TP: 604 (59.9%)	n/a (FP)
	No CPA	FN: 405 (40.1%)	n/a (TN)

The raw AIS (grey), AIS CPAs (blue), JVD detected CPAs (red), and AMAR (yellow) position are shown in Figure 36 for deployments 1 and 2.

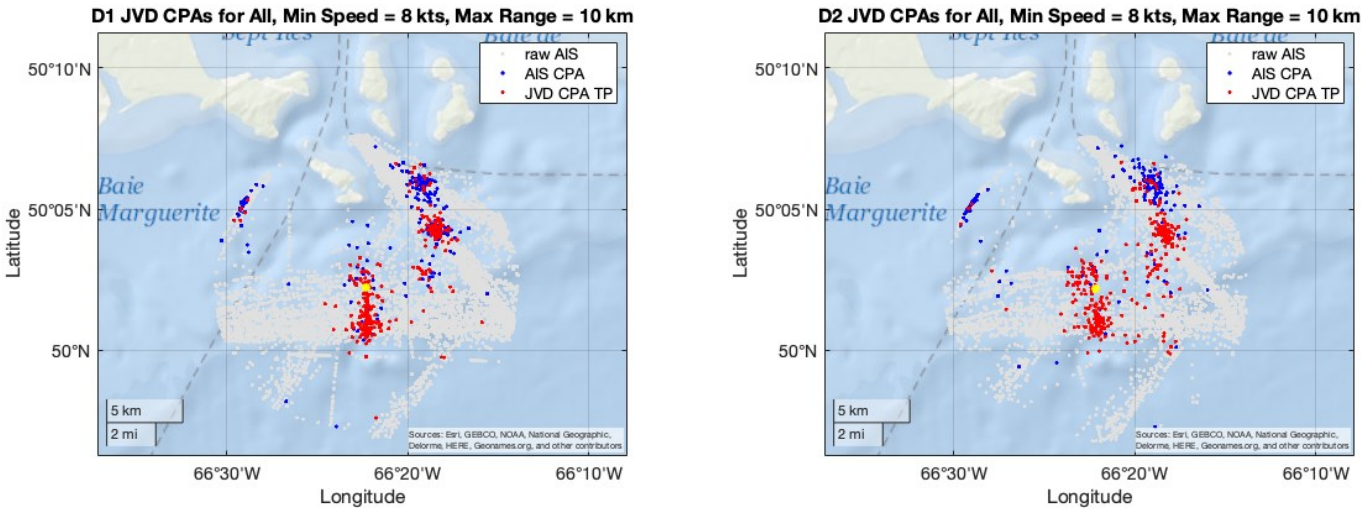

Deployment 1 Deployment 2

Figure 36: Geospatial view of JASCO detector CPAs. It shows the AMAR location as the yellow star, the grey dots are the raw AIS, the blue dots are the AIS CPAs which are the JASCO FN CPAs, and the red dots are the JASCO TP CPAs.

There are an increased number of TP CPAs (red) near the AMAR, and the number of FN CPAs (blue) tends to increase towards the northwest and northeast forming clusters in the shipping lanes that are there. A potential reason for FN CPAs could be that those ships are further away from the AMAR, and hence, they tend to have a lower SNR.

5.2.2 DEMON Vessel Detector

Table 6 and Figure 37 shows the results and corresponding geospatial plots for the DEMON detector CPAs for the two deployments.

Table 6: Detection results for the DEMON detector.

Confusion matrix		AIS (1009 CPAs)	
		CPA	No CPA
DEMON detector	CPA	TP: 796 (78.9%)	n/a (FP)
	No CPA	FN: 213 (21.1%)	n/a (TN)

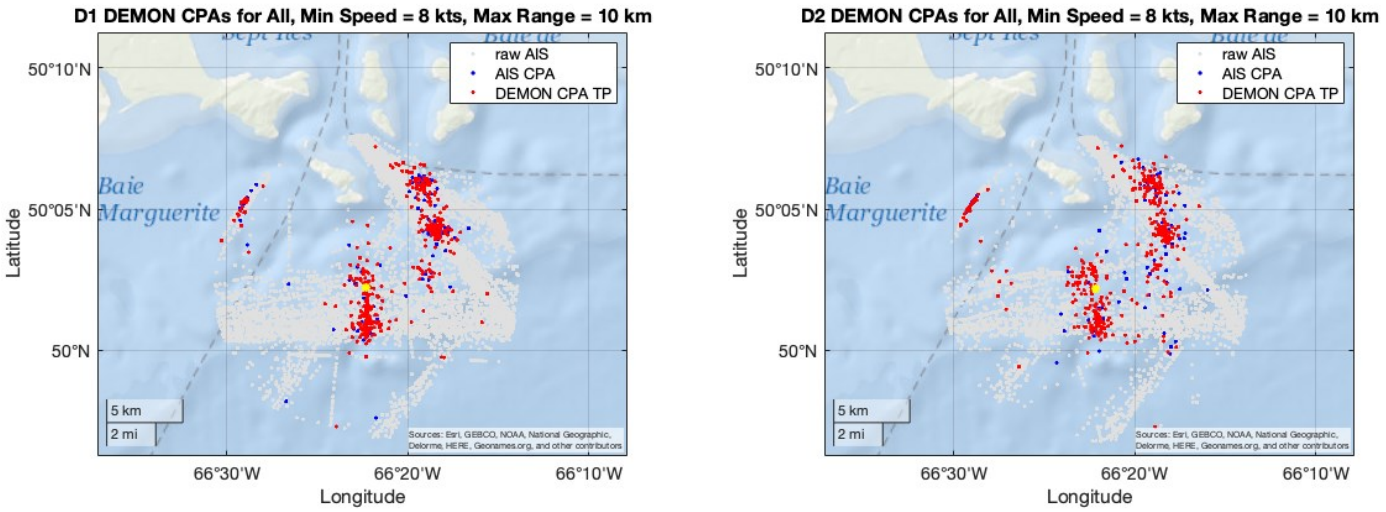

Deployment 1 Deployment 2

Figure 37: Geospatial view of DEMON detector CPAs. It shows the AMAR location as the yellow star, the grey dots are the raw AIS, the blue dots are the AIS CPAs which are the DEMON FN CPAs, and the red dots are the DEMON TP CPAs.

The DEMON detector (796 TP CPAs) appears to have performed better than the JASCO detector (604 TP CPAs) especially towards the northwest and northeast.

The JASCO detector is more dependent on the SNR. It looks at the signal levels, so the probability of it having a lower performance on low SNRs is higher than that of the DEMON detector. The DEMON detector does not depend as much on SNR. It is looking for a specific pattern which is the amplitude modulation of the cavitation noise, and it should therefore perform better on low SNRs which is shown in Figure 37.

5.2.3 Combined JASCO / DEMON Detector

To improve the existing JASCO's vessel detector's performance, the DEMON detector could be incorporated with it. The combined detector would look for either a JASCO or DEMON CPA match within the 21-minute time tolerance.

Table 7 and Figure 38 shows the results and corresponding geospatial plots for the combined JASCO/DEMON detector CPAs for the two deployments.

Table 7: Detection results for the combined JASCO/DEMON detector.

Confusion matrix		AIS (1009 CPAs)	
		CPA	No CPA
JASCO / DEMON detector	CPA	TP: 881 (87.3%)	n/a (FP)
	No CPA	FN: 128 (12.7%)	n/a (TN)

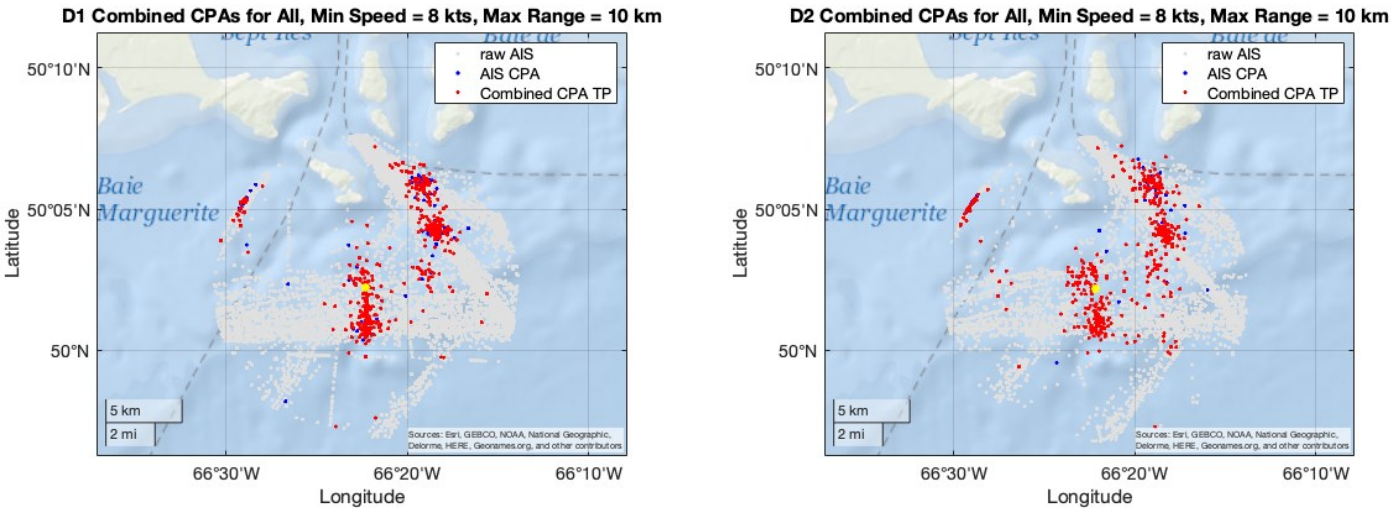

Deployment 1 Deployment 2

Figure 38: Geospatial view of Combined Detector CPAs. It shows the AMAR location as the yellow star, the grey dots are the raw AIS, the blue dots are the AIS CPAs which are the combined FN CPAs, and the red dots are the combined TP CPAs.

Establishing confidence in using acoustic methods to determine a vessel's presence and closest point of approach is important. The results presented above demonstrate that 87.3% of the combined JASCO/DEMON detector results were corroborated using the AIS ground truth data.

The number of true positive CPAs have significantly improved for the combined JASCO/DEMON detector. Further away from the AMAR towards the northwest and

northeast, there are still some number of false negative CPAs (blue), but their number 128 (12.7%) is significantly lower for the combined detector when compared to the original JASCO vessel detector which is 405 (40.1%).

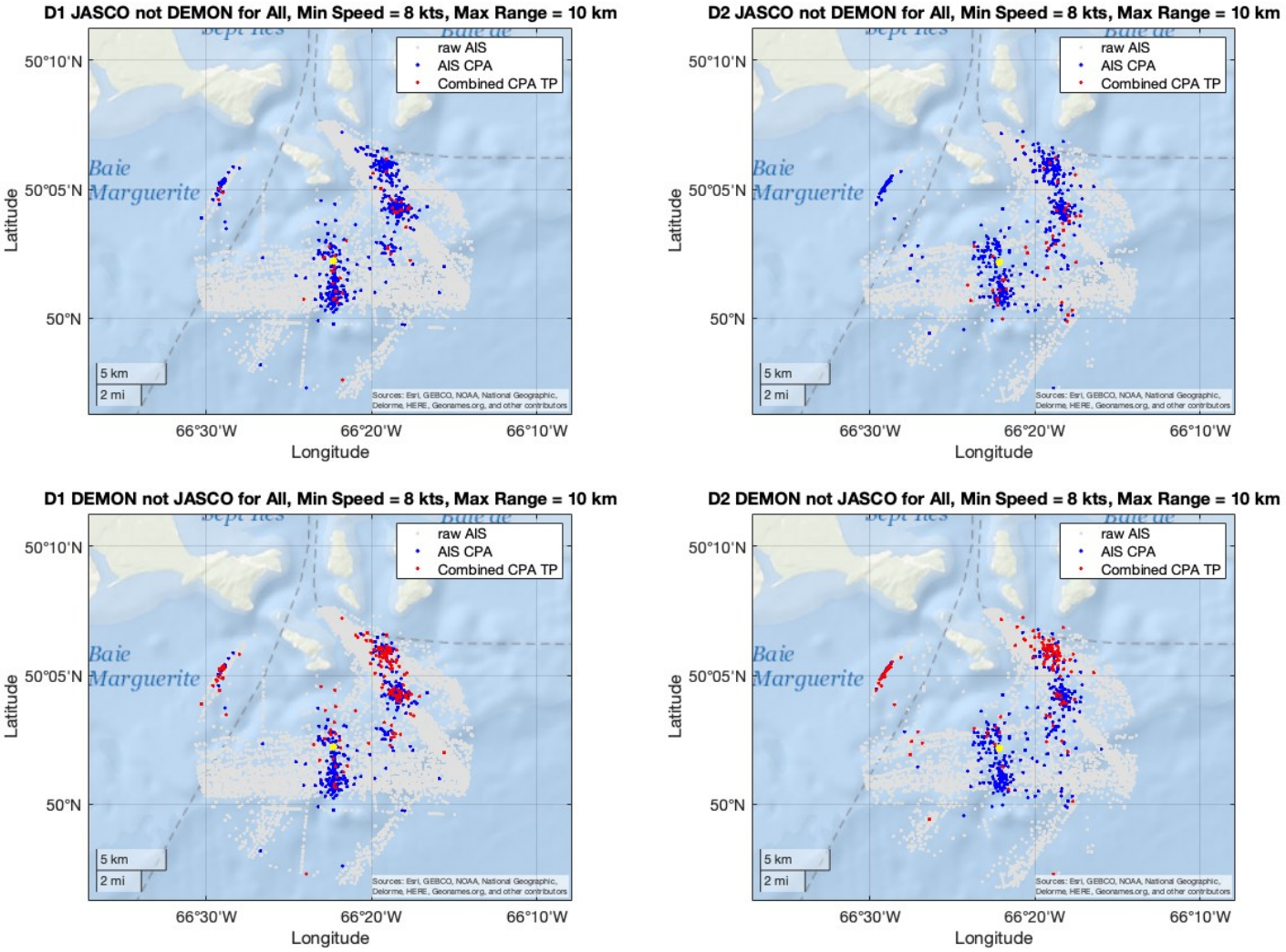

Deployment 1 Deployment 2

Figure 39: Geospatial view of Comparative Performance of the JASCO and DEMON Detectors for Deployment 1 (left) and Deployment 2 (right). It shows the AMAR location as the yellow star, the grey dots are the raw AIS, and the blue dots are the AIS CPAs. The upper plots show the JASCO TP CPAs (red) which were missed by the DEMON detector, and the lower plots illustrate the DEMON TP CPAs (red) which were missed by the JASCO detector.

Figure 39 upper plots show the TP CPAs (red) that the JASCO detector found but that the DEMON detector missed. Conversely the lower plots illustrate the TP CPAs for the DEMON detector where they were missed by the JASCO detector. The DEMON detector identified a significant number of CPAs in the direction of the northwest and northeast towards the shore. As can be seen, the DEMON detector outperformed the JASCO detector for identifying the vessel CPAs from both deployments.

The percentage of true positive CPAs as a function of range to 10 km for the JASCO, DEMON, and combined detectors for both deployments are shown in Figure 40.

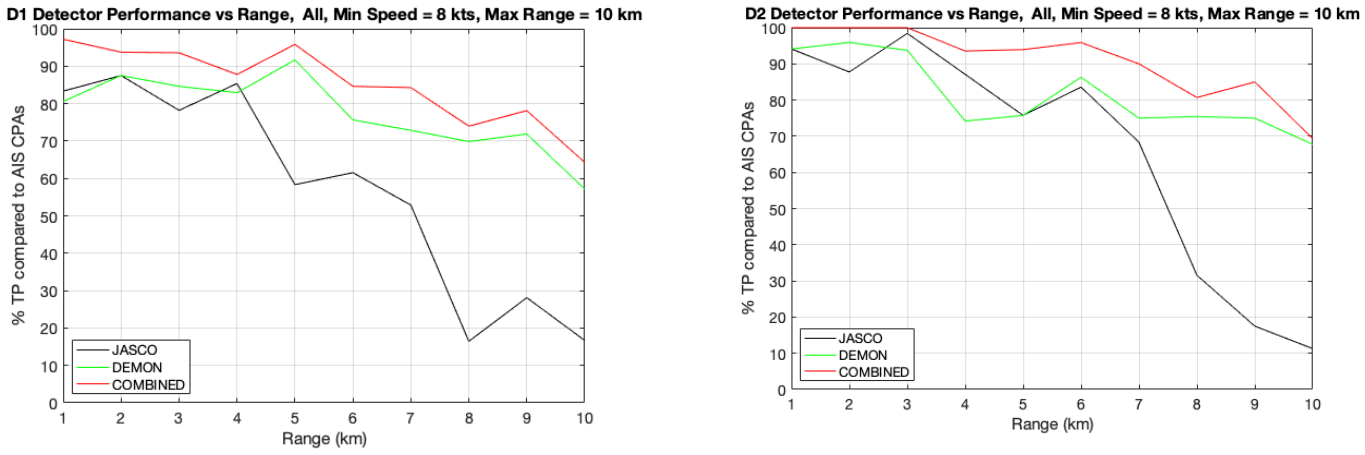

Deployment 1 Deployment 2

Figure 40: Percentage of true positive CPAs for the JASCO, DEMON, and combined detectors. The black line is the JASCO detector, the green line is the DEMON detector, and the red line is the combined detector.

The percent of true positive CPAs is similar for the JASCO and DEMON detectors up to 4 km (Deployment 1) and about 6 km (Deployment 2). Beyond these ranges the DEMON detector outperforms the JASCO detector to the maximum range evaluated of 10 km. As a result, the combined detector demonstrates at least 87 % accuracy in identifying the true positive CPAs out to the 10 km range maximum.

5.3 The Oceanographic Characteristics of Port of Sept-Îles

The JASCO detector performed better during Deployment 2 than Deployment 1 as can be seen in Figure 40. The long-term average noise levels for Deployments 1 and 2 are shown in Figure 41.

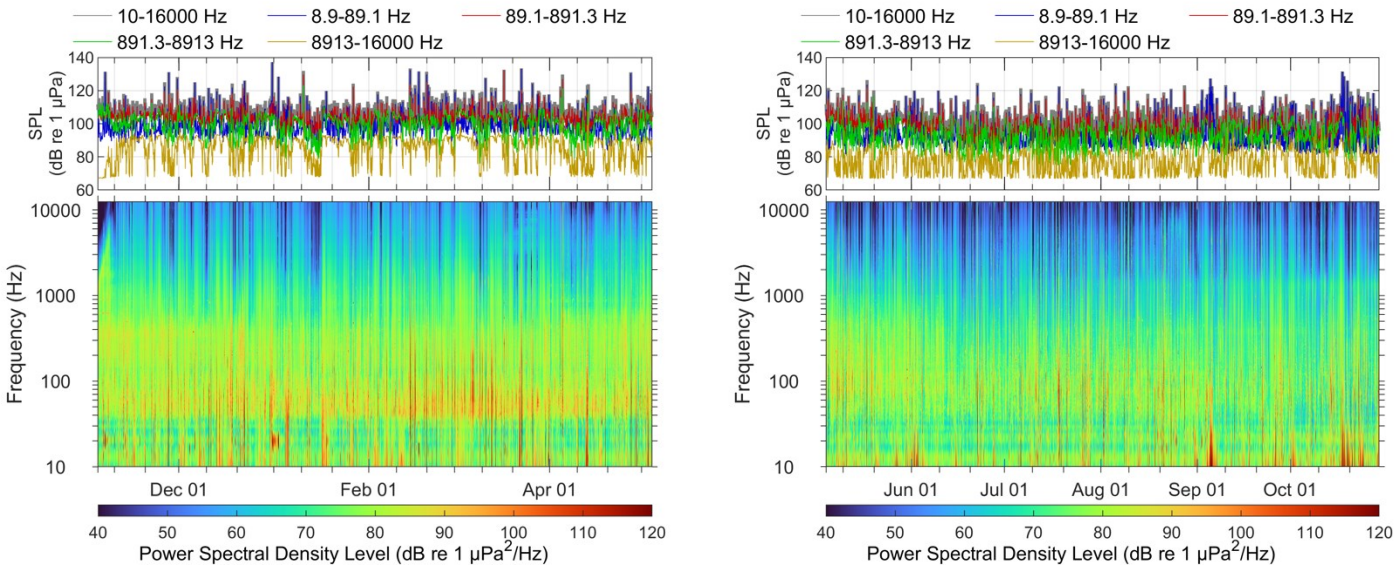

Deployment 1 Deployment 2

Figure 41: Long-term average noise levels for Deployments 1 and 2.

The first deployment covered the winter and spring months whereas the second deployment covered the summer and fall months. The background noise was higher during Deployment 1 than during Deployment 2 and was likely due to "environmental forces such as solar heating, wind mixing, and currents" (p.34) (Martin, 2019). As a result, the JASCO detector performed better during Deployment 2. However, the DEMON detector performance is similar for both deployments. As mentioned above, the JASCO detector is more dependent on the SNR. Areas with higher background noise (i.e. periods of intense weather conditions and higher sea states, contributions from distance vessels, etc.) will have lower SNRs and as a result the JASCO detector may not perform as well. However,

the DEMON detector does not depend as much on SNR and therefore will still likely perform well.

The sound speed profiles (SSPs) for both deployments can be seen in Figure 42 (Deployment 1) and Figure 43 (Deployment 2).

Deployment 1

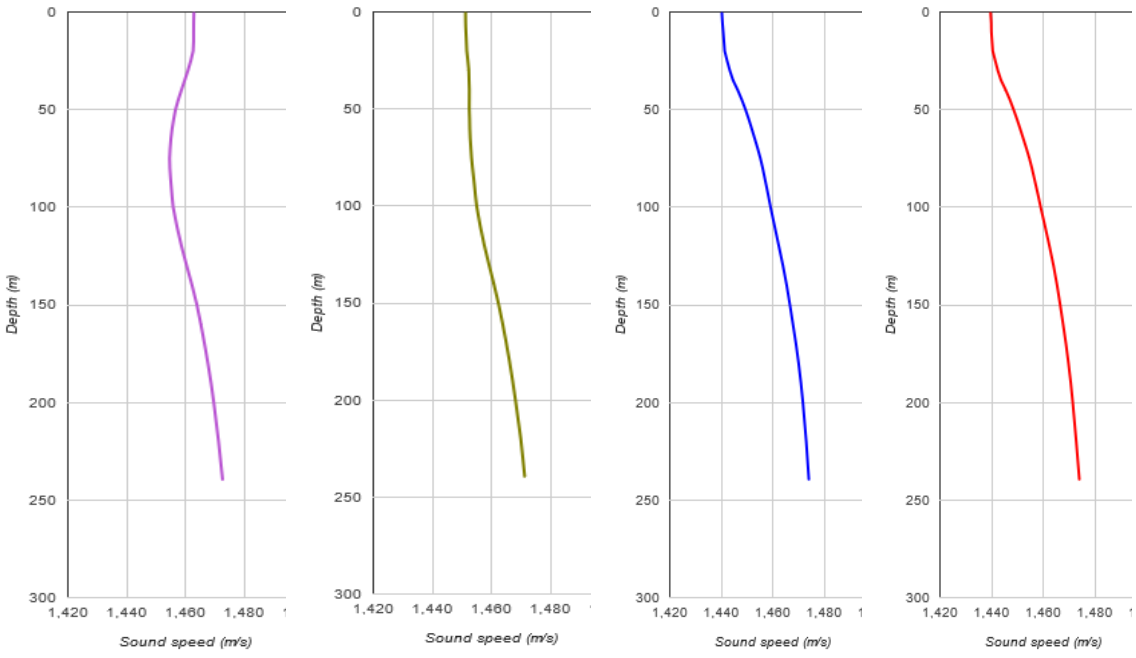

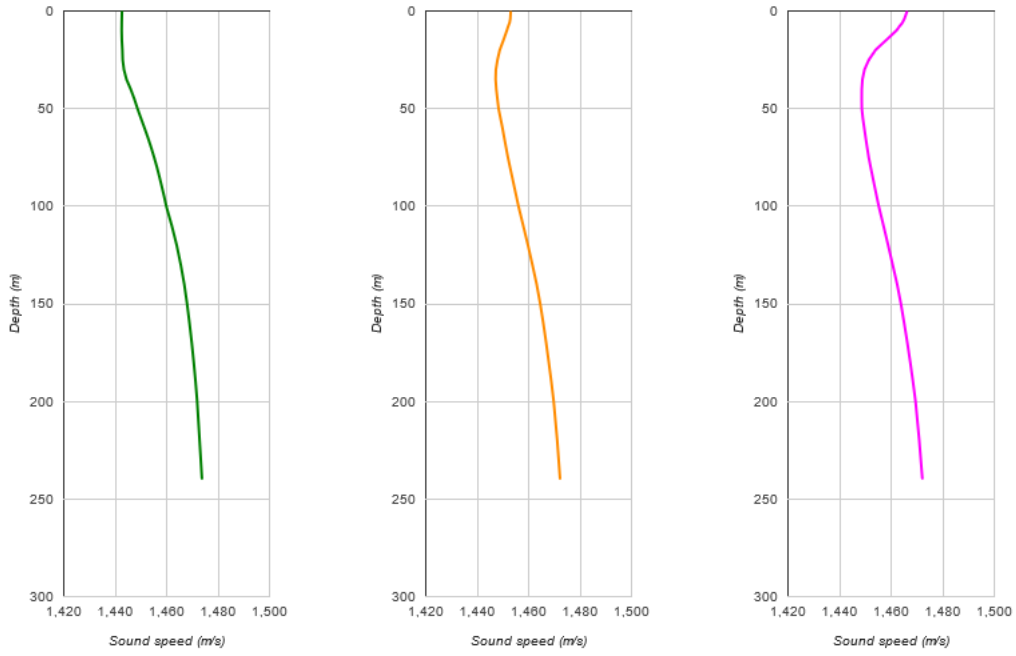

Figure 42: Monthly SSPs for Deployment 1.

Deployment 2

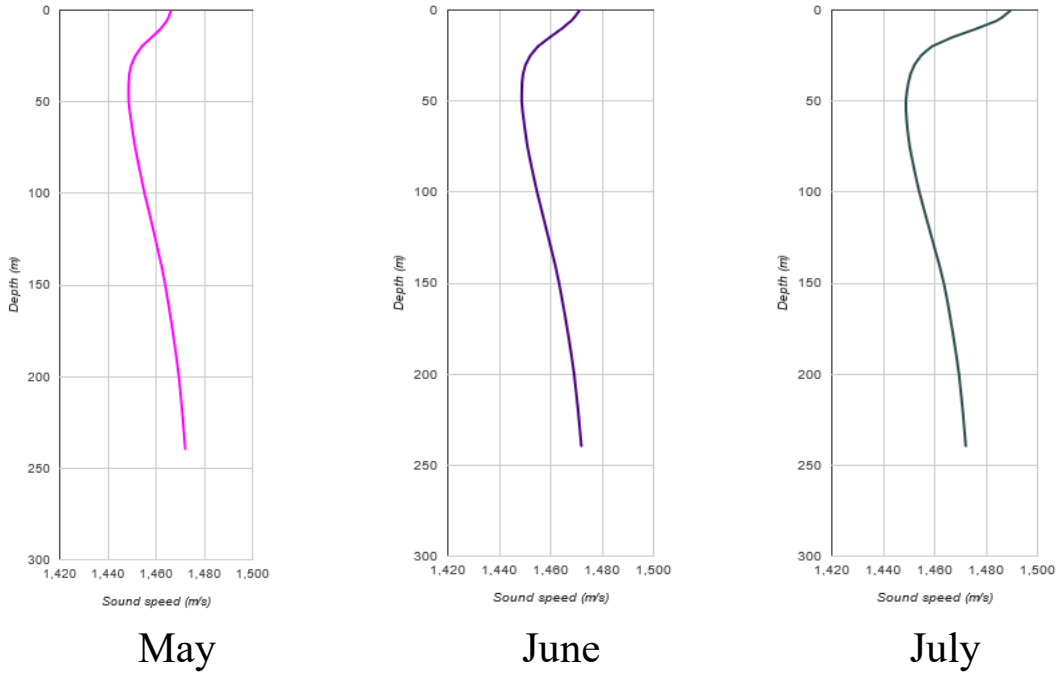

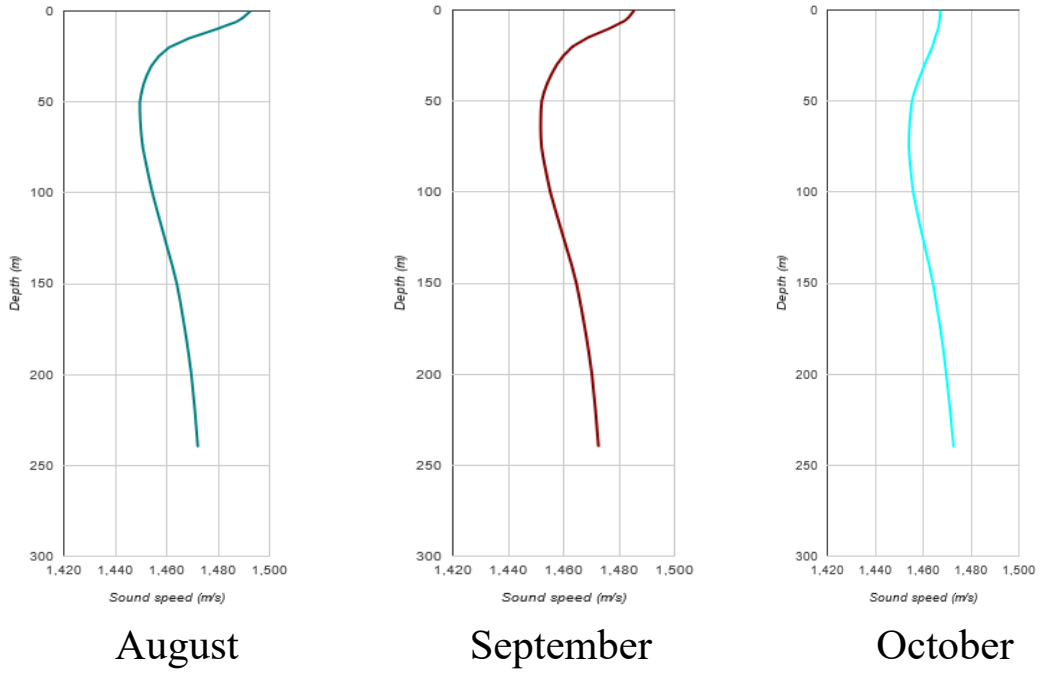

Figure 43: Monthly SSPs for Deployment 2.

Underwater acoustic propagation modeling was done using a ray tracer. For example, the propagation loss up to 10 km in February (deployment 1) can be seen in Figure 44.

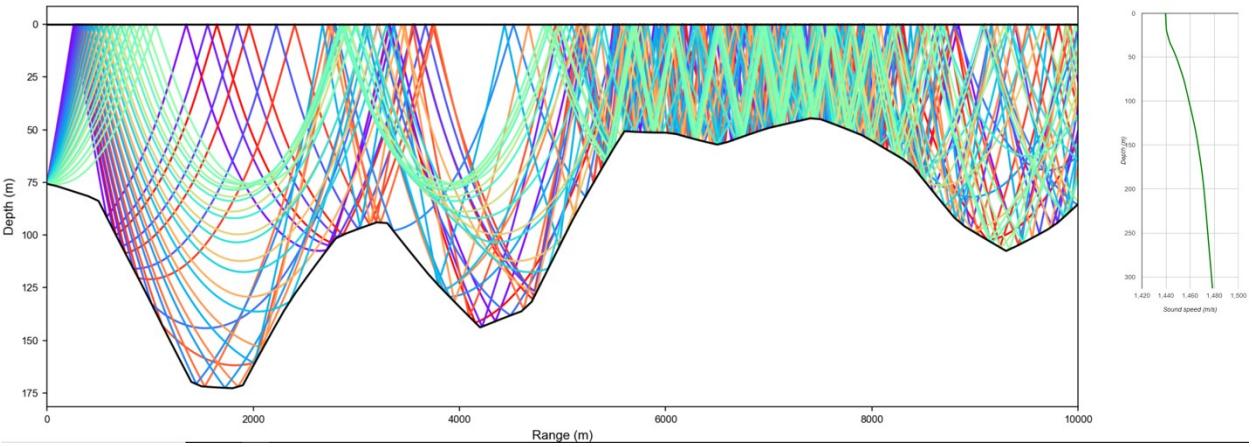

Figure 44:The propagation loss up to 10 km in February (deployment 1).

There are propagation paths to the AMAR up to 4 km and between 5 and 10 km. However, there are very few propagation paths between 4 and 5 km. These distances correspond to the percentage of JASCO true positive CPAs (Figure 40, deployment 1). There is a higher percentage of JASCO true positive CPAs up to 4 km, and there is a drop between 4 and 5 km which also agrees with the propagation plot (Figure 44). However, the performance of the JASCO detector decreases after 5 km. Therefore, other factors, perhaps environmental as discussed earlier, play a role in the decrease of the percentage of JASCO true positive CPAs beyond 5 km (Figure 40, deployment 1).

Figure 45 shows the propagation loss up to 10 km in August (deployment 2).

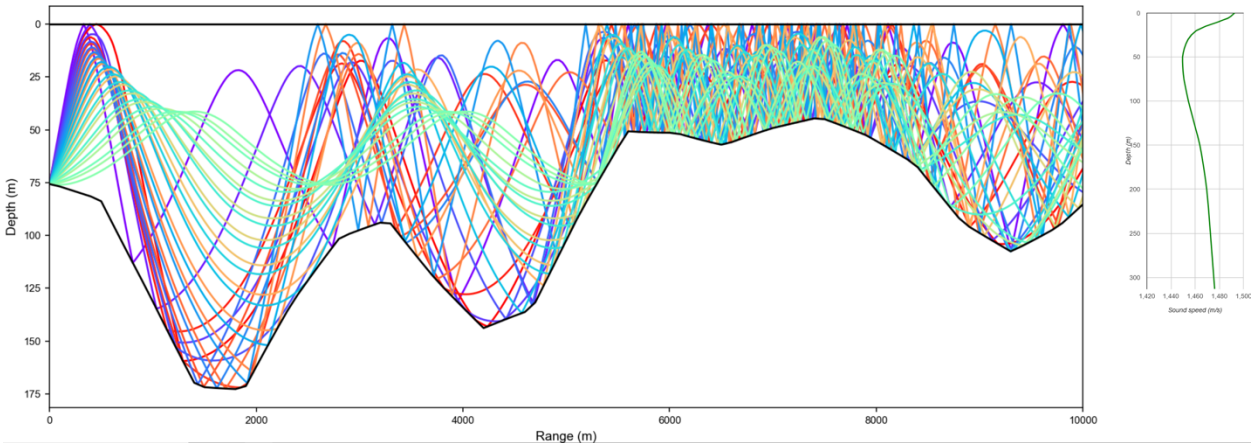

Figure 45: The propagation loss up to 10 km in August (deployment 2).

Propagation paths to the AMAR are more numerous beyond 5 km and persist up to 9 km. However, the percentage of JASCO true positive CPAs decreases after 6 km (Figure 40, deployment 2). To summarise, during deployment 2 the background noise is lower (Figure 41), and there are propagation paths to the AMAR between 5 and 9 km (Figure 45). Therefore, the JASCO decrease in the percentage of true positive CPAs after 6 km perhaps is due to ships with lower SNR.

5.3.1 Sound Propagation in Shallow and Deep Waters

Initially sound waves propagate as spherical surfaces (spherical spreading) (Martin, 2019; JASCO Applied Sciences, 2019; Seto, 2021). Transmission loss due to spherical spreading is given by (Martin, 2019):

$$20log_{10}\frac{R}{1\ m}\ dB, \text{where R is range}$$

When the waves encounter horizontal boundaries such as the seabed and sea-surface, the propagation tends to cylindrical spreading (Martin, 2019; JASCO Applied Sciences, 2019; Seto, 2021) and the associated transmission loss is given by (Martin, 2019):

$$10log_{10}\frac{R}{1\ m}\ dB$$

Both spherical and cylindrical spreading are only rough approximations to actual spreading loss in the ocean. Neither considers the refraction that occurs because of the dependence of sound speed on temperature, salinity and pressure (depth).

"Colder and fresher water has a lower sound speed and conversely warmer and saltier water has a higher sound speed. As the water depth increases the pressure increases the water density slightly, which increases the sound speed (Jensen et al., 2011)" (p.34) (Martin, 2019).

Moreover, "when the sound speed changes with depth" (p.34) (Martin, 2019), the sound rays can be trapped in a surface propagation duct or deep sound channel (Martin, 2019; JASCO Applied Sciences, 2019).

Additionally, in shallow water seabed and sea surface interactions "reflect, absorb and scatter the sounds" (p.33) (Martin, 2019). Furthermore, the "knowledge of the bottom

shape and composition, the surface roughness and the sound's wavelength" (p.34) (Martin, 2019) play an important role in propagation effects.

Chapter 6: Discussion

6.1 False Positives

This is a difficult category as there is no legal requirement for some vessel types to carry or use an AIS transmitter (Lowes et al., 2022). For example, local fishing and recreational boats or other small vessels might not have an AIS system on board (Lowes et al., 2022). Other vessels may not, for various reasons, have their AIS system on.

Another factor is that the AIS data were filtered to a maximum range of 10 km and minimum speed of 8 knots. There are vessels at longer ranges and lower speeds that have been detected by the JASCO and DEMON detectors but were not included in the statistics.

Therefore, false positive classification may not be reliable for the reasons discussed above and acoustic data which correspond to false positives CPAs should be manually verified and evaluated for the presence of vessels by listening to the audio recordings and looking at the spectrograms.

6.2 False Negatives

False negatives could be due to vessel distance to the sensor, source level, vessel class, vessel orientation, vessel engine status, background noise, and other underwater propagation conditions (Lowes et al., 2022). There also could be a need for threshold refinements (Lowes et al., 2022).

6.2.1 Vessel Distance to the Sensor

Vessel distance to the sensor could be a factor. If a vessel is at CPA, it is difficult to detect tonals due to cavitation, and Lloyds' mirror and Doppler effects (Delarue, 2021).

6.2.2 Cavitation

When a vessel is at CPA, propeller cavitation noise can mask a tonal.

6.2.3 Lloyds' Mirror

Lloyd's Mirror Effect is produced by acoustic interferences between direct and surface reflected propagation paths causing alternatively constructive (in-phase) and destructive (out-of-phase) interferences at the receiver (Carey, 2009; McKenna et al., 2012; Audoly, 2015). It results in the u-shaped frequency-dependent interference patterns centered at the CPA that can be observed in a spectrogram (McKenna et al., 2012; Audoly, 2015). If there is severe fading due to Lloyds' mirror effect, tonals can be masked (Seto, 2021).

6.2.4 Doppler Effect

When a vessel is transiting relative to the acoustic sensor, the relative motion between the two, create Doppler effects (Seto, 2021). When the range is decreasing (vessel approaching) we get a higher frequency version of the transmitted vessel acoustic signal, and the frequency will be shifted to higher frequencies. However, when the range is increasing (vessel departing), we get a lower frequency version of the transmitted vessel acoustic signal, and the frequencies will be shifted to lower frequencies. Therefore, we observe the change in frequency which is a Doppler effect (Seto, 2021).

The JASCO tonal detector requires a tonal to be present for 32 seconds continuously at the same frequency. If we are tracking a constant frequency, and there is a Doppler shift, the frequency does not stay stable for the detector's duration of 32 seconds indicating that there is enough frequency change to stop tracking the tonal. Another factor could be that some vessels' acoustic signatures are not clean, meaning they could be distorted, so we do not get a constant frequency over the necessary duration.

The 11-minutes-moving-average-number-of-tonals is used to overcome the issues discussed in sections 6.2.1 - 6.2.4. Vessels are quieter when they are approaching the sensor then when they are leaving, because the vessel itself is shielding the sound coming from the propeller. Therefore, when the stern of a vessel is facing the sensor, there is a direct path to the propeller noise source which results in additional or more distinguishable tones. By averaging over 11 minutes (5 minutes before, 1 current minute, 5 minutes after) the detector can average between the times when it does and does not detect tones.

6.2.5 Source Level

According to MacGillivray et al. (2021) there is a strong correlation between the source level and AIS vessel class which depends on vessel mean speed and length. Source level depends on and, generally increases with vessel speed (Arveson et al., 2000; MacGillivray et al., 2021). Also, longer ships displace more water, generating more flow noise, especially in cases where they are maneuvering (Seto, 2021).

6.2.6 Vessel Class

Vessel class plays a significant role. For example, sail boats can sail with their engines turned off, and hence, be very quiet, while still transmitting AIS information (Lowes et al., 2022). Selecting a particular AIS category will help address this problem.

There are some distinct differences between a ship and small vessel or boat. Small vessels or boats are relatively small in size (length, width, depth of the hull) in comparison with large ships. Additionally, ships are usually powered by large and heavy marine diesel engines that are mounted or coupled to the hull, whereas a small vessel or boat generally uses smaller engines such as an outboard engine (Seto, 2021). Moreover, the size of the propeller of a ship is greater than that of a small vessel or boat.

Based on these differences, the URN of a small vessel or boat will be different than that of a ship. Small vessels will typically have lower radiated power due to smaller and less powerful drive trains and propellers, and they also tend to have much less machinery on board (Seto, 2021). Therefore, in general, we expect a small vessel or boat to produce less tonals (Seto, 2021). However, small vessels or boats will produce higher frequency tonals as their shafts turn faster and they can accelerate to very high velocities.

6.2.7 Vessel's Orientation

Vessel orientation relative to the AMAR is important (Lowes et al., 2022). When a vessel is approaching the sensor, the vessel itself may obstruct the direct path between the propeller and the hydrophone. However, as a vessel passes CPA and begins to move away from the AMAR, the propeller would be more acoustically visible to the hydrophone thereby maximizing the detectability of the cavitation noise (Lowes et al., 2022).

Also, as mentioned above, when a ship is maneuvering, it generates more flow noise, so it will be harder to detect tonals (Seto, 2021).

6.2.8 Vessel Engine

Vessel engine status is also important. Some ships could be idling, but still transmitting AIS data (Lowes et al., 2022). However, the AIS data would indicate zero speed. In this thesis, setting a minimum speed threshold has eliminated this problem. It is recommended to consider the AIS Navigational Status to overcome other issues related to the vessel engine (MarineTraffic, from https://help.marinetraffic.com/hc/en-us/articles/205426887-What-kind-of-information-is-AIS-transmitted-, last viewed July 5, 2022).

6.2.9 Background Noise

Background noise is generated by geophonic sounds, biophony and anthrophony (JASCO Applied Sciences, 2019).

According to the JASCO vessel detector criteria, the SPL in the 40–315 Hz decidecade shipping band must be at least 3 dB higher than the lower of the left and right sided 360-minute mean for a possible vessel detection to occur (Delarue, 2021). Events such as a noisy vessel transiting slowly, periods of increased sea state and associated weather conditions, distance vessels noise, saturation from cavitation, and Lloyds' mirror effect due to multipaths, will fill the background up with energy. The vessel noise has to be higher than the background for a substantial amount of time to permit its detection. If the tonals are masked and the SPL is not meeting the 3 dB exceedance requirement, the ship event will not be detected. Another reason could be that the background noise can be higher before and after the current time, which can elevate the background estimate and make detection less likely.

Chapter 7: JASCO Detector Thresholds Analysis

It may be possible to improve the JASCO vessel detector's performance by further analyzing the criteria thresholds it uses. This section presents an analysis of these.

The JASCO detector used the parameters and associated thresholds shown in Table 8 for the vessel detection and CPA determination.

Table 8: The JASCO detector threshold.

Parameter	JASCO detector default threshold
f_{min} flag (Hz)	40
f_{max} flag (Hz)	315
Minimum broadband SPL (dB)	105
Shipping to background threshold (dB)	3
Minimum number of moving average tonals	3
Background window duration (in minutes)	720
Minimum shipping duration (in minutes)	5
Maximum shipping duration (in minutes)	360
Typical shipping passing duration (in minutes)	30
Shipping to RMS threshold (dB)	12
Anthropogenic shoulder (in minutes)	15

Selection of a maximum range of 10 km and minimum speed of 8 knots resulted in an initial data set of 1090 AIS CPAs. Note that this number differs slightly from the 1009

used in section 5.2 as it was performed before the final analysis was conducted and there were slight differences in the parameters used to down select the AIS CPA dataset.

Table 9 shows the results for deployment 1 and 2 separately and combined. The JASCO detector produced 593 true positive CPA matches, and 497 false negative CPA matches. These numbers were used as a baseline for further analysis of the individual parameter values used with the objective of increasing the JASCO detector's overall performance.

Table 9: The JASCO detector.

	JASCO detector		
	Deployment 1 (D1)	Deployment 2 (D2)	D1 + D2
AIS CPA Data	559	531	**1090**
Number of true positive CPAs	295	298	**593**
Number of false negative CPAs	264	233	**497**
Moving average number of tonals less than 3	64	37	101
Number of shipping tonals less than 3	84	73	157
SPL in the shipping band (40–315 Hz) is less than 3 dB above the 12 h mean	163	145	308
SPL in the shipping band is not within 12 dB of the system unweighted SPL	0	8	8

For each individual parameter the range of new threshold values to be assessed are shown in Table 10. They were selected based on a range of values that could cover shallow and deep waters scenarios.

Table 10: New thresholds.

Parameter	New threshold	
	Lower	Upper
Minimum number of moving average tonals	1	6
Background window duration (in minutes)	120	780
Minimum shipping duration (in minutes)	2	6
Maximum shipping duration (in minutes)	60	420
Shipping to background threshold (dB)	1	6
Shipping to RMS threshold (dB)	3	18

The next step was to test the new thresholds and run the statistics on them. The results are available in Appendix A (Table 14 - Table 25). Table 11 shows that the final parameters shown in the first column have significantly improved the number of true positive CPA matches when compared with the original thresholds.

Table 11: Number of TP and FN CPAs, and their percentage for the parameters with the original and new thresholds.

JASCO detector parameters	Number of true positive CPAs	Percent	Number of false negative CPAs	Percent
Original thresholds	593	54 %	497	46 %
Minimum number of moving average tonals equal to 1	624	57 %	466	43 %
Background window duration (in minutes) equal to 120	624	57 %	466	43 %
Minimum shipping duration (in minutes) equal to 2	692	63 %	398	37 %

There is also an improvement of four additional true positive CPAs when the background window duration set to 780 minutes. Additionally, there is an insignificant improvement of one detection for a shipping to RMS threshold (dB) equal to 18. There is no change in the number of true positive CPAs for maximum shipping duration of 420 minutes. For the remaining parameters, the number of true positive CPAs have increased.

The next step was to run the analysis using the combination of revised parameter thresholds highlighted in grey in Table 12 that resulted in an improved number of true positive and false negative CPAs. Default values were used for the other parameters. The parameter combinations were based on four random selections of revised parameter thresholds. Runs were performed as shown in Table 12.

Table 12: The combination of parameters with the original and new thresholds for four runs.

Parameter	**Threshold**			
	Run 1	**Run 2**	**Run 3**	**Run 4**
Minimum number of moving average tonals	**1**	**1**	3 (default)	**1**
Background window duration (in minutes)	**120**	720 (default)	**120**	**120**
Minimum shipping duration (in minutes)	5 (default)	**2**	**2**	**2**
Maximum shipping duration (in minutes)	360	360	360	360
Shipping to background threshold (dB)	3	3	3	3
Shipping to RMS threshold (dB)	12	12	12	12

The results are available in Appendix A (Table 26 - Table 29). Table 13 summarises the results of the four runs.

Table 13: The number of TP and FN CPAs, and their percentage for the four runs

	Number of true positive CPAs	Percent	Number of false negative CPAs	Percent
Original thresholds	593	54 %	497	46 %
Run 1	655	60 %	435	40 %
Run 2	699	64 %	391	36 %
Run 3	734	67 %	356	33 %
Run 4	755	69 %	335	31 %

Run 4, the combination of the three new thresholds values, resulted in the overall highest number of true positive CPAs, and consequently, in the lowest number of false negative CPAs. The number of true positive CPAs has increased by 15 %.

7.1 Discussion of the Assessment of the JASCO Detector Thresholds

The analysis's results have shown that the JASCO detector's performance depends primarily on three parameters which are the minimum number of moving average tonals, background window duration, and minimum shipping duration.

The default threshold for the minimum number of moving average tonals was 3, whereas the new threshold was set to 1. One of the possible explanations could be that we are getting detections from small vessels or Lake vessels.

As discussed earlier, smaller vessels will typically have a lower radiated power as a result of a smaller and less powerful drive train and propeller, and they also require less machinery on board (Seto, 2021). Therefore, in general, we expect a small vessel produce less tonals (Seto, 2021).

Lake vessels are known as "lakers" (Figure 46). Lakers are long, narrow and flat (Harbron, 2014). Lake vessels may have different sound signatures from larger ocean-going vessels, however, it is not well explored or documented.

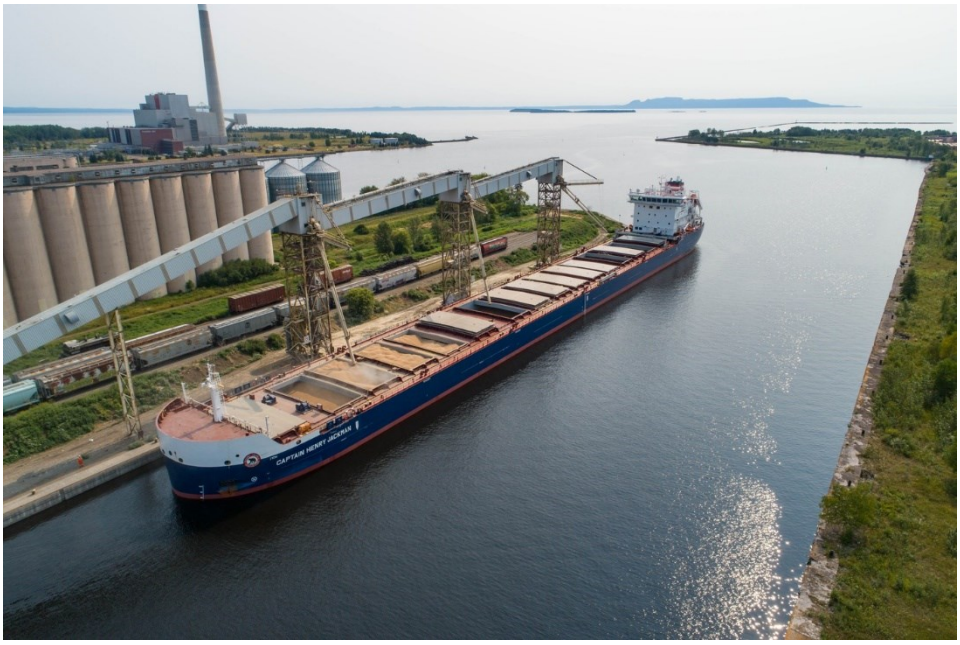

Figure 46: The dry-bulk carrier, the Captain Henry Jackman (CMC, 2021).

The default threshold for background window duration was 720 minutes which is normally suitable for open waters. The new shorter threshold was set to 120 minutes.

Events including a slower vessel transiting with a louder sound signature, periods of intense sea/ocean and weather conditions, or distance vessels noise, can last a fair amount of time resulting in an increased background noise level. As was discussed, the vessel noise has to be higher than the background for a substantial amount of time to permit its detection. Shortening the background window essentially helps with faster recovery of the background ambient noise level thereby facilitating the 3 dB exceedance requirement.

The default threshold for the minimum shipping duration was 5 minutes, whereas the revised threshold was set to 2 minutes. As discussed before, we could be getting detections from smaller quicker vessels. Shortening the minimum shipping duration would help with their detection.

Another factor could be that AMAR is duty cycled for these deployments. A shipping event would only be detectable during the 5 minutes and 40 seconds AMAR recording cycle. This is followed by a sleep period of 9 minutes and 20 seconds where no acoustic data are collected. Therefore, there is a possibility of missing the detection of a vessel if it was only detectable for a short period of time. Shortening the minimum shipping duration showed that it helps with the true positive CPA detections.

The water depth of the AMAR location was about 75 metres which is relatively deep (Figure 11). There were an increased number of JASCO true positive CPAs near the AMAR with the number of JASCO false negative CPAs increasing towards the northwest and northeast. One of the possible explanations could be due to the shallower water found there (Figure 11). Therefore, the revised parameters which are optimized for shallow water, demonstrated the lowest overall number of JASCO false negative CPAs in comparison with the default ones which are more applicable to deeper waters. One of the future works could be to compare the number of true positive CPAs in the shallow waters versus deep waters. This comparison will give some insights into the choice of parameters thresholds which could be more suitable for shallow or deep waters. The default thresholds were used for the rest of the parameters and this analysis concluded that they were already optimal for the deployment area.

Based on this assessment it is recommended to optimize the existing JASCO vessel detection criteria by changing some of the threshold values. It is suggested to change the moving average number of tonals to 1, the background window duration to 120 minutes, and the minimum shipping duration to 2 minutes. This optimization is recommended for the Sept-Îles region, and other similar deployment areas.

Chapter 8: Recommendation for Future Work

DEMON Processing is widely used for ship detection and classification (Pollara et al., 2016; Pollara et al., 2017a; Lowes et al., 2022). There are a number of implementations of DEMON Processing (Hanson et al., 2008; Fillinger et al., 2009; Fillinger et al., 2011; Chung et al., 2011; Pollara et al., 2016; Pollara et al., 2017a; Pollara et al., 2017b; Reis et al., 2019; Lowes et al., 2022). These papers suggest several improvements, address challenges, and highlighted limitations of the DEMON Processing. The standard approach (Chung et al., 2011) has been described earlier in this thesis.

DEMON Processing allows the identification of tonals (e.g. shaft and blade rate, and their harmonics) which can be used for ship detection and classification (Chung et al., 2011; Pollara et al., 2016; Pollara et al., 2017a; Pollara et al., 2017b; Lowes et al., 2022).

This thesis implemented a DEMON detector, and demonstrated some applications of DEMON Processing for passive acoustic data.

8.1 Overall Limitations

As discussed in section 6.1, false positive JASCO and DEMON CPAs could be due to a vessel not carrying an AIS transmitter (Lowes et al., 2022) or because the JASCO and DEMON detections were only compared to a subset of the AIS vessel data (<10 km and > 8 knots). Therefore, there may be vessels at longer ranges and lower speeds that have been detected by the JASCO and DEMON detectors.

For the JASCO, DEMON, and combined detectors, the statistics for false positive and true negative CPAs could not be obtained at this stage.

8.2 Overall Improvements

One suggestion is to estimate the heading of a vessel based on the AIS course over ground. Vessel orientation could be useful for exploring false negative CPAs. It is also proposed to extend the 10 km maximum range to a longer range based on the location and assessment of AIS data. For example, one of the main shipping lanes near the Port of Sept-Îles is at approximately 15 km range from where the AMAR was deployed. This resulted in the AMAR getting a number of CPAs at longer ranges which significantly contributed to the number of false positive CPAs for the evaluation criteria (<10 km and > 8 knots). However, these CPAs could be true positive detections. The speed limit of 8 knots also plays an important role. The optimal speed range has to be further explored.

It is recommended to run the DEMON Processing on the entire one-year of acoustic data combined with a manual analysis of some percentage of the data set. Manual analysis would permit the annotation of vessel and boat presence by listening to the audio recordings and looking at their spectrograms. This would permit a more detailed analysis of the DEMON detector's performance when compared to the AIS data and JASCO detector.

For the DEMON processing undertaken to date only the largest peak was saved for CPA determination resulting in the inability to detect two vessels at CPA at the same time. Therefore, it is recommended to track and save additional peaks to improve the performance. This could help with vessel detection, especially for the case of identifying two or more vessels transiting past the recorder at similar times. This should increase the number of true positive CPAs. Moreover, the ratio between blade rate and shaft rate will give a number of propeller blades which could be used for vessel classification.

Furthermore, it is suggested to continue analysing the DEMON data, and find the optimal time difference between the peaks to distinguish between different vessel events, the peak distance in minutes, and time tolerance between AIS and DEMON data.

It is suggested to save additional SPL peaks for the JASCO detector. It is also recommended to use the optimized thresholds for the JASCO detector for datasets acquired in environments like that of the Sept Iles deployment location. Finally, another suggestion is to further investigate the other potential causes for false negative CPAs that were discussed earlier in the detector performance section.

Leal's et al. (2015) paper presented a method for automatic ship classification according to their type using Artificial Neural Networks and Support Vector Machines (Reis et al., 2019). In addition, Meir et al. (2012) showed decision-making algorithm for acoustic vessel classification. Machine learning techniques for detecting and classifying vessels could be researched and applied in the future.

Chapter 9: Conclusion

All three detectors were able to access and document the number of vessels in the area around the Port of Sept-Îles within the 10 km evaluation range.

When run on the entire one-year subset of acoustic data set, the JASCO vessel detector had a CPA determination accuracy rate of almost 60% in comparison with the AIS data, whereas the DEMON detector performed better with an overall accuracy rate of 79%. The DEMON detector performance is 19% higher than that of the JASCO detector. The combination of the two detectors resulted in a 87% CPA determination accuracy rate, an improvement of 27% in comparison with the JASCO detector, and 8% in comparison with the DEMON detector.

The analysis of the different JASCO detector parameters with different thresholds resulted in an increase of true positive CPAs by 15%. Suggestions for optimizing the JASCO detector and the existing JASCO vessel detection criteria have been proposed and recommendations for the further optimization of the AIS data and DEMON detector have been put forward.

References

Abrahamsen, K. (2012). The ship as an underwater noise source. The Journal of the Acoustical Society of America, 17. https://doi.org/10.1121/1.4772953

André, M., Rizzuto, E., & Gaggero, T. (2010). Underwater radiated noise. SILENV European Collaborative Project, deliverable D1.3.

Arveson, P. T., & Vendittis, D. J. (2000). Radiated noise characteristics of a modern cargo ship. The Journal of the Acoustical Society of America, 107(1), 118–129. https://doi.org/10.1121/1.428344

Audoly, C. (2015). Noise Sources. Ship Underwater Radiated Noise Patterns. AQUA (Achieve QUieter Oceans by shipping noise footprint reduction) FP7 - Collaborative Project n°314227. Retrieved from http://www.aquo.eu/downloads/AQUO_R2.9_Ship_URN_Patterns_V1.0.pdf

Baldacci, A., & Haralabus, G. (2006). Adaptive normalization of active sonar data. NATO Undersea Research Centre. Retrieved from https://www.researchgate.net/publication/228543582_Adaptive_normalization_of_active_sonar_data

Bahtiarian, M. (2019). Quieting Ships to Protect the Marine Environment Workshop Final Report. Report #481**,** ACENTECH.

Bretschneider, H., Bosschers, J., Choi, G. H., Ciappi, E., Farabee, T., Kawakita, C., & Tang, D. (2014). Specialist committee on hydrodynamic noise. Final report and recommendations to the 27th ITTC.

Bright Hub Engineering. (2009). Variable pitch propellers and their uses in marine engineering. Naval Architecture & Ship Design for Marine Engineers. Retrieved from https://www.brighthubengineering.com/naval-architecture/32845-cpp-controllable-pitch-propellers-explained/

Blair, H. B., Merchant, N. D., Friedlaender, A. S., Wiley, D. N., & Parks, S. E. (2016). Evidence for ship noise impacts on humpback whale foraging behaviour. Biology letters, 12(8), 20160005. https://doi.org/10.1098/rsbl.2016.0005

Canadian Sailings. (2018). A new dawn for Port of Sept-Îles. Retrieved from https://canadiansailings.ca/a-new-dawn-for-port-of-sept-les/

Castellote, M., Clark, C., & Lammers, M. (2012). Acoustic and behavioural changes by fin whales (Balaenoptera physalus) in response to shipping and airgun noise. Biological Conservation*,* 147, 115–122. doi: 10.1016/j.biocon.2011.12.021

Carey, W.M. (2009). Lloyd's mirror—image interference effects. Acoustics Today. Retrieved from https://acousticstoday.org/wp-content/uploads/2019/09/LLOYD'S-MIRROR—IMAGE-INTERFERENCE-EFFECTS-William-M.-Carey.pdf

Cerna, M., & Harvey, F.A. (2000). The Fundamentals of FFT-Based Signal Analysis and Measurement (Application Note 041). National Instruments. Retrieved from https://www.sjsu.edu/people/burford.furman/docs/me120/FFT_tutorial_NI.pdf

Chamber of Marine Commerce (CMC). (2021). New Great Lakes eco ship setting records. Retrieved from https://www.marinedelivers.com/2021/08/new-great-lakes-eco-ship-setting-records/

Chung, K., Sutin, A., Sedunov, A., & Bruno, M. (2011). DEMON Acoustic Ship Signature Measurements in an Urban Harbor. Advances in Acoustics and Vibration. https://doi.org/10.1155/2011/952798

Cranford, T. W., & Krysl, P. (2015). Fin whale sound reception mechanisms: skull vibration enables low-frequency hearing. PloS one, 10(1), e0116222. https://doi.org/10.1371/journal.pone.0116222

Cruz, E., Lloyd, T., Bosschers, J., Lafeber, F.H., Vinagre, P., & Vaz, G. (2021). Study on inventory of existing policy, research and impacts of continuous underwater noise in Europe. EMSA report EMSA/NEG/21/2020. WavEC Offshore Renewables and Maritime Research Institute Netherlands. Retrieved from https://www.researchgate.net/publication/355477751_SOUNDS_STATUS_OF_UNDERWATER_NOISE_FROM_SHIPPING_STUDY_ON_INVENTORY_OF_EXISTING_POLICY_RESEARCH_AND_IMPACTS_OF_CONTINUOUS_UNDERWATER_NOISE_IN_EUROPE

Damas, M. D. (2006). Study of tons and their characteristics for use in a ship classifier based on neural networks (Master dissertation). Federal University of Rio de Janeiro - COPPE-PEE.

Delarue, Julien. 2021. Passive Acoustic Monitoring, Port of Sept-Îles: Marine Mammal Detections and Ambient Noise Characterization: Nov 2020-May 2021. Document 02509, Version 1.0. Technical report by JASCO Applied Sciences for INREST.

DOSITS. (n.d.). Introduction to Signal Levels. Retrieved from https://dosits.org/science/advanced-topics/introduction-to-signal-levels/ (Last viewed May 12, 2022).

Erbe, C., Marley, S.A., Schoeman, R., Smith, J.N., Trigg, L.E., & Embling, C.B. (2019). The Effects of Ship Noise on Marine Mammals—A Review. Frontiers in Marine Science. https://doi.org/10.3389/fmars.2019.00606

Fillinger, L., Sutin, A., & Sedunov, A. (2009). Cross-correlation of ship noise for water traffic monitoring. The Journal of the Acoustical Society of America, 126, 2251. https://doi.org/10.1121/1.3249259

Fillinger, L., Sutin, A., & Sedunov, A. (2011). Acoustic ship signature measurements by cross-correlation method. The Journal of the Acoustical Society of America, 129, 774 – 778. https://doi.org/10.1121/1.3365315

Government of Canada. (2021). Maritime Mobile Service Identities (MMSIs) and Maritime Identities (MIs). Retrieved from https://www.ic.gc.ca/eic/site/smtgst.nsf/eng/h_sf06198.html

Great Lakes Guide (n.d.). St. Lawrence River. Retrieved from https://greatlakes.guide/watersheds/st-lawrence (Last viewed August 1, 2022).

Halliday, W. D., Insley, S. J., Hilliard, R. C., de Jong, T., & Pine, M. K. (2017). Potential impacts of shipping noise on marine mammals in the western Canadian Arctic. Marine Pollution Bulletin, 123, 73-82. https://doi.org/10.1016/j.marpolbul.2017.09.027

Hanson, D., Antoni, J., Brown, G., & Emslie, R. (2008). Cyclostationarity for Passive Underwater Detection of Propellor Craft: A Development of DEMON Processing. Proceedings of Acoustics 2008. Retrieved from https://www.acoustics.asn.au/conference_proceedings/AAS2008/papers/p63.pdf

Harbron, D. J. (2014). Lake Carriers. The Canadian Encyclopedia. Retrieved from https://www.thecanadianencyclopedia.ca/en/article/lake-carriers

Harris, F. (1978). On the use of windows for harmonic analysis with the discrete Fourier transform. Proceedings of the IEEE, 66, 51-83. Retrieved from https://www.cs.cmu.edu/afs/cs/user/bhiksha/WWW/courses/dsp/spring2013/WWW/schedule/readings/windows_comparison2_harris.pdf

Hewlett-Packard. (1985). The Fundamentals of Signal Analysis, Application Note 243. Retrieved from https://www.hpmemoryproject.org/an/pdf/an_243.pdf

Hildebrand, J. A., Frasier, K. E., Helble, T. A., & Roch, M. A. (2022). Performance metrics for marine mammal signal detection and classification. The Journal of the Acoustical Society of America, 151(1), 414. https://doi.org/10.1121/10.0009270

Hildebrand, J.A. (2004). Sources of Anthropogenic Sound in the Marine Environment. Retrieved from https://www.mmc.gov/wp-content/uploads/hildebrand.pdf

INREST. (2017). Observatoire environnemental de la baie de Sept-Îles.

Tilden, S.J., Max, S., Blair, J.J., Alegria, F.A., Balestrieri, E., Björsell, N., Calvin, J., Dallet, D., Daponte, P., Vito, L.D., Goncharenko, A.M., Greer, D., Liggiero, R., Linnenbrink, T.E., Rapuano, S., & Xu, F. (2011). IEEE Std.1241-2010 - IEEE Standard for Terminology and Test Methods for Analog-to-Digital Converters (Revision of IEEE Std.1241-2000). https://doi.org/10.1109/IEEESTD.2011.5692956.

International Maritime Organization (IMO). (n.d.). AIS transponders. Retrieved from https://www.imo.org/en/OurWork/Safety/Pages/AIS.aspx (Last viewed July 5, 2022).

International Maritime Organization (IMO). (2010). IMO MEPC59 Noise from Commercial Shipping and its Adverse Impacts on Marine Life – Report of the Correspondence Group. 17th ASCOBANS Advisory Committee Meeting. Retrieved from https://www.ascobans.org/sites/default/files/document/AC17_4_11_IMO-MEPC59_NoiseWGReport_1.pdf

JASCO Applied Sciences (n.d.). Detection_levels. JASCO internal document. (Last viewed May 18, 2022).

JASCO Applied Sciences. (2019). Underwater acoustics: noise and the effects on aquatic life. A pocket handbook 4th edition (interim).

Jensen, F. B., Kuperman, W. A., Porter, M. B., & Schmidt, H. (2011). Computational Ocean Acoustics. 2nd edition. AIP Series in Modern Acoustics and Signal Processing. AIP Press - Springer, New York. 794 p.

Kschischang, R. F. (2015). The Hilbert Transform. The Edward S. Rogers Sr. Department of Electrical and Computer Engineering, University of Toronto. Retrieved from https://www.comm.utoronto.ca/frank/notes/hilbert.pdf

Lobo, V. (2002). Ship noise classification. A contribution to prototype based classifier design (Doctoral dissertation). New University of Lisbon, College of Science and Technology. Retrieved from https://www.novaims.unl.pt/vlobo/Publicacoes/4_2_2_Tese_total.pdf

Lowes, G.J., Neasham, J., Burnett, R., Sherlock, B., & Tsimenidis, C. (2022). Passive Acoustic Detection of Vessel Activity by Low-Energy Wireless Sensors. Journal of Marine Science and Engineering, 10(2), 248. https://doi.org/10.3390/jmse10020248

Leal, N., Leal, E., & Sanchez, G. (2015). Marine vessel recognition by acoustic signature. ARPN Journal of Engineering and Applied Sciences. Retrieved from http://www.arpnjournals.org/jeas/research_papers/rp_2015/jeas_1115_2919.pdf

MacGillivray, A., & de Jong, C. A. (2021). Reference Spectrum Model for Estimating Source Levels of Marine Shipping Based on Automated Identification System Data. Journal of Marine Science and Engineering, 9(4), 369. https://doi.org/ 10.3390/jmse9040369

MarineTraffic Density Maps. (2021). Map data. Retrieved from https://www.marinetraffic.com/en/ais/home/centerx:56.3/centery:-15.5/zoom:2

MarineTraffic. (n.d.). What kind of information is AIS-transmitted? Retrieved from https://help.marinetraffic.com/hc/en-us/articles/205426887-What-kind-of-information-is-AIS-transmitted- (Last viewed July 5, 2022).

Maritime Information Portal. (2020). Automatic Identification System (AIS) on Ships. Retrieved from https://www.marinfo.gc.ca/e-nav/docs/ais-index-en.php

Marley, S. A., Salgado Kent, C. P., Erbe, C., & Thiele, D. (2017). A tale of two soundscapes: comparing the acoustic characteristics of urban versus pristine coastal dolphin habitats in Western Australia. Acoustics Australia, 45, 159–178. doi: 10.1007/s40857-017-0106-7

Martin, B. (2013). Computing cumulative sound exposure levels from anthropogenic sources in large data sets. Proceedings of Meetings on Acoustics, 19(1). https://doi.org/10.1121/1.4800967

Martin, S. B., Gaudet, B. J., Klinck, H., Dugan, P. J., Miksis-Olds, J. L., Mellinger, D. K., Mann, D. A., Boebel, O., Wilson, C. C., Ponirakis, D. W., & Moors-Murphy, H. (2021). Hybrid millidecade spectra: A practical format for exchange of long-term ambient sound data. JASA express letters, 1(1), 011203. https://doi.org/10.1121/10.0003324

Martin, S.B. (2019). One minute at a time: advancing our ability to estimate effects of human sound on marine life (Doctoral dissertation). Dalhousie University. Retrieved from https://dalspace.library.dal.ca//handle/10222/76377

McKenna, M. F., Ross, D., Wiggins, S. M., & Hildebrand, J. A. (2012). Underwater radiated noise from modern commercial ships. The Journal of the Acoustical Society of America, 131(1), 92–103. https://doi.org/10.1121/1.3664100

Merchant, N. D., Fristrup, K. M., Johnson, M. P., Tyack, P. L., Witt, M. J., Blondel, P., & Parks, S. E. (2015). Measuring acoustic habitats (Appendix S1, PAMGuide tutorial). Methods in ecology and evolution, 6(3), 257–265. https://doi.org/10.1111/2041-210X.12330

Meir, T., Tsionskiy, M., Sutin, A., & Salloum, H.R. (2012). Decision Learning Algorithm for Acoustic Vessel Classification. Homeland Security Affairs, 8. Retrieved from https://www.hsaj.org/articles/211

Mooney, T.A., Di Iorio, L., Lammers, M.O., Lin, T., Nedelec, S.L., Parsons, M., Radford, C.A., Urban, E., & Stanley, J.A. (2020). Listening forward: approaching marine biodiversity assessments using acoustic methods. Royal Society Open Science, 7. https://doi.org/10.1098/rsos.201287

National Oceanic and Atmospheric Administration (NOAA). (2021). What is ocean noise? National Ocean Service website. Retrieved from https://oceanservice.noaa.gov/facts/ocean-noise.html

Oliveira, R., Lima, B., & Ebecken, N. (2010). The Use of Multi-Way Analisys in the Classification Task of Passive SONAR Contacts. Mecánica Computacional. Computational Intelligence Techniques for Optimization and Data Modeling, 29. Retrieved from https://www.researchgate.net/publication/49175840_The_Use_of_Multi-Way_Analisys_in_the_Classification_Task_of_Passive_SONAR_Contacts

Parks, S. E., Ketten, D. R., O'Malley, J. T., & Arruda, J. (2007). Anatomical predictions of hearing in the North Atlantic right whale. Anatomical record (Hoboken, N.J. : 2007), 290(6), 734–744. https://doi.org/10.1002/ar.20527

Perlman, D., Stanford, J.M., & Wallischeck, E.Y. (2017). Concept of Operations: SeaTA - Enhanced Travel Time Estimates and Traffic Management Practices for the St. Lawrence Seaway. Retrieved from https://rosap.ntl.bts.gov/view/dot/34625

Pollara, A., Sutin, A., & Salloum, H.R. (2016). Improvement of the Detection of Envelope Modulation on Noise (DEMON) and its application to small boats. OCEANS 2016 MTS/IEEE Monterey, 1-10. doi: 10.1109/OCEANS.2016.7761197

Pollara, A., Sutin, A. & Salloum, H. (2017a). Passive acoustic methods of small boat detection, tracking and classification. The Proceedings of the 2017 IEEE International Symposium on Technologies for Homeland Security (HST), 1–6. https://doi.org/10.1109/THS.2017.7943488

Pollara, A., Sutin, A., & Salloum, H. (2017b). Modulation of high frequency noise by engine tones of small boats. The Journal of the Acoustical Society of America, 142(1), EL30. https://doi.org/10.1121/1.4991345

Port of Sept-Îles (n.d.). Port of Sept-Îles. Retrieved from https://www.portsi.com/port/?lang=en (Last viewed December 14, 2021).

Port of Vancouver. (2020). ECHO Program 2019 voluntary vessel slowdown trial in Haro Strait and Boundary Pass. Retrieved from https://www.portvancouver.com/wp-content/uploads/2020/08/ECHO-Program-2019-voluntary-vessel-slowdown-in-Haro-Strait-and-Boundary-Pass-final-report.pdf

Pricop, M., Chitac, V., Gheorghe, F., Pazara, T., Oncica, V., Atodiresei, D., & Pricop, C. (2010). Underwater radiated noise of ships' machinery in shallow water. Proceedings of the 2nd International Conference on Manufacturing Engineering, Quality and Production Systems. Retrieved from https://www.researchgate.net/publication/308693751_Underwater_Radiated_Noise_of_Ships%27Machinery_in_Shallow_Water

Reis, C.D., Padovese, L.R., & Oliveira, M.C. (2019). Automatic detection of vessel signatures in audio recordings with spectral amplitude variation signature. Methods in Ecology and Evolution, 10, 1501 - 1516. https://doi.org/10.1111/2041-210X.13245

Seto, M. L. (2021). Underwater Acoustic Engineering. Lecture materials.

Saunders, J. C., Rintelmann, W. F., & Bock, G. R. (1979). Frequency selectivity in bird and man: a comparison among critical ratios, critical bands and psychophysical tuning curves. Hearing research, *1*(4), 303–323. https://doi.org/10.1016/0378-5955(79)90003-0

Shaw, G., & Kaczkowski, V. (2015). St. Lawrence Seaway. The Canadian Encyclopedia. Retrieved from https://www.thecanadianencyclopedia.ca/en/article/st-lawrence-seaway

Simard, Y., Roy, N., Gervaise, C., & Giard, S. (2016). Analysis and modeling of 255 source levels of merchant ships from an acoustic observatory along St. Lawrence Seaway. The Journal of the Acoustical Society of America, 140(3), 2002. https://doi.org/10.1121/1.4962557

Scharf, B. (1970). Critical bands. In Tobias, J.V. (ed.). Foundations of Modern Auditory Theory. Volume 1. Academic Press, New York. pp. 157–202.

Sound on Sound (SOS). (n.d.). Glossary. Retrieved from https://www.soundonsound.com/glossary/band-pass-filter-bpf (Last viewed May 8, 2022).

Southall, B.L. (2005). Shipping noise and marine mammals: a forum for science, management, and technology. Final Report of the National Oceanic and Atmospheric Administration (NOAA) International Symposium. U.S. NOAA Fisheries, Arlington, Virginia, May 18–19, 2004, 40. Retrieved from http://beamreach.org/wiki/images/4/47/2004NoiseReport.pdf

Southall, B.L., Scholik-Schlomer, A.R., Hatch, L.T., Bergmann, T., Jasny, M.D., Metcalf, K., Weilgart, L.S., & Wright, A.J. (2017). Underwater Noise from Large Commercial Ships—International Collaboration for Noise Reduction. Encyclopedia of Maritime and Offshore Engineering. https://doi.org/10.1002/9781118476406.emoe056

Southall, B.L., Bowles, A.E., Ellison, W.T., Finneran, J.J., Gentry, R.L., Greene, C.R., Jr Kastak, D., Ketten, D.R., Miller, J.H., Nachtigall, P.E., Richardson, W.J., Thomas, J.A., & Tyack, P.L. (2007). Marine mammal noise exposure criteria: initial scientific recommendations. Aquatic Mammals, 33, 411– 521. doi: 10.1578/AM.33.4.2007.411

Southall, B.L., Finneran, J.J., Reichmuth, C., Nachtigall, P.E., Ketten, D.R., Bowles, A.E., Ellison, W.T., Nowacek, D.P., & Tyack, P.L. (2019). Marine Mammal Noise Exposure Criteria: Updated Scientific Recommendations for Residual Hearing Effects. Aquatic Mammals. https://doi.org/10.1578/AM.45.2.2019.125

Southall, B.L., Nowacek, D.P., Bowles, A.E., Senigaglia, V., Bejder, L., & Tyack, P.L. (2021). Marine Mammal Noise Exposure Criteria: Assessing the Severity of Marine Mammal Behavioral Responses to Human Noise. Aquatic Mammals, 47(5), 421-464. https://doi.org/10.1578/AM.47.5.2021.421

Struzinski, W. A., & Lowe, E. D. (1984). A performance comparison of four noise background normalization schemes proposed for signal detection systems. The Journal of the Acoustical Society of America, 76, 1738-1742. https://doi.org/10.1121/1.391621

Viswanathan, M. (2017). Understanding Analytic Signal and Hilbert Transform. GaussianWaves, Signal Processing for Communication Systems. Retrieved fromhttps://www.gaussianwaves.com/2017/04/analytic-signal-hilbert-transform-and-fft/

Wisniewska, D. M., Johnson, M., Teilmann, J., Siebert, U., Galatius, A., Dietz, R., & Madsen, P. T. (2018). High rates of vessel noise disrupt foraging in wild harbour porpoises (Phocoena phocoena). Proceedings. Biological sciences, 285(1872), 20172314. https://doi.org/10.1098/rspb.2017.2314

Yang, Y. (2017). A Signal Theoretic Approach for Envelope Analysis of Real-Valued Signals. IEEE Access, 5, 5623-5630. Retrieved from https://ieeexplore.ieee.org/stamp/stamp.jsp?arnumber=7891054

Appendix A: Results of JASCO Detector Threshold Analysis

Table 14: Minimum number of moving average tonals equal to 1.

	Minimum number of moving average tonals equal to 1		
	Deployment 1 (D1)	Deployment 2 (D2)	D1 + D2
AIS CPA Data	559	531	**1090**
Number of true positive CPAs	319	305	**624**
Number of false negative CPAs	240	226	**466**
Moving average number of tonals less than 1	21	15	36
Number of shipping tonals less than 1	61	62	123
SPL in the shipping band (40–315 Hz) is less than 3 dB above the 12 h mean	159	145	304
SPL in the shipping band is not within 12 dB of the system unweighted SPL	0	8	8

Table 15: Minimum number of moving average tonals equal to 6.

	Minimum number of moving average tonals equal to 6		
	Deployment 1 (D1)	Deployment 2 (D2)	D1 + D2
AIS CPA Data	559	531	**1090**
Number of true positive CPAs	241	245	**486**
Number of false negative CPAs	318	286	**604**
Moving average number of tonals less than 6	166	136	302
Number of shipping tonals less than 6	132	107	239
SPL in the shipping band (40–315 Hz) is less than 3 dB above the 12 h mean	164	149	313
SPL in the shipping band is not within 12 dB of the system unweighted SPL	0	9	9

Table 16: Background window duration (in minutes) equal to 120.

	Background window duration (in minutes) equal to 120		
	Deployment 1 (D1)	Deployment 2 (D2)	D1 + D2
AIS CPA Data	559	531	**1090**
Number of true positive CPAs	309	315	**624**
Number of false negative CPAs	250	216	**466**
Moving average number of tonals less than 3	66	37	103
Number of shipping tonals less than 3	80	68	148
SPL in the shipping band (40–315 Hz) is less than 3 dB above the 2 h mean	169	155	324
SPL in the shipping band is not within 12 dB of the system unweighted SPL	0	8	8

Table 17: Background window duration (in minutes) equal to 780.

	Background window duration (in minutes) equal to 780		
	Deployment 1 (D1)	Deployment 2 (D2)	D1 + D2
AIS CPA Data	559	531	**1090**
Number of true positive CPAs	301	296	**597**
Number of false negative CPAs	258	235	**493**
Moving average number of tonals less than 3	65	37	102
Number of shipping tonals less than 3	83	73	156
SPL in the shipping band (40–315 Hz) is less than 3 dB above the 13 h mean	161	144	305
SPL in the shipping band is not within 12 dB of the system unweighted SPL	0	8	8

Table 18: Minimum shipping duration (in minutes) equal to 2.

	Minimum shipping duration (in minutes) equal to 2		
	Deployment 1 (D1)	Deployment 2 (D2)	D1 + D2
AIS CPA Data	559	531	**1090**
Number of true positive CPAs	354	338	**692**
Number of false negative CPAs	205	193	**398**
Moving average number of tonals less than 3	43	32	75
Number of shipping tonals less than 3	68	62	130
SPL in the shipping band (40–315 Hz) is less than 3 dB above the 12 h mean	139	134	273
SPL in the shipping band is not within 12 dB of the system unweighted SPL	0	8	8

Table 19: Minimum shipping duration (in minutes) equal to 6.

	Minimum shipping duration (in minutes) equal to 6		
	Deployment 1 (D1)	Deployment 2 (D2)	D1 + D2
AIS CPA Data	559	531	**1090**
Number of true positive CPAs	283	293	**576**
Number of false negative CPAs	276	238	**514**
Moving average number of tonals less than 3	65	35	100
Number of shipping tonals less than 3	85	73	158
SPL in the shipping band (40–315 Hz) is less than 3 dB above the 12 h mean	167	147	314
SPL in the shipping band is not within 12 dB of the system unweighted SPL	0	9	9

Table 20: Maximum shipping duration (in minutes) equal to 60.

	Maximum shipping duration (in minutes) equal to 60		
	Deployment 1 (D1)	Deployment 2 (D2)	D1 + D2
AIS CPA Data	559	531	**1090**
Number of true positive CPAs	264	276	**540**
Number of false negative CPAs	295	255	**550**
Moving average number of tonals less than 3	64	37	101
Number of shipping tonals less than 3	93	80	173
SPL in the shipping band (40–315 Hz) is less than 3 dB above the 12 h mean	163	145	308
SPL in the shipping band is not within 12 dB of the system unweighted SPL	0	8	8

Table 21: Maximum shipping duration (in minutes) equal to 420.

	Maximum shipping duration (in minutes) equal to 420		
	Deployment 1 (D1)	Deployment 2 (D2)	D1 + D2
AIS CPA Data	559	531	**1090**
Number of true positive CPAs	295	298	**593**
Number of false negative CPAs	264	233	**497**
Moving average number of tonals less than 3	64	37	101
Number of shipping tonals less than 3	84	73	157
SPL in the shipping band (40–315 Hz) is less than 3 dB above the 12 h mean	163	145	308
SPL in the shipping band is not within 12 dB of the system unweighted SPL	0	8	8

Table 22: Shipping to background threshold (dB) equal to 1.

	Shipping to background threshold (dB) equal to 1		
	Deployment 1 (D1)	Deployment 2 (D2)	D1 + D2
AIS CPA Data	559	531	**1090**
Number of true positive CPAs	299	291	**590**
Number of false negative CPAs	260	240	**500**
Moving average number of tonals less than 3	64	37	101
Number of shipping tonals less than 3	85	73	158
SPL in the shipping band (40–315 Hz) is less than 1 dB above the 12 h mean	97	110	207
SPL in the shipping band is not within 12 dB of the system unweighted SPL	0	8	8

Table 23: Shipping to background threshold (dB) equal to 6.

	Shipping to background threshold (dB) equal to 6		
	Deployment 1 (D1)	Deployment 2 (D2)	D1 + D2
AIS CPA Data	559	531	**1090**
Number of true positive CPAs	254	274	**528**
Number of false negative CPAs	305	257	**562**
Moving average number of tonals less than 3	66	39	105
Number of shipping tonals less than 3	90	75	165
SPL in the shipping band (40–315 Hz) is less than 6 dB above the 12 h mean	238	205	443
SPL in the shipping band is not within 12 dB of the system unweighted SPL	0	8	8

Table 24: Shipping to RMS threshold (dB) equal to 3.

	Shipping to RMS threshold (dB) equal to 3		
	Deployment 1 (D1)	Deployment 2 (D2)	D1 + D2
AIS CPA Data	559	531	**1090**
Number of true positive CPAs	221	218	**439**
Number of false negative CPAs	338	313	**651**
Moving average number of tonals less than 3	66	42	108
Number of shipping tonals less than 3	96	91	187
SPL in the shipping band (40–315 Hz) is less than 3 dB above the 12 h mean	174	149	323
SPL in the shipping band is not within 3 dB of the system unweighted SPL	223	198	421

Table 25: Shipping to RMS threshold (dB) equal to 18.

	Shipping to RMS threshold (dB) equal to 18		
	Deployment 1 (D1)	Deployment 2 (D2)	D1 + D2
AIS CPA Data	559	531	**1090**
Number of true positive CPAs	295	299	**594**
Number of false negative CPAs	264	232	**496**
Moving average number of tonals less than 3	64	37	101
Number of shipping tonals less than 3	84	73	157
SPL in the shipping band (40–315 Hz) is less than 3 dB above the 12 h mean	163	145	308
SPL in the shipping band is not within 18 dB of the system unweighted SPL	0	5	5

In the first run, the moving average number of tonals was set to 1 and the background window duration to 120 minutes (Table 26).

Table 26: Run 1 with moving average number of tonals equals to 1 and background window duration (in minutes) equals to 120.

	Run 1		
	Deployment1 (D1)	Deployment2 (D2)	D1 + D2
AIS CPA Data	559	531	**1090**
Number of true positive CPAs	335	320	**655**
Number of false negative CPAs	224	211	**435**
Moving average number of tonals less than 1	21	16	37
Number of shipping tonals less than 1	59	58	117
SPL in the shipping band (40–315 Hz) is less than 3 dB above the 2 h mean	166	155	321
SPL in the shipping band is not within 12 dB of the system unweighted SPL	0	8	8

In the second run, the moving average number of tonals was set to 1 and the minimum shipping duration to 2 minutes (Table 27).

Table 27: Run 2 with moving average number of tonals equals to 1 and minimum shipping duration (in minutes) equals to 2.

	Run 2		
	Deployment1 (D1)	Deployment2 (D2)	D1 + D2
AIS CPA Data	559	531	**1090**
Number of true positive CPAs	363	336	**699**
Number of false negative CPAs	196	195	**391**
Moving average number of tonals less than 1	13	12	25
Number of shipping tonals less than 1	49	54	103
SPL in the shipping band (40–315 Hz) is less than 3 dB above the 12 h mean	136	133	269
SPL in the shipping band is not within 12 dB of the system unweighted SPL	0	8	8

In the third run, the background window duration was set to 120 minutes and minimum shipping duration to 2 minutes (Table 28).

Table 28: Run 3 with background window duration (in minutes) equals to 120 and minimum shipping duration (in minutes) equals to 2.

	Run 3		
	Deployment1 (D1)	Deployment2 (D2)	D1 + D2
AIS CPA Data	559	531	**1090**
Number of true positive CPAs	372	362	**734**
Number of false negative CPAs	187	169	**356**
Moving average number of tonals less than 3	47	33	80
Number of shipping tonals less than 3	68	57	125
SPL in the shipping band (40–315 Hz) is less than 3 dB above the 2 h mean	142	136	278
SPL in the shipping band is not within 12 dB of the system unweighted SPL	0	8	8

Finally for the fourth run, the moving average number of tonals was set to 1 along with a background window duration equal to 120 minutes and a minimum shipping duration of 2 minutes (Table 29).

Table 29: Run 4 with moving average number of tonals equals to 1, background window duration (in minutes) equals to 120 and minimum shipping duration (in minutes) equals to 2.

	Run 4		
	Deployment1 (D1)	Deployment2 (D2)	D1 + D2
AIS CPA Data	559	531	**1090**
Number of true positive CPAs	391	364	**755**
Number of false negative CPAs	168	167	**335**
Moving average number of tonals less than 1	13	12	25
Number of shipping tonals less than 1	46	47	93
SPL in the shipping band (40–315 Hz) is less than 3 dB above the 2 h mean	136	133	269
SPL in the shipping band is not within 12 dB of the system unweighted SPL	0	8	8

Appendix B: Equipment Specifications

AMAR

AMAR G4 Technical Specifications

Environmental

Operating temperature:	−5 to 50 °C
Storage temperature:	−18 to 55 °C

Hydrophones and Arrays

Customizable options from various manufacturers
Sensitivities and frequencies tailored to your needs

Example sensitivities:	−164 dB re 1 V/µPa @ 1 kHz −210 dB re 1 V/µPa @ 1 kHz
Example frequencies:	1 Hz to 50 kHz 5 Hz to 100 kHz 20 Hz to 200 kHz
Acoustic sensors:	Omnidirectional hydrophones Directional hydrophones Vector sensors Small spatial arrays Small linear arrays

Memory, Recording and Timing

Removable flash memory:	Up to 10 TB on 512 GB SD cards
Data format:	WAV, CSV
Clock accuracy (manufacturer's specification):	
Built-in clock:	5 ppm w/ 4.6 ppm aging over 20 yrs
Optional TCXO clock:	0.7 ppm w/ 1 ppm aging in first year
Optional CSAC:	10 ppb
Time sync options:	GPS PPS, NMEA (60 µs accuracy) AMARlink (1 s accuracy)

Power

Operating voltage:	7.8–24 V_{DC}
Batteries:	Alkaline, others upon request
AC power adapter:	110–240 V, 50–60 Hz, 0.5 A

4 to 16 Acoustic Channels

Resolution:	24 bits
Sample rates:	8, 16, 32, 64, 128, 256, 512 ksps sampled synchronously
Spectral noise floor:	Better than −150 dB re FS per root Hz at all sample rates

Seven Oceanographic Sensor Channels

Sensor options:	Oxygen, salinity, acidity/pH, depth, turbidity, orientation (roll-pitch-yaw), temperature, others upon request	
Four analog channels:	Sample rate:	1 sps
	Resolution:	10 bits
	Voltage:	0 to +5 V
Three serial channels:	One RS-232 and Two configurable as RS-232, RS-422, RS-485, or 3.3 V logic level	

Communications

ACE and UD:	Configure via Wi-Fi. Magnetic reed switches to start/stop recording.
PVC and AL:	Wired Comms Box to connect via Ethernet. Activation plug to turn on/off.

C-Lander

Specifications

Depth rating	250 m [820 ft] (with 48D-PVC External Battery Packs) 500 m [1640 ft] (with 48D-AL External Battery Packs)	
Total height	63 in [1600 mm]	
Cylinder outer diameter	24 in [610 mm]	
	With anchor	Without anchor
Weight in air	258 kg [569 lbs]	132 kg [291 lbs]
Weight in seawater	85 kg [188 lbs]	−25 kg [−56 lbs]
Material	Float body: Syntactic foam HDPE (high density polyethylene) Acetal thermoplastic 316 stainless steel Anchor Plate Assembly: Steel Acetal thermoplastic	
Acoustic sensor options	Up to 4 omnidirectional hydrophones 50 cm tetrahedral hydrophone array Directional hydrophones Vector/particle motion sensors (GTI M20 or similar)	
Measures	Imperial	

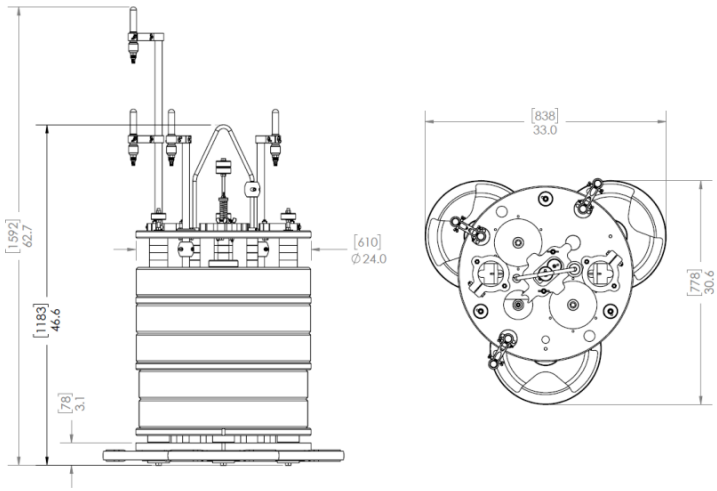

Hydrophone

GeoSpectrum Technologies Inc.
Customizing Detection

M36-100

The M36-100 is a wide-band omni-directional hydrophone designed for marine observation. It comes with a pre-amplified output of 0 to 35 dB (selectable on order) with current or voltage signalling.

Characteristics	
Nominal Voltage Sensitivity (without preamp)	-200 dBV re 1 µPa @ 20°C
Size	7.8" length, 1.3" max OD
Depth Rating	2500 m
Storage and Operating Temperatures	-40 to +70°C
Acceleration Sensitivity	<1.5 mbar/g, in air, any axis
Labelling	Calibration parameters, serial number, date
Connector	MCBH-8M
Pre-Amplifier	
Preamp signalling	Current, single ended voltage or, differential voltage (selectable on order)
Gain	0 – 35 dB (selectable on order)
Input Voltage	6.8 VDC nominal 4.5 – 30 VDC operating range
Band Pass	5 Hz HPF, no LPF installed (unless otherwise specified)
IRN	<140 nV/√Hz @10 Hz <4 nV/√Hz @1 kHz
Current Draw	1.3 mA (at 6.8 VDC) 4.2 mA with current signalling preamp